University of Bologna

Enabling Techniques and Algorithms for Integrated

Communication and Navigation Satellite Systems

by

Lina Deambrogio

Coordinator:
Prof. **Luca Benini**

Supervisor:
Prof. **Giovanni Emanuele Corazza**

March 2012

To my family

Any sufficiently advanced technology is indistinguishable from magic

Arthur C. Clarke

Contents

List of Figures

List of Tables

List of Acronyms

ACF Auto-Correlation Function

AGNSS Assisted-GNSS

AltBOC Alternate Binary Offset Carrier

BOC Binary Offset Carrier

CBA Cross-Band Aiding

CFAR Constant False Alarm Rate

C/N0 Carrier to Noise density ratio

CNR Carrier-to-Noise Ratio

CUR Complete Uncertainty Region

DBF Distributed Beamforming

DLL Delay Lock Loop

DPE Direct Position Estimation

EKF Extended Kalman Filter

EMLP Early-minus-Late Power

FFT Fast Fourier Transform

FLL Frequency Lock Loop

GNSS Global Navigation Satellite Systems

IFFT Inverse Fast Fourier Transform

IMU Inertial Measurement Unit

INS Inertial Navigation System

KF Kalman Filter

LOS Line of Sight

LS Least Squares

MAT Mean Acquisition Time

ML Maximum Likelihood

NCO Numerically Controlled Oscillators

OMAT Overall Mean Acquisition Time

OS Open Service

P Position

PDI Pre-detection Integration

PF Particle Filters

PLL Phase Lock Loop

PRN Pseudo Random Noise

PRS Public Regulated Service

PSA Pseudorange Sharing Algorithm

PSD Power Spectral Density

PV Position-Velocity

PVT Position Velocity and Time

RAIM Receiver Autonomous Integrity Monitoring

RUR Reduced Uncertainty Region

ROC Receiver Operating Characteristics

RSS Received Signal Strength

SNR Signal to Noise Ratio

SoO Signal of Opportunity

SS Spread Spectrum

SSB Single Side Band

TC Threshold Crossing

TTFF Time To First Fix

UEE User Equipment Error

UERE User Equivalent Range Error

UR Uncertainty Region

URE User Range Error

VDLL Vector Delay Lock Loops

VDFLL Vector Delay Frequency Lock Loop

VPLL Vector Phase Lock Loop

WSN Wireless Sensor Networks

Introduction

Motivation and Goals

This thesis is the outcome of the work performed within my PhD research activities. The focus of my research has been on Global Navigation Satellite Systems (GNSS) and in particular on the design of aiding schemes and the evaluation of their feasibility and advantages.

GNSS technology has impacted greatly on society and has become a fixture in everyday life, significantly changing people's habits and their way of interacting with their surroundings and each other. Indeed GNSS applications have grown into being fundamental tools for many common activities, the most significative being positioning services, i.e. car navigation, but also for mobile phone operations and control of power grids, through the exploitation of GNSS clocks. Moreover, the pervasive diffusion of GNSS-capable devices has laid the grounds for developing many exciting new application and location-based services. As a consequence, the demand for ubiquitous and reliable positioning has grown significantly and has become the driver of many research efforts by both the academia and the industry.

While very adapt and accurate in open sky environments, GNSS technology has well known limitations in constrained environments or in the presence of large errors affecting the transmitted signal that may cause considerable performance degradation, and in worst cases, the inability of producing a positioning solution.

Aiding techniques able to integrate GNSS receivers with assistance information can thus become the key for overcoming GNSS limitations and complementing its main features. By merging together two different systems, the integrated solution has the potential to considerably surpass stand-alone device performance and provide a tool that can be used in every operating condition. This will allow to employ GNSS technology also in areas where its use has been limited due to poor performance and extend the location-based services market.

In the context of the so-called system-of-systems, that comprises the new and modernized navigation satellite systems, novel augmentation and regional systems, emerging technologies able to achieve autonomous positioning and telecommunication infrastructures, fusing together all available information is just a matter of defining the best possible solution in a specific scenario and exploiting system complementarities.

Depending on the point in the receiver processing chain where assistance is applied, many different integration techniques can be envisaged. The most intuitive schemes work at the position level and rely on providing additional measurements to the receiver to improve its availability in scenarios where satellite signal reception is hindered by obstacles. This is useful for localization but becomes crucial for safety operation and emergency services working indoor and in challenging outdoors scenarios where sky visibility is limited. Furthermore, more complex techniques can also be employed at the physical level to improve receiver performance and especially synchronization capabilities that allow to achieve a faster position fix and guarantee enhanced robustness against errors affecting the satellite signals.

Aiding relies on the definition of new powerful concepts, as peer-to-peer cooperation, Inertial Navigation System (INS) hybridization and vector architectures, that, if on one hand provide the basis for developing innovative solutions, on the other raise interesting challenges to be considered and analyzed.

During my PhD I have dealt with these issues, proposing techniques and novel ideas which have contributed to the definition of viable solutions in the field of navigation. These design solution have been proposed in the framework of several projects in the National and International arena [9] [10] [11] that have provided proof of their applicability as well as the identification of the trade-offs related to the practical constraints of realistic systems.

Thesis Outline

This thesis is organized in two parts that tackle respectively the problem of aiding in GNSS receivers at the position level and at the physical level.

Part I deals with aiding strategies at the position level. The aim of assistance provided at this level is to improve position estimation availability by providing missing equations to the navigation processor. Exploiting the pervasive presence of (NAV-COM) devices, the exchange proposed in this thesis is conducted in a

peer-to-peer fashion and integration is proposed in two different manners: either through the exchange of terrestrial ranging information or GNSS-only assitance. Their performance analysis has been carried out considering different application scenarios and receiver types.

Part II considers the problem of aiding at the physical level. These types of aiding techniques require to enter the receiver synchronization blocks in order to supply assistance in speeding-up initial operation and improve robustness against signal degradation and receiver dynamics. In this context the initial acquisition block has been considered with the aim of proposing a code strategy able to achieve synchronization in dual-band receivers targeting a reduction of the mean acquisition time. Tracking blocks, on the other hand, have been considered to test the feasibility of advanced solutions that rely on integration with external information sensors and cross-signal aiding.

Original Contributions

The activities performed during the three years of this doctorate study led me to obtain original scientific contributions in several fields. Regarding aiding techniques operating at the positioning level, the main contributions are the following:

- Introduction of novel integration schemes that rely on the exchange of information in a peer-to-peer fashion;

- Design of a GNSS-data only algorithm to improve availability of the positioning solution [6];

- Design of a hybrid techniques to improve receiver accuracy [6].

Regarding physical level aiding techniques the main contributions are:

- Design of a novel code acquisition strategy for dual-band receivers that is based on the exchange of timing information between the different bands;

- Exploitation of the timing structures of the Galileo Open Service (OS) signals;

- Evaluation of the benefits in terms of mean acquisition time in allowing uni and bi-directional information flow between the acquisition engines [1], [2];

- Introduction of an innovative ultra-tight integration scheme that is based on the synthesis of an artificial correlation peak obtained through inertial system information [3];

- Analysis of the feedback generation process in vector tracking loops;

- Analysis of the feasibility of vector phase tracking [4].

Part I

Position Level Aiding Techniques

The goal of a GNSS receiver is to provide users their precise position anytime and anywhere. Finding the three dimension user position relies on the determination of the distance between the receiver and three or more satellites with known positions and resolving the resulting system of equations in the receiver coordinates. The range can be determined as the multiplication between the time needed by the signal transmitted by the satellite to reach the receiver and the speed of light. Since accurate synchronization between satellite and receiver clocks cannot be guaranteed, the distance measured this way is not the geometric distance but a pseudo-range. In fact, even though satellite clocks are very accurate and stable and all satellite transmission can be considered synchronous, receiver clocks do not have the same level of accuracy.

In order to provide the user position is thereby necessary to consider in the computation the misalignment between satellite and receiver clocks as an additional unknown and use measurements from a further satellite to provide all the required equations to resolve the system in the user coordinates and clock error. The minimum required number of satellites for position computation is thus equal to four.

The system of pseudorange equations is typically resolved using iterative Least Squares (LS) or Kalman filtering [12]. For both methods, the pseudorange equations are linearized about some initial estimates of the receiver position and clock bias. Differently from the LS method that relies only on the measurements at a given time and initial estimates of the unknowns, Kalman filtering allows also to include in the computation additional information as past measurements and the receiver motion model.

In the following the detailed description of the GNSS position computation block will be presented and aiding techniques that aim at improving positioning accuracy and availability will be discussed.

Chapter 1

Positioning Techniques

1.1 Position Determination

Position computation relies on the resolution of a system of at least four equations in the receiver coordinates. The distance between satellite and receiver can be computed by measuring the amount of time elapsed between the transmission of the satellite signals and their reception. Since all the satellite transmit their signals synchronously, the different times of arrival at the receiver are due to their different distances. As shown in 1.1, the receiver generates pseudorange measurements by multiplying the propagation delays by the speed of light.

$$\rho_i^1 \;\; = \;\; c \cdot \tau_i^1 \tag{1.1}$$
$$\vdots \;\; = \;\; \vdots$$
$$\rho^N \;\; = \;\; c \cdot \tau_i^N$$

For a generic satellite j the pseudorange measurement is related to the position of the receiver by 1.2.

$$\rho_i^j = \sqrt{(x^j - x_i)^2 + (y^j - y_i)^2 + (z^j - z_i)^2} + c(b_i - b^j) + I_i^j + T_i^j + e_i + n_i \tag{1.2}$$

where:

- (x_i, y_i, z_i) is the receiver position at time instant t_i;

- (x^j, y^j, z^j) is the j-th satellite position at transmission time t_t;

- b^j is the j-th satellite clock bias at transmission time t_t;

- b_i is the receiver clock bias at time instant t_i;

- I_i^j and T_i^j are the ionospheric and tropospheric delays respectively;

- e_i represents other various transmission delays (e.g. multipath);

- n_i is the receiver noise;

- c is the speed of light.

The equation unknowns are (x_i, y_i, z_i, b_i), since the tropospheric delay T_i^j can be computed from an a priori model and similarly the ionospheric delay I_i^j and satellite clock bias b^j may be estimated from an a priori model whose coefficients are part of the broadcast ephemerides [13].

For both the LS and the Kalman filtering methods, the pseudorange equations are then linearized with a Taylor expansion about some initial estimates of the receiver position and clock bias (x_0, y_0, z_0, b_0). The first order linearized pseudorange equation becomes:

$$\rho_i^j = \rho_0^j - \frac{(x^j - x_0)}{\rho_0^j}\Delta X_i - \frac{(y^j - y_0)}{\rho_0^j}\Delta Y_i - \frac{(z^j - z_0)}{\rho_0^j}\Delta Z_i + c(b_i - b^j) + I_i^j + T_i^j + e_i + n_i$$

$$(1.3)$$

where $\rho_0^j = \sqrt{(x^j - x_0)^2 + (y^j - y_0)^2 + (z^j - z_0)^2}$ is the geometric range at the initial position and $\Delta X_i = x_i - x_0$, $\Delta Y_i = y_i - y_0$, $\Delta Z_i = z_i - z_0$ are the increments in user position.

Therefore it can be obtained:

$$
\begin{aligned}
\delta\rho_i^j &= \rho_i^j - \rho_0^j + cb^j - I_i^j - T_i^j - e_i \\
&= -\frac{(x^j - x_0)}{\rho_0^j}\Delta X_i - \frac{(y^j - y_0)}{\rho_0^j}\Delta Y_i - \frac{(z^j - z_0)}{\rho_0^j}\Delta Z_i + cb_i
\end{aligned}
\tag{1.4}
$$

$$
\begin{bmatrix} \delta\rho_i^1 \\ \vdots \\ \delta\rho_i^N \end{bmatrix} = \begin{bmatrix} -\frac{(x^1 - x_0)}{\rho_0^j} & -\frac{(y^1 - y_0)}{\rho_0^j} & -\frac{(z^1 - z_0)}{\rho_0^j} & 1 \\ \vdots & \vdots & \vdots & \vdots \\ -\frac{(x^N - x_0)}{\rho_0^j} & -\frac{(y^N - y_0)}{\rho_0^j} & -\frac{(z^N - z_0)}{\rho_0^j} & 1 \end{bmatrix} \cdot \begin{bmatrix} \Delta X_i \\ \Delta Y_i \\ \Delta Z_i \\ cb_i \end{bmatrix}
$$

That can be written as:

$$\Delta\rho = \mathbf{H}_i\left[\Delta X_i, \Delta Y_i, \Delta Z_i, cb_i\right]^T \tag{1.5}$$

When using iterative least squares or a Kalman filter the vector of corrections is calculated and then added to the initial estimates (x_0, y_0, z_0, b).

1.2 Kalman Filtering

The peculiarity of the Kalman filter is that also a priori knowledge on the receiver motion or other additional information can be blended in the navigation system in order to improve position estimation accuracy.

The standard Kalman equations can be subdivided into two blocks: the first one is responsible for predicting the user position knowing the receiver transition model; the second is in charge of correcting the predictions by exploiting measurement information. The final optimal estimate is obtained through a weighted mean of the a priori estimate and the measurement correction. Depending on the filter gain, either the prediction or the correction are considered more in the final estimation.

The KF algorithm, first introduced in its discrete-time formulation in [12], offers an efficient and optimal solution to PVT estimation when the system under consideration is linear and the random measurements errors follow a Gaussian distribution.

The discrete KF aims at estimating recursively the state of a dynamic system described by the following equations:

$$
\begin{aligned}
\mathbf{x}_k^- &= \mathbf{F}_k \hat{\mathbf{x}}_{k-1} + \mathbf{w}_k \\
\mathbf{w}_k &\sim \mathcal{N}(0, \mathbf{Q}_k)
\end{aligned}
\tag{1.6}
$$

where:

- $\mathbf{x}_k$ is the Kalman filter vector state at time instant t_k composed of the user position coordinates and clock bias; with $\mathbf{x}_i^-$ representing the predicted state vector at time instant i obtained by considering just the system transition model (a priori estimation) and $\hat{\mathbf{x}}_i$ the a posteriori estimation after measurement correction;

- $\mathbf{F}_k$ is the system transition matrix describing the user dynamics;

- $\mathbf{w}_k$ is the process noise vector that accounts for uncertainties on the system model and is synthesized as a Gaussian variable with zero mean and covariance matrix Q_k;

The Kalman filter computes at each iteration also the reliability of the computed solution through the estimation covariance matrix P_k:

$$\mathbf{P}_k^- = \mathbf{F}_k \hat{\mathbf{P}}_{k-1} \mathbf{F}_k^T + \mathbf{Q}_k \tag{1.7}$$

analogously to the state vector, $\mathbf{P}_i^-$ represents the a priori covariance matrix and $\mathbf{F}_i$ the system transition matrix.

The measurement information is then used to correct the estimations obtained using the mathematical model only.

$$\begin{aligned} \mathbf{z}_k &= \mathbf{H}_k \mathbf{x}_k^- + \mathbf{n}_k \\ \mathbf{v}_k &\sim \mathcal{N}(0, \mathbf{R}_k) \end{aligned} \tag{1.8}$$

where:

- $\mathbf{z}_k$ are the observations;

- $\mathbf{H}_k$ is the observation matrix linking the state vector to the measurements;

- $\mathbf{n}_k$ is the measurement noise, modeled as Gaussian noise with zero mean and covariance R_k.

The final estimation is thus obtained as:

$$\hat{\mathbf{x}}_k = \mathbf{x}_k + \mathbf{K}_k[\mathbf{z}_k - \mathbf{H}\mathbf{x}_k^-] \tag{1.9}$$

$$\hat{\mathbf{P}}_k = (\mathbf{I} - \mathbf{K}_k \mathbf{H}_k)\mathbf{P}_{k-1}^- \tag{1.10}$$

where the Kalman filter gain is computed as:

$$\mathbf{K}_k = \frac{\mathbf{P}_k^- \mathbf{H}_k^T}{\mathbf{H}_k \mathbf{P}_k^- \mathbf{H}_k^T + \mathbf{R}_k} \tag{1.11}$$

However, due to the non-linear nature of the observation likelihood for distance measurements in GNSS applications, some linearizations and approximations are needed to transform the KF into the Extended Kalman Filter (EKF), suitable for non-linear systems [14]. The EKF is the nonlinear version of the Kalman filter which linearizes about the current mean and covariance.

In EKF filter, the state transition and observation models can be non-linear functions of the state vector.

$$\begin{aligned} \mathbf{x}_k &= f(\hat{\mathbf{x}}_{k-1}) + \mathbf{w}_k \\ \mathbf{z}_k &= h(\mathbf{x}_k) + \mathbf{n}_k \end{aligned}$$

The function f can be used to compute the predicted state from the previous estimate and, similarly, the function h can be used to compute the predicted measurement from the predicted state. However, f and h cannot be applied to the covariance directly. Instead a matrix of partial derivatives is computed.

$$\mathbf{F}_k = \left.\frac{\partial f}{\partial x}\right|_{\hat{\mathbf{x}}_k^-}$$

$$\mathbf{H}_k = \left.\frac{\partial h}{\partial x}\right|_{\hat{\mathbf{x}}_k^-}$$

At each timestep the Jacobian is evaluated with current predicted states $\mathbf{x}_k^-$. These matrices can be used in the Kalman filter equations. This process essentially linearizes the non-linear function around the current estimate.

Predict Phase In this phase of the computation the state vector is predicted from the a priori knowledge of the user dynamics. The predicted state can be obtained as:

$$\mathbf{x}_k^- = f(\hat{\mathbf{x}}_{k-1})$$

While the predicted estimate covariance is calculated as:

$$\mathbf{P}_k^- = \mathbf{F}_k \hat{\mathbf{P}}_{k-1} \mathbf{F}_k^\top + \mathbf{Q}_k$$

Update Phase In the second stage of the EKF algorithm, the predicted state is updated and corrected thanks to the measurement information. The innovation or measurement residual and the innovation (or residual) covariance are given by:

$$\tilde{\mathbf{y}}_k = \mathbf{z}_k - h(\hat{\mathbf{x}}_k^-)$$

$$\mathbf{S}_k = \mathbf{H}_k \mathbf{P}_k^- \mathbf{H}_k^\top + \mathbf{R}_k$$

The optimal Kalman gain is:

$$\mathbf{K}_k = \mathbf{P}_k^- \mathbf{H}_k^\top \mathbf{S}_k^{-1}$$

The final a posteriori estimations of the vector state and the covariance matrix are then:

$$\hat{\mathbf{x}}_k = \hat{\mathbf{x}}_k^- + \mathbf{K}_k \tilde{\mathbf{y}}_k$$

$$\hat{\mathbf{P}}_k = (\mathbf{I} - \mathbf{K}_k\mathbf{H}_k)\mathbf{P}_k^-$$

It is worthwhile noting that, in literature alternative techniques based on Bayesian filtering are also considered for position estimation. In [15], a thorough survey of different methods is reported. In particular, attention is given to Particle Filters (PF) for dealing with nonlinear/nonGaussian systems, which would not be properly described by the Kalman filter error models, and advanced positioning techniques as Direct Position Estimation (DPE) algorithms that are introduced to enhance receiver robustness by jointly processing all received signals.

1.3 Pseudorange Models and Performance

Pseudorange measurements in GNSS receivers can be perturbed by many error contributions: due to space, control and user segment irregularities as well as receiver conditions. In order to model correctly the errors, it is fundamental to account for each contribution but it is nevertheless important to consider measurement noise, which increases with signal attenuation, and the effect of multipath, which causes delayed reflected signals.

Different models can be used to characterize pseudorange measurements. In particular, two different models have been considered in this thesis: the User Equivalent Range Error (UERE) and the attenuation dependent model that relies on the Carrier to Noise density ratio (C/N0).

1.3.1 User Equivalent Range Error

The UERE is a measure of the error in the range measurement to each satellite as seen by the receiver. UERE varies because of random variations in the satellite signal, signal propagation characteristics, and user measurement processes.

It can be obtained by assuming all error contributions as statistically independent and normally distributed. Error sources can be classified in different classes: as User Range Error (URE), encompassing errors linked to the space and control segments, and User Equipment Error (UEE) comprising the errors attributable to the user segment [16]. In particular the following error sources can be identified:

- ephemeris and clock;

- ionosphere: the delay introduced depends on the frequency and on the density of electrons along the propagation path;

- troposphere: the propagation delay depends on the pressure, temperature and humidity of the air;

- multipath: due to the reflections of the transmitted signal near the receiver;

- receiver noise;

- uncompensated relativistic effects.

As noted above, each k-th error source can be modeled as a random variable, which is Gaussian with zero mean and standard deviation σ_k. Given the independency of all error terms, the UERE is computed as the square root of the sum of all contributions. Over the long term (days to months) UERE closely resembles a Gaussian distribution and is equivalent for each satellite [17]. All pseudorange measurements can thus be described as independently affected by an error modeled as a Gaussian random variable with zero mean and a standard deviation σ_{UERE}:

$$\sigma_{UERE} = \sqrt{\sum_k \sigma_k^2} \qquad (1.12)$$

In order to improve the accuracy of the solution, compensation techniques can be put into place at the receiver. The more basic ones depend on the prediction of the errors using models and coefficients broadcasted in the navigation data. In advanced or professional receivers more complex algorithms can be used to cancel the largest error contribution (e.g. ionospheric delay) [18], [19], [20]. Thus, the error affecting the measurements has to be intended as a residual error after the receiver has applied all corrections and mitigated the effect of each error source. An example of the error budget for GNSS measurements is shown in table 1.1, reporting the error contribution mean values for the single-frequency GPS receiver case [18]. However, it is worthwhile noting that accuracy losses, due to unmodeled errors, as for example severe multipath or RF interferences, can also induce biases in the pseudorange evaluation and are not taken into account with this error model.

Segment Source	Error Source	Std Error (m)
Space	Satellite Clock Stability	3.0
	Satellite Perturbation	1.0
	Other (thermal radiation, et c)	0.5
Control	Ephemeris Prediction Error	4.2
	Other (thrusters performance, etc)	0.9
User	Ionospheric Delay	5.0
	Tropospheric Delay	1.5
	Receiver Noise and Resolution	1.5
	Multipath	2.5
	Other (interchannel bias, etc)	0.5
System UERE	Total (rms)	8.0

Table 1.1: Pseudorange error budget for a single-frequency GPS receiver

1.3.2 Attenuation Dependent Error Model

In real scenarios, characterizing pseudorange measurements as in 1.3.1 may not be accurate enough to describe received signal power and multipath errors. In these cases, the error component should be modeled as a Gaussian random variable with zero mean and a standard deviation expressed as a function of the C/N_0.

C/N_0 is an essential measure of the quality of a GNSS signal that relies on assuming that the noise has infinite bandwidth and thus power. Noise is thereby characterized as noise power per unit of bandwidth. On the other hand, Signal to Noise Ratio (SNR) considers the noise power in a known limited bandwidth [21].

Measurements standard deviation can be obtained as [22]:

$$\sigma = \sqrt{a + b^2 \cdot 10^{\frac{-C/N_0}{10}}} \tag{1.13}$$

The constants a and b are chosen empirically by assessing the actual observed measurement errors.

In [23], the predicted UERE values for Galileo are shown as functions of the elevation angle, and the receiver type. Thus, a model that describes the relationship

between the C/N_0 and the satellite elevation angle α should be found. In particular, the path loss attenuation strongly impacts on the C/N_0 and follows the rule:

$$A_0(\alpha) = \sqrt{R^2 + S^2 - 2SR\cos 90° - \alpha - \arcsin \frac{R}{S}} \cos \alpha \qquad (1.14)$$

where R is the Earth radius, S is the satellite height.

It must be noted that, in a real scenario, the experienced C/N_0 is not only a function of the attenuation loss, but it is strongly dependant on the antenna pattern, on the atmospheric losses, on the receiver design, and on the scenario under evaluation. In literature, some empirical models are known [22], [24]. These models have been used in the following, yielding for the open sky scenario the C/N_0 Vs elevation angle behavior shown in figure 1.1.
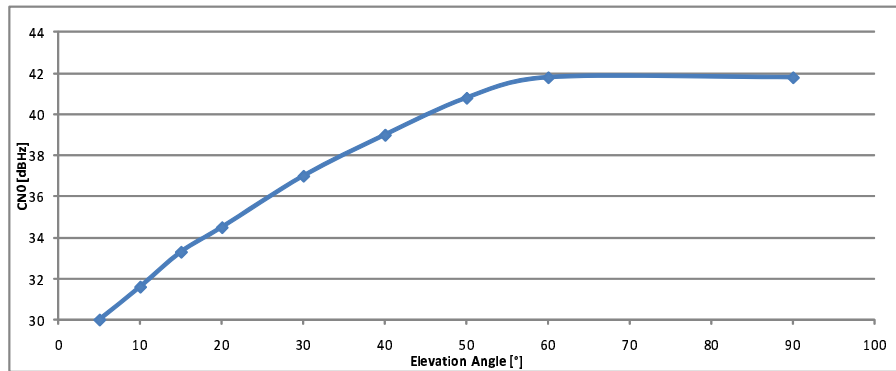
Figure 1.1: Nominal C/N_0 Vs Elevation Angle - Open Sky conditions

By matching the values of $\sigma(a, b)$ with the UERE reported in [23], the following values for the parameters (a, b) have been obtained: for mass-market receivers $a = 12$ and $b = 255$ and for professional receivers $a = 0.48$ and $b = 44$.

In table 1.2, the values of pseudorange error standard deviation are reported for the open sky scenario.

Elevation Angle [°]	C/N_0 [dBHz]	L1 mass-market [m]	L1/E5 professional [m]
5	30	8.78	1.55
10	31.6	7.55	1.35
15	33.3	6.51	1.18
20	34.5	5.92	1.08
30	37	5	0.93
40	39	4.49	0.85
50	40.8	4.17	0.80
60	41.8	4.04	0.78
90	41.8	4.04	0.78

Table 1.2: Pseudorange standard deviation in Open Sky scenarios

Figure 1.2 reports the pseudorange standard deviation trends for mass market and professional receivers at different elevation angles in open sky environments.

By considering, for the light indoor and the deep indoor cases, behaviors similar to figure 1.1 but with reduced values of C/N_0, the corresponding pseudorange standard deviation can be computed straightforwardly. In the following, the assumption of 8dB loss for the light indoor case, and 25dB for the deep indoor have been envisaged.

Elevation Angle [°]	C/N_0 [dBHz]	L1 mass-market [m]	L1/E5 professional [m]
5	22	20.55	3.56
10	23.6	17.20	2.99
15	25.3	14.28	2.49
20	26.5	12.55	2.19
30	29	9.69	1.71
40	31	7.98	1.42
50	32.8	6.79	1.22
60	33.8	6.25	1.13
90	33.8	6.25	1.13

Table 1.3: Pseudorange standard deviation in Light Indoor scenarios

Elevation Angle [°]	C/N_0 [dBHz]	L1 mass-market [m]	L1/E5 professional [m]
5	5	143.44	24.75
10	6.6	119.32	20.59
15	8.3	98.13	16.94
20	9.5	85.49	14.75
30	12	64.15	11.07
40	14	51.00	8.81
50	15.8	41.50	7.17
60	16.8	37.02	6.40
90	16.8	37.02	6.40

Table 1.4: Pseudorange standard deviation in Deep Indoor scenarios
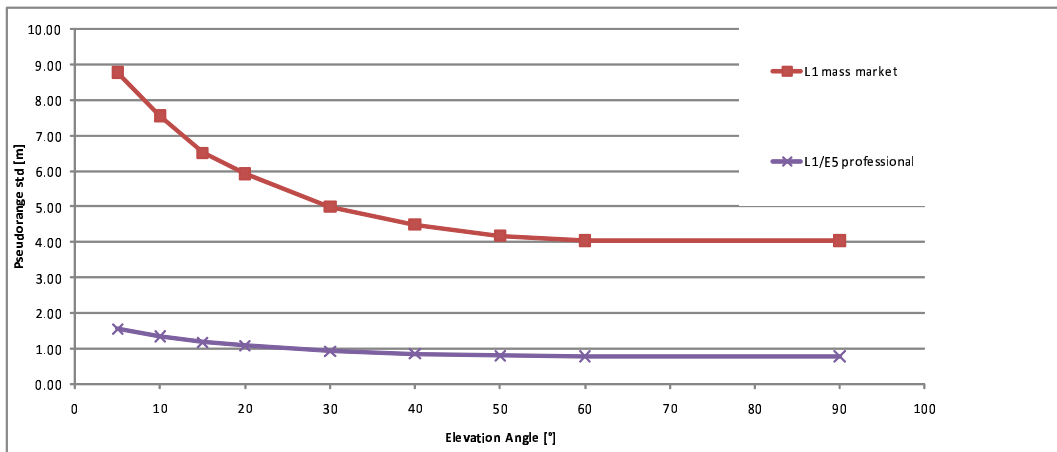
Figure 1.2: Pseudorange standard deviation Vs Elevation Angle in Open Sky scenarios

1.4 Aiding Techniques

Position based services for support, safety and commercial uses have witnessed a great diffusion in the last years, consequently GNSS have assumed growing importance. The availability of new services has opened the way to the definition of localization based applications for an increasing number of activities, but this, in turn, has lead to the definition of more stringent requirements for position accuracy, integrity, continuity of service, but more so for position availability. The need to guarantee improved performance has attracted the interest of both academia and industry, and many efforts are being devoted to satisfy the evermore challenging requirements.

As known, GNSS receivers need at least four satellites in visibility to solve the Position Velocity and Time (PVT) equations. Since this is generally achieved only in open sky environments, in harsh scenarios, where signal reception is heavily degraded or obstructed, GNSS-based localization degrades or completely fails.

In these cases, the state of the art offers different approaches to aid GNSS receivers.

Many techniques that rely on blending information from different systems have been investigated in [25], [26] and [27].

The most widely used scheme fuses information coming from GNSS sensors with inertial sensor estimations. INSs are self-contained navigation schemes in which measurements provided by accelerometers and gyroscopes, are used to compute the position and orientation (attitude) of an object relative to a known initial state. Usually, integration is performed through the use of a Kalman filter that is responsible for blending together the information coming from both the GNSS and the INS. The simplest scheme, the *loose integration*, performs hybridization at the position level by fusing together the position and velocity computed independently by the GNSS and by the INS. The GNSS computes the position starting from the estimation of the pseudorange measurements to at least for satellites, while the INS computes the position by integrating the information coming from its sensors. Data from both navigation systems are then submitted to a linear Kalman filter that combines them in order to achieve a more precise final solution, obtained by weighting the information from the GNSS receiver and the INS according to the SNR of the received signals and the reliability of the inertial sensor outputs. While on one hand this integration scheme is fairly simple to implement and provides better accuracy than both standalone GNSS and INS, on the other, it has limitations

due to the dependence on satellite visibility. If only raw GNSS measurements are available, integration is possible at the pseudorange level through a *tight integration* scheme. With tight hybridization, the integration block can fuse raw data and INS outputs to reach an improved position solution even with signal blockage or signal degradation. In these cases, when there are less than four received channels a PVT solution cannot be achieved with a navigation processor, but it can be achieved by the integrated receiver. This coupling technique is more robust to signal blockage than the loose approach, since each GNSS measurements is combined independently with INS outputs. However, being based on pseudoranges, this integration scheme requires non-linear equations in the Kalman filter, making this type of hybridization more complex to be achieved. The block diagram representing the two hybridization techniques is reported in figure 1.3.
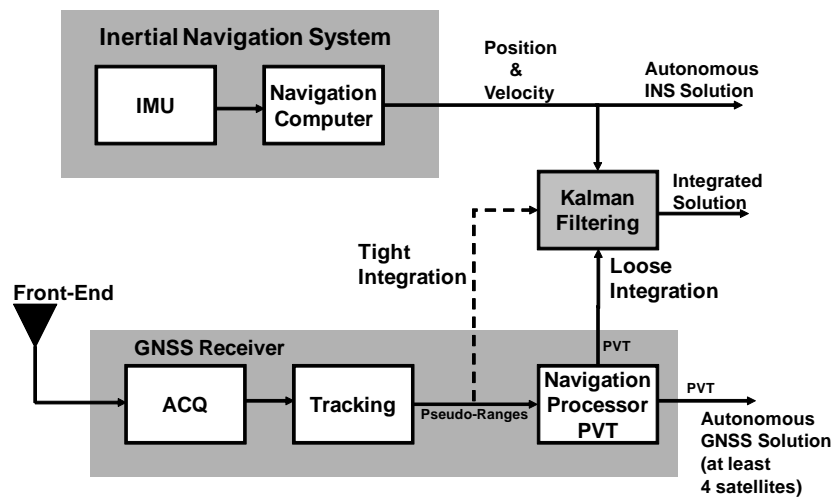
Figure 1.3: Loose and Tight Integration Schemes

Chapter 2

Peer-to-peer Positioning Techniques

The schemes proposed in 1.4, require the users to have additional sensors installed on their devices and this is not usually the case especially for pedestrians. On the other hand, the rapid worldwide growth in the number of GNSS users and the diffusion of hybrid navigation-communication (NAV-COM) devices have allowed to develop the concept of peer-to-peer cooperative localization. The paradigm of Peer-to-Peer (P2P) cooperative localization, relies on the exploitation of direct communication links among nodes in a network to exchange aiding information. The literature on cooperative peer-to-peer schemes is rather scarce. In [28] a possible architecture for P2P positioning is presented where indoor nodes are able to compute their position by dead reckoning and correct their estimations either through aiding provided by neighboring peers or through GNSS positioning, when sufficient satellite visibility is present. However, no collaboration between peers in terms of GNSS technology is considered.

My contribution to this topic is in the design and analysis of innovative P2P aiding techniques for cooperative positioning. The concept at the base of these aiding schemes is that all peers belonging to the same network have positions and velocities that are correlated to each other, thereby the exchange of information and the sharing of resources can become the means for achieving increased positioning capabilities especially in those scenarios where triangulation would be impossible for a single user. The presence of a P2P network becomes in these cases instrumental for achieving reliable positioning since it allows the exchange of range layer information between the peers and provides the missing equations in the PVT sys-

tem. In particular two different strategies are herein investigated: the first approach provides the exchange of GNSS data only, while the second approach consists in a hybrid terrestrial-satellite positioning technique. In the former method, the missing equations necessary for the PVT solution can be obtained by using the pseudorange measurements between the aiding peers and one or more satellites out of the user visibility; the latter consists in the transmission of the estimated distances between the nodes that are able to compute terrestrial ranging, and on the use of a hybrid set of equations where peers can be considered as pseudo-satellites.

In particular two situations can be envisaged:

- Indoor scenarios where GNSS signals are completely obstructed; hence, aiding becomes fundamental and cooperative techniques must be used, as depicted in figure 2.1.

- Outdoor environments where GNSS signals are not completely obstructed; however stand-alone GNSS receivers may eventually receive signals from an insufficient number of satellites, as shown in figure 2.2.
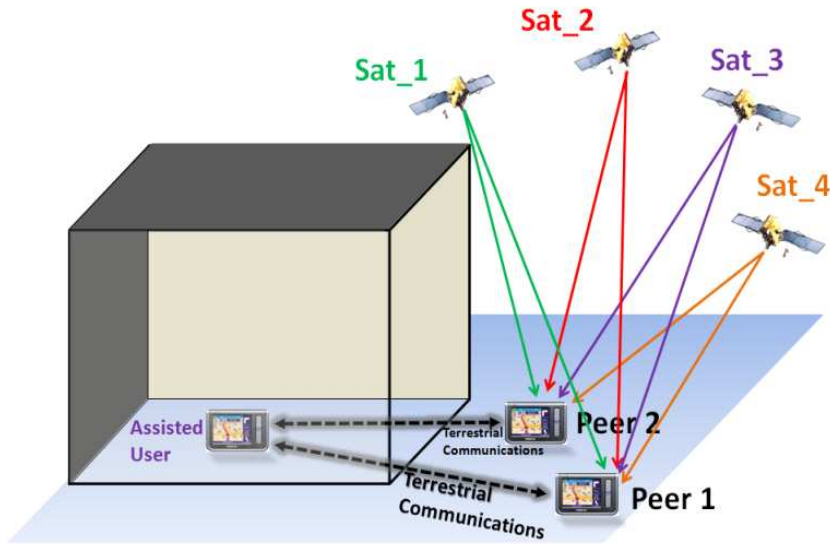
Figure 2.1: P2P typical indoor scenario

2.1   Pseudorange Sharing Algorithm

Pseudorange Sharing Algorithm (PSA) is proposed as a way to improve the availability and continuity of the positioning solution. In the algorithm, additional GNSS
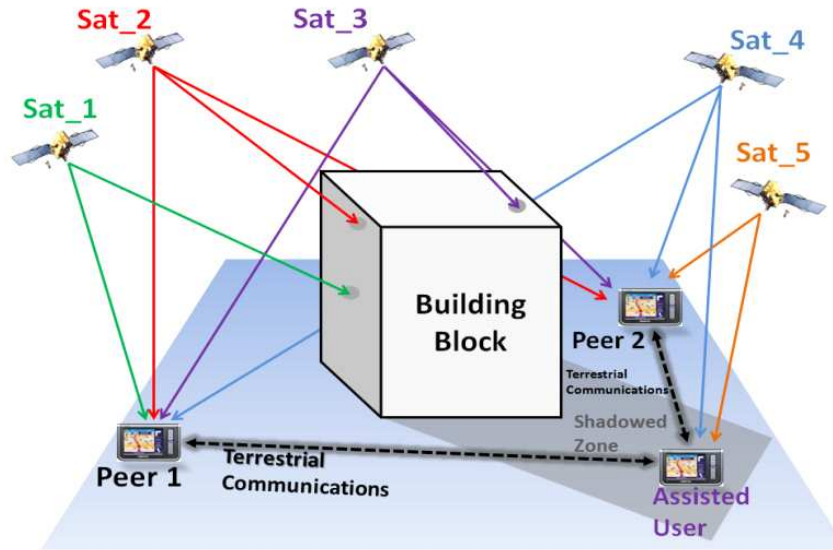
Figure 2.2: P2P typical outdoor scenario

ranging information are fused inside the navigation Kalman filter in order to supply missing equations when the user lacks visibility to the required number of satellites. This aiding technique relies on the exchange of the pseudorange measurements between neighboring peers and satellites not in visibility to the user. The algorithm does not require to correct the exchanged pseudoranges depending on the distance between the aiding and aided peers, causing the positioning solution to be biased towards the aiding peer position. Nonetheless it can be instrumental in providing a coarse position estimation in those scenarios where the line-of-sight between the user and the satellites is not guaranteed (like in urban canyons and indoor scenarios). In order to set correctly the matrices in the Kalman filter not only the pseudorange measurements but also the coordinates of the additional satellites must be passed on to the user.

2.1.1 Algorithm Parameters

Several parameters have been considered to analyze the behaviour of the proposed algorithm. Since the integrated user position is obtained through a Kalman filter, one of the most critical aspects is to set correctly the filter matrices. In particular the initial setting of the model matrices and the appropriate weighting of the available measurements are fundamental in limiting the algorithm convergence time. The algorithm paremeters are reported in the following:
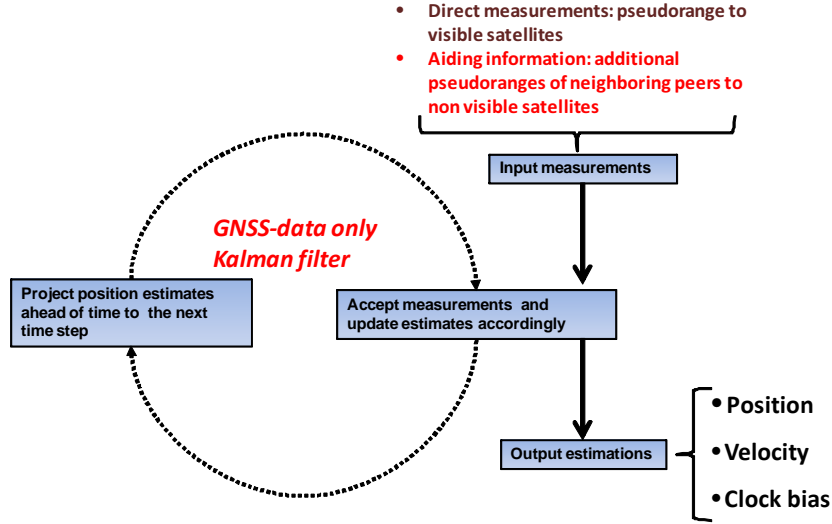
Figure 2.3: GNSS-data only Fusing Algorithm

- **System model matrices:** Depending on the knowledge of the initial user position, the initial estimate covariance matrix, P, and the model reliability matrix, Q, can be set differently. In particular the bigger the uncertainty on the initial position, the bigger should be the covariance values in the P matrix.

- **Measurement model matrix:** Depending on the application scenario and the assistance provided by the peers in the network the measurements provided to the estimation filter can either be direct pseudorange measurements, calculated by the user itself, or additional ranging information coming from neighboring peer. For direct measurements the accuracy depends on the noisiness of the available measurements that is generally modeled as additional Gaussian noise with a given standard deviation σ_{ρ_D}. The standard deviation is here computed as a function of C/N_0 since errors affecting the measurements increase with the signal attenuation as in 1.3.2. Additional aiding measurements, on the other hand, are all weighted the same. Since they are intrinsically affected by a bias due to the distance between aiding peer and aided user, their associated variance is set much higher than that of direct measurements as σ_{ρ_A} that accounts for aiding reliability and is a parameter that needs to be optimized in order to provide the best positioning solution.

When an initial clock synchronization between the peers in the network takes place, all clock misalignments can be considered almost equal; if this is not the case,

in order to account for the additional unknowns, the state filter must be modified and to resolve the positioning solution more equations are needed. In particular one additional state must be considered for every non-synchronized aiding peer.

2.1.2 Algorithm Description

For the indoor scenario and static receivers a Position (P) model can be employed to describe the system evolution in time, while a Position-Velocity (PV) model is more suited to limited dynamic outdoor scenarios.

The state vector in the first case can be considered equivalent to:

$$\mathbf{x}_k = [x_k, y_k, z_k, b_k] \tag{2.1}$$

while the system model can be represented as:

$$
\begin{aligned}
f(\mathbf{x}_k, \mathbf{w}_k) &= \mathbf{F}_k \hat{\mathbf{x}}_{k-1} + \mathbf{G}_k \mathbf{w}_k \\
&= \mathbf{I}_{4x4} \hat{\mathbf{x}}_{k-1} + \Delta t \mathbf{I}_{4x4} \mathbf{w}_k
\end{aligned}
$$

where Δt is the time between two consecutive algorithm iterations and $\mathbf{Q}_k = diag([\sigma_{\dot{x}}^2, \sigma_{\dot{y}}^2, \sigma_{\dot{z}}^2, \sigma_{\dot{b}}^2])$. The $\mathbf{Q}_k$ matrix takes into account the un-modeled dynamics and non-linearities white velocities and clock drift variances.

On the other hand, with the PV model the state vector becomes:

$$\mathbf{x}_k = \left[x_k, y_k, z_k, b_k, vx_k, vy_k, vz_k, \dot{b}_k \right] \tag{2.2}$$

$$
\begin{aligned}
f(\mathbf{x}_k, \mathbf{w}_k) &= \mathbf{F}_k \hat{\mathbf{x}}_{k-1} + \mathbf{G}_k \mathbf{w}_k \\
&= \begin{pmatrix} \mathbf{I}_{4x4} & \Delta t \mathbf{I}_{4x4} \\ 0 & \mathbf{I}_{4x4} \end{pmatrix} + \begin{pmatrix} \frac{\Delta t}{2} \mathbf{I}_{4x4} \\ \Delta t \mathbf{I}_{4x4} \end{pmatrix} \mathbf{w}_k
\end{aligned}
$$

and $\mathbf{Q}_k = diag([\sigma_{\ddot{x}}^2, \sigma_{\ddot{y}}^2, \sigma_{\ddot{z}}^2, \sigma_{\ddot{b}}^2])$ where white accelerations disturbances are considered.

In both cases the observation vector is given by

$$\mathbf{z}_k = [\rho_{D_k}, \rho_{A_k}] \tag{2.3}$$

where ρ_{D_k} are the direct pseudorange measurements and ρ_{A_k} the aiding pseudoranges at time instant k.

As mentioned above, the measurements must be weighted accordingly in the EKF by considering $\mathbf{R}_k = diag\left(\left[\sigma_{\rho_{D1_k}}{}^2, \ldots, \sigma_{\rho_{DN_k}}{}^2, \sigma_{\rho_{A1_k}}{}^2, \ldots, \sigma_{\rho_{AN_k}}{}^2\right]\right)$.

It is worthwhile noting that in order to limit the bias to the resulting position and allow algorithm convergence, only measurements to satellites not in direct visibility to the user are exchanged and each pseudorange to a non visible satellite is provided by one aiding peer only. Different assistance exchange strategies can be envisaged to optimize the algorithm performance and convergence time.

2.1.3   Simulation Environments

The PSA algorithm is evaluated in different scenarios where the user receives less than the required number of satellites, thus depends on aiding information to obtain the position solution.

In the following the options/parameters considered during the simulations are presented:

- **Receiver type:** the P2P network is comprised of both mass-market and professional receivers. The two types of users differ from one another in the quality of the available measurements.

- **Scenario Environment:** the algorithm can be tested considering both indoor and outdoor scenarios. The main difference in the two scenarios is the distance between aiding and aided peers. In indoor simulations, all peers are restricted in a confined area with limited relative distances; in outdoor scenarios, on the other hand, the aiding peers are deployed far from the aided user. The former scenario represents the optimal case for the pseudorange exchange algorithm since the bias due to to the exchange of pseudorange information without correction is very limited.

- **Mobility:** user mobility allows to test the algorithm with a variable number of visible satellites. Whenever the user has visibility of a sufficient number of satellites no aiding is needed, otherwise aiding is required.

- **Number of aiding peers:** increasing numbers of aiding peers allow, especially in the outdoor scenario, to provide aiding when needed.

2.1.4 Indoor Simulation Results

Figure 2.4 shows the indoor environment and the configuration parameters used to test the PSA. The blue point represents the user (Unknown Peer) located in the deep indoor zone (with no satellites visibility), while the green diamonds are the three aiding peers located in either the light indoor zone or the outdoor zone (with satellite visibility).
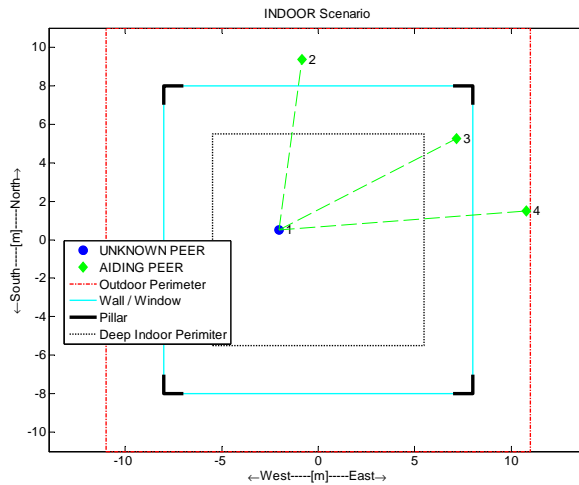
Figure 2.4: Indoor environment used for the simulation

In the first simulation the Unknown Peer (UP) is static and all aiding peers are classified as mass-market. The exchanged information of the aiding peers arrive at the user asynchronously, the initial UP's guessed position is set to its exact coordinates and the maximum random bias is chosen equal to ± 150 km. The following figures report the PSA algorithm performance considering $300T_s$ (each T_s is equal to 1 second). Figure 2.5 shows the Horizontal Cumulative Distribution Function (CDF) and reports the Root Mean Square Error (RMSE) after $300T_s$ that, in this case, is equal to 10.408 m.
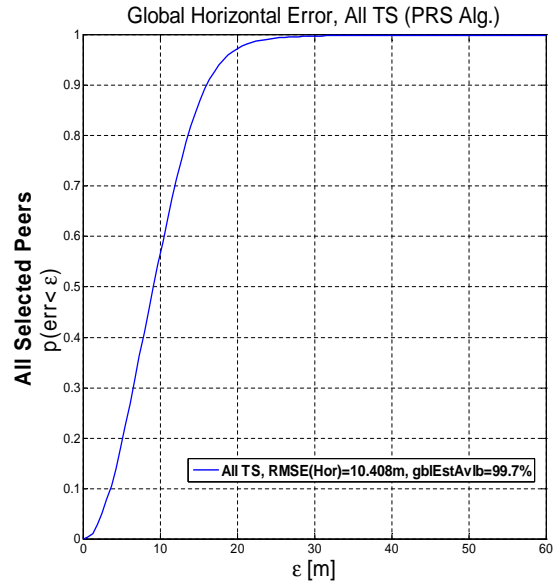
Figure 2.5: Horizontal Cumulative Distribution Function and RMSE for indoor simulation

Figure 2.6 and Figure 2.7 show the PSA performance: the horizontal error stabilizes around the value of 10.408 m after three steps, that is the Convergence Time (CT) as shown in the magnified Figure 2.7.
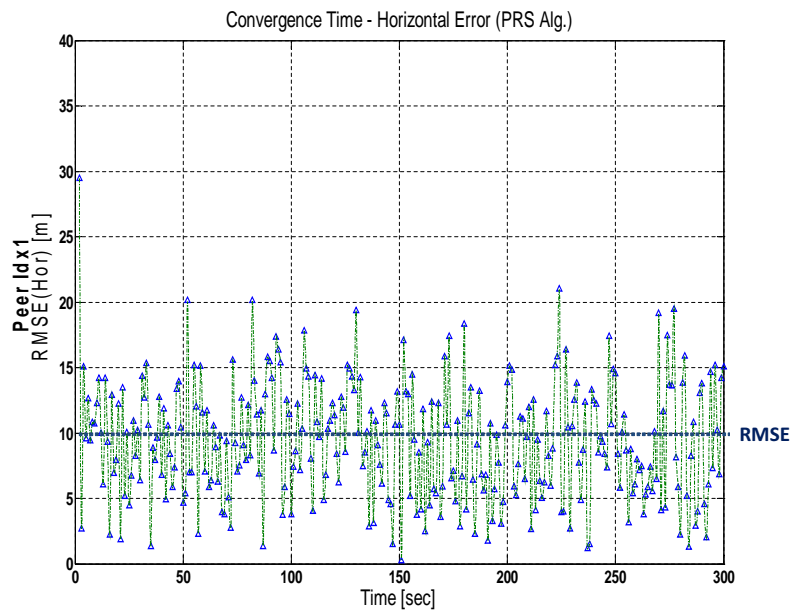
Figure 2.6: Unknown Peer horizontal errors
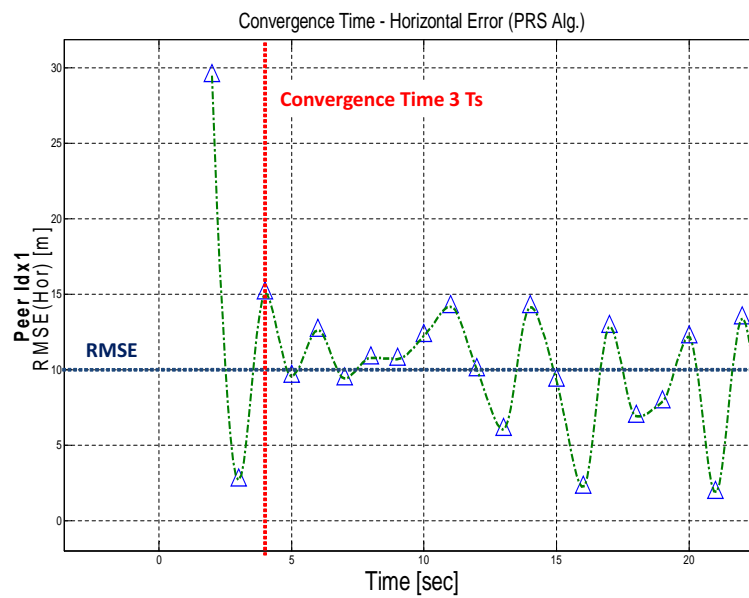
Figure 2.7: Unknown Peer horizontal errors: convergence time at the third step

Figure 2.8 presents graphically the UP horizontal error trend. The figure is made of different color blocks reporting the horizontal error at every estimation time instant: blue colors refer to small position errors, red colors refer to large errors and white zones correspond to the cases in which position calculation is not achievable due to insufficient satellite visibility.
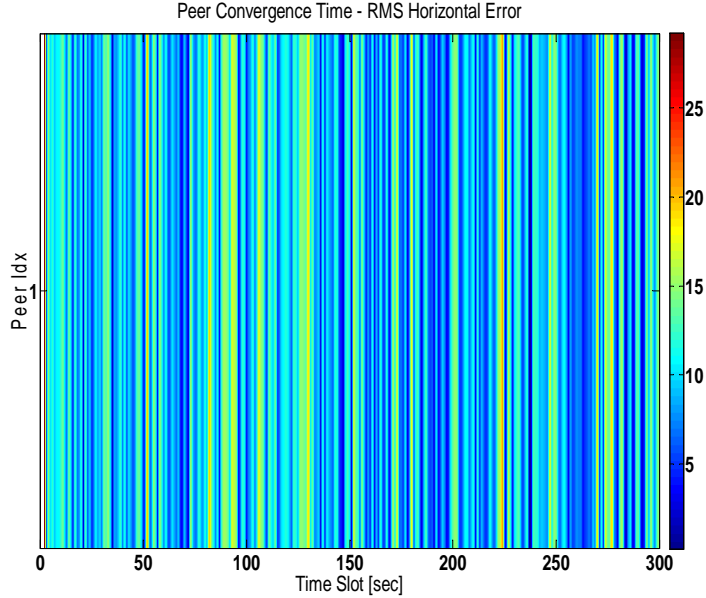
Figure 2.8: Graphical representation of Horizontal Errors trend

Table 2.1 reports the simulation results for the indoor case. The table reports the simulation identifier (Sim), the number of UPs (UP), the number of Aiding Peers (AP), the synchronization mode (Sync), the user mobility (Mobility), the number of Professional Aiding Peers (Pro), the number of simulated time instants (T_s), the initial guess for UP's position (IP) and the maximum random bias (Bias). Simulations 1 and 3 show performance without and with professional aiding peers in a static configuration. Simulations 2 and 4 show performance in a dynamic scenario, where the assisted peer moves inside the environment (random point model with a max speed equal to 2 m/sec); mobility worsens performance in term of RMSE. Finally simulation 5 shows performance degradation in term of RMSE and convergence time (CT) when the initial guess for the UP's position is the center of the Earth.

Sim	UP	AP	Mobility	Pro	T_s	IP	Bias	RMSE	CT
1	1	3	Static	0	300	Exact	150km	10.408m	3
2	1	3	Dynamic	0	300	Exact	150km	19.328m	3
3	1	3	Static	3	300	Exact	150km	6.611m	3
4	1	3	Dynamic	3	300	Exact	150km	16.653m	3
5	1	3	Dynamic	0	300	Earth Center	150km	18.711m	6

Table 2.1: Simulation results for the indoor environment

2.1.5 Outdoor Simulation Results

Figure 2.9 shows the outdoor environment and the configuration parameters used to test the the PSA. The blue point represents the user (Unknown Peer) located in street number 1, while the green points represent five aiding peers randomly distributed inside the urban environment.
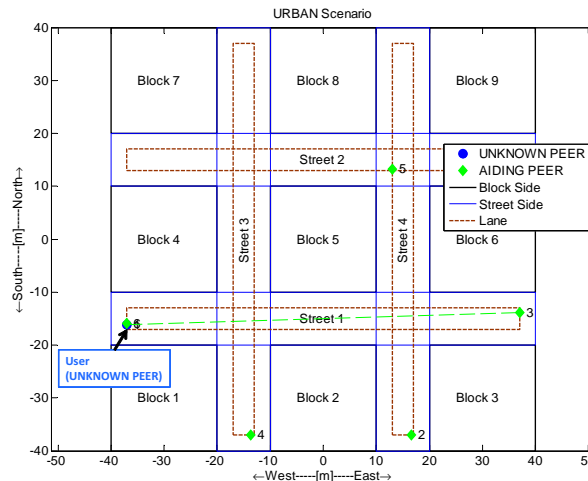
Figure 2.9: OUTDOOR

In the first simulation the Unknown Peer (UP) is a dynamic peer moving along street number 1 with a maximum speed of 2 m/sec, and all aiding peers are classified as mass market users. The exchanged information of the aiding peers arrive to the user asynchronously (Asynchronous Peers), the IP initial guess position is chosen equal to its exact position and the maximum random bias is 150 km. As in the indoor case, the following figures report the PSA performance in $300T_s$ (each T_s is equal to 1 second). Figure 2.10 shows the Horizontal CDF and reports the RMSE

after $300T_s$ that in this case is equal to 16.135 m.
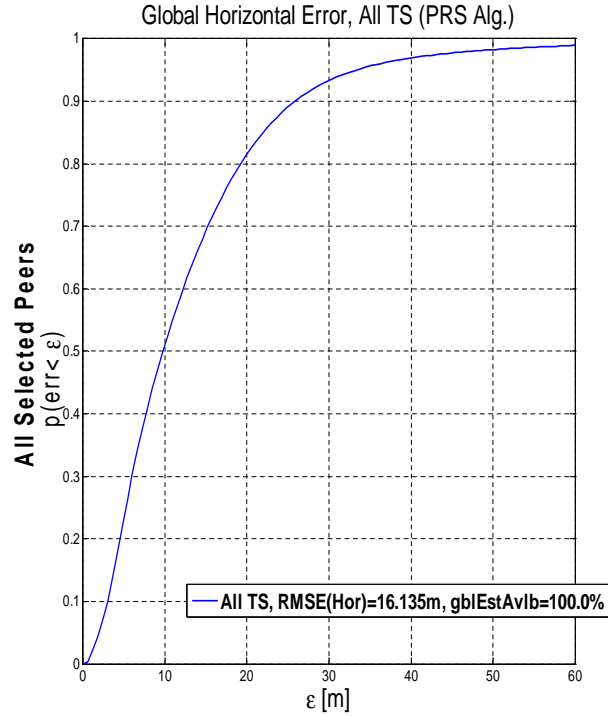
Figure 2.10: Horizontal Cumulative Distribution Function and RMSE for outdoor simulation

Figure 2.11 and Figure 2.12 show the PSA performance: the Horizontal Error stabilize around the value of 16.135 m after one step, that is the Convergence Time (CT) as shown in the magnified Figure 2.12. Convergence time is greatly reduced since the collaborating peers have a greater satellite visibility and the DOP is improved.
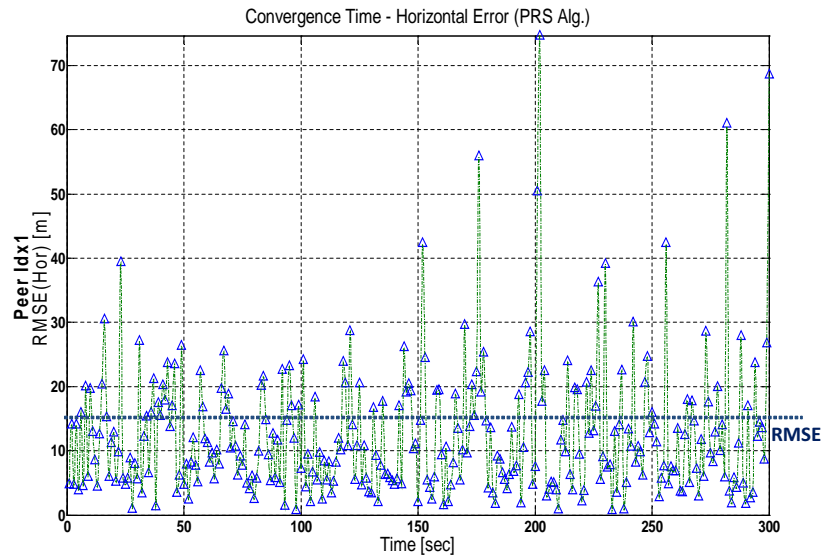
Figure 2.11: Horizontal Errors of Unknown Peer calculated position
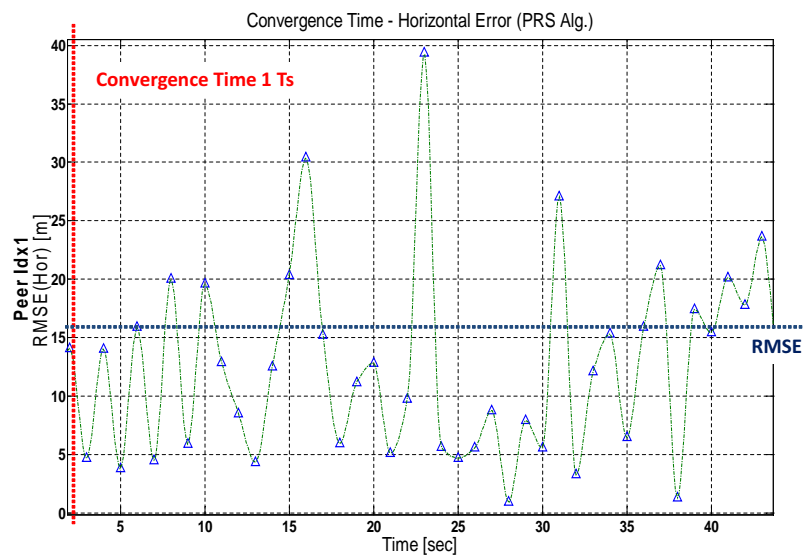
Figure 2.12: Horizontal Errors of Unknown Peer calculated position: convergence time at the first step

Figure 2.13 presents graphically the UP horizontal error trend. The figure is made of different color blocks reporting the horizontal error at every estimation time instant: blue colors refer to small position errors, red colors refer to large errors and white zones correspond to the cases in which position calculation is not achievable due to insufficient satellite visibility. Figures 2.11 and 2.13 show in particular how in outdoor environments the horizontal error is more unstable than in the indoor case due to the larger distances between the peers and because the integration phase is interrupted when the UP is able to perform autonomous positioning: this fact causes more instability inside matrices of the Kalman filter that must be often re-initialized.
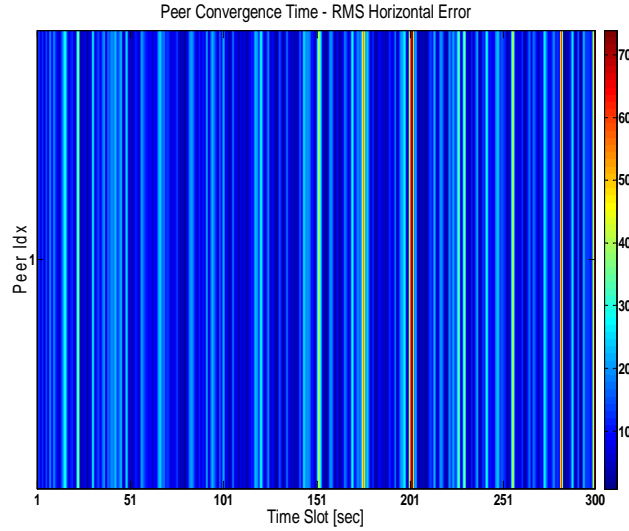
Figure 2.13: Graphical representation of Horizontal Errors trend

Table 2.2 reports the simulation results for the outdoor case. In the table we report different simulations (Sim), the number of Unknown Peers (UP), the number of Aiding Peers (AP), user mobility (Mobility), the number of Professional Aiding Peers (Pro), the number of simulated time steps (T_s), the initial UP position guess (IP) and the maximum random bias (Bias). In simulation 1 and 2 performance in terms of RMSE are comparable with and without professional aiding peers. This is because all aiding peers send their pseudorange without any correction dependent on their position and error correction capabilities, moreover all aiding is weighted the same in the Kalman filter. Simulation 3 has a longer convergence time with respect time simulation 1 and 2 since the initial position guess is the center of the Earth.

Sim	UP	AP	Mobility	Pro	T_s	IP	Bias	RMSE	CT
1	1	5	Dynamic	0	300	Exact	150km	16.135m	1
2	1	5	Dynamic	5	300	Exact	150km	15.050m	1
3	1	5	Dynamic	0	300	Earth Center	150km	16.240m	3

Table 2.2: Simulation results for the outdoor environment

The use of P2P algorithms can be instrumental for improving position solution availability. In particular the exchange of aiding information through the PSA algorithm can allow to obtain coarse positioning even in the cases where the user has scarce satellite visibility like in deep-indoor or urban scenarios.

2.2 Hybrid Positioning Technique

Since it is reasonable to expect that a typical P2P network will be characterized by different classes of receivers, each with its peculiar functions, the impact of the presence of professional receivers alongside mass-market devices has been considered in case of hybrid information integration. In particular the assumption that professional receivers will include multi-band signal processing has been made.

2.2.1 Professional Receivers

As known, the received signal power in GNSS applications is extremely weak due to the very long propagation distance, thus correct detection is susceptible to strong interfering signals. The first advantage in having frequency diversity is the enhanced robustness against jamming attempts since if the detection of the signal on one band is hindered by an interferer the receiver can switch to the other unencumbered band or, alternatively, information can be exchanged between the different bands. Other specific advantages on operating over multiple bands rely on the possibility of exploiting the different chip rates and thus the potential for increased tracking accuracy using signals with an higher chip rate, greatly improving the overall positioning performance and enabling high precision applications. Furthermore, multi-frequency receivers can provide autonomous ionospheric delay estimation and thus be able to remove almost completely one of the most significant error sources in positioning [18].

Propagation through the Ionosphere, in fact, influences electromagnetic wave propagation due to the presence of ionized gas molecules that release free electrons. The electron density along the path length, referred to as the total electron count

(TEC), is a space-time varying parameter expressed in units (TECU - TEC Units) of electrons/m^2 and depends on various factors (e.g. time of day, user location, satellite elevation angle, etc.) [29]. The delay induced by the group refractive index (group delay) and phase refractive index (phase advance), based on the first order model and expressed in meters, can be respectively written as:

$$\Delta S_{iono,g} = \frac{40.3TEC}{f^2} \quad [m] \tag{2.4}$$

$$\Delta S_{iono,p} = -\frac{40.3TEC}{f^2} \quad [m] \tag{2.5}$$

In professional receivers the ionospheric additional delay can be estimated by measuring the corresponding delay of the electromagnetic waves at multiple frequencies and exploiting the Ionosphere dispersive nature [18]. In particular, if the high-end receiver operates in the Galileo OS bands E1 and E5, the pseudo-ranges can be written as:

$$\rho_{E1} = c(T_u - T_s) + c(\delta t^u - \delta t^s + \delta t_{D-E1}) = Range + c(\delta t^u - \delta t^s + \delta t_D) \tag{2.6}$$

$$\rho_{E5} = c(T_u - T_s) + c(\delta t^u - \delta t^s + \delta t_{D-E5}) = Range + c(\delta t^u - \delta t^s + \delta t_D) \tag{2.7}$$

where δt_D is the total time offset due to ionospheric effects δt_{iono}, tropospheric effects δt_{tropo}, multipath δt_{MP}, receiver hardware offsets δt_{hw} and receiver noise δt_{NOISE}.

In the ideal case, all errors sources except the ionospheric can be neglected and δt_D become equal to $\delta t_{iono} = \frac{\Delta S_{iono,g}}{c}[sec]$

$$\rho_{E1} \cong Range + c(\delta t_{iono}^{E1}) \tag{2.8}$$

$$\rho_{E5} \cong Range + c(\delta t_{iono}^{E5}) \tag{2.9}$$

In the absence of measurement errors, the traditional approach for range estimation allows professional dual band receivers to remove almost all of the ionospheric effect by making two different ranging measurements on two different frequencies. Combining pseudo-range ρ_{E1} and ρ_{E5} made on both $E1$ and $E5$ enables the estimation of both the $E1$ and $E5$ delays. The path length difference on the $E1$ signal can be estimated using the following expression:

$$\Delta S_{I,Cor}^{E1} = \left(\frac{f_{E5}^2}{f_{E5}^2 - f_{E1}^2}\right)(\rho_{E1} - \rho_{E5}) \tag{2.10}$$

And for the $E5$ signal:

$$\Delta S_{I,Cor}^{E5} = \left(\frac{f_{E1}^2}{f_{E5}^2 - f_{E1}^2}\right)(\rho_{E1} - \rho_{E5}) \tag{2.11}$$

By subtracting these estimated corrections $\Delta S_{I,Cor}^{E1}$ and $\Delta S_{I,Cor}^{E5}$ from the pseudo-range measurements made on each band ρ_{E1} and ρ_{E5}, as shown in 2.12 and 2.13, the position accuracy improves considerably.

$$\rho_{E1}^{iF} = Range + c(\delta t_{iono}^{E1} - \Delta S_{I,Cor}^{E1}) \tag{2.12}$$

$$\rho_{E5}^{iF} = Range + c(\delta t_{iono}^{E5} - \Delta S_{I,Cor}^{E5}) \tag{2.13}$$

Some residual errors are usually still present in the Iono-Free Pseudoranges 2.12 and 2.13, because 2.10 and 2.11 are estimated quantities but nevertheless by correcting the ionospheric delay the quality of the measurements is greatly enhanced.

It is worthwhile noting that, in realistic scenarios the presence of measurement errors (i.e. incomplete multipath mitigation) can further affect the accuracy of the corrected range estimation. In these cases the traditional approach may not provide the best performance, thereby different dual-frequency ionospheric correction methods should be considered to minimize the estimation error as in [29].

Therefore, it is clear that although professional multi-frequency receivers require a considerable complexity increase both in the front end and in the digital baseband processing blocks, the achievable improvements are compelling. Moreover, as P2P networks are based on the cooperation between different kind of users (high-end and mass-market), accuracy and robustness is the key parameters, and the presence of high-end receivers may be fundamental in improving positioning accuracy of the network.

2.2.2 Algorithm Parameters

As in 2.1.1, several parameters have been considered to analyze the behaviour of the algorithm. The algorithm paremeters are reported in the following:

- **System model matrices:** Depending on the knowledge of the initial user position, the initial estimate covariance matrix, P, and the model reliability matrix, Q, can be set differently. In particular the bigger the uncertainty on the initial position, the bigger should be the covariance values in the P matrix.

- **Measurement model matrix:** Differently from the PSA, additional ranging information is provided by means of terrestrial ranging techniques implying the use of a hybrid set of equations where the peers can be considered as pseudo-satellites. In this context, the presence of professional peers, that have more accurate knowledge of their position, is beneficial to the solution of the navigation equations. The measurements provided to the estimation filter are in this case either the direct pseudorange measurements, calculated by the user itself, or additional terrestrial ranging information coming from neighboring peer. In order to be able to discriminate between mass-market and professional receivers, the noisiness of the available measurements are modeled as additional Gaussian noise with a given standard deviation σ_{UERE}. The standard deviation is here computed as a function of the different error contributions as in 1.3.1. The additional ranging information must be weighted properly by taking into account both peer position uncertainty and ranging errors.

Given that (x_k, y_k, z_k) are the receiver coordinates and $(x_k^{pi}, y_k^{pi}, z_k^{pi})$ the i-th peer coordinates, the observation vector is in this case:

$$\mathbf{z}_k = [\rho_{D_k}, \mathbf{r}_k] \tag{2.14}$$

with $\mathbf{r}_k$ representing the terrestrial ranges between peers:

$$\mathbf{r}_k = \sqrt{(x_k^{pi} - x_k)^2 + (y_k^{pi} - y_k)^2 + (z_k^{pi} - z_k)^2} + n_k \tag{2.15}$$

Eventual clock misalignments between the peers can be dealt with considering round-trip measurements.
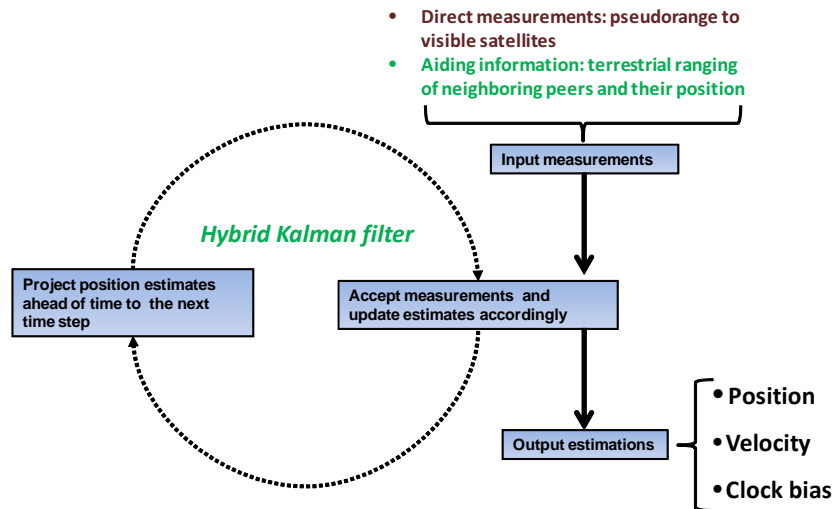
Figure 2.14: Hybrid data Fusing Algorithm

2.2.3 Simulation Environments

The hybrid positioning algorithm is evaluated in different scenarios where the user receives less than the required number of satellites, thus depending on aiding information to obtain the position solution.

In the following the options/parameters considered during the simulations are presented:

- **Receiver type:** the P2P network is comprised of both mass-market and professional receivers. The two types of users differ from one another in the quality of the available measurements.

- **Scenario Environment:** the wanted user has direct visibility of only three satellites, and is thus unable to compute its position in a standalone fashion. For the hybrid case the possible exchange protocols for the terrestrial link should be designed to best suit the application scenario: Ultra Wide Band (UWB) seems to be an excellent choice for the indoor pedestrian case, while the 802.11p Wireless Access for Vehicular Environments (WAVE) is best suited for the outdoor vehicular one. For the simulations we have considered an error standard deviations on the terrestrial ranging information equal to σ_t=0.3 m. All pseudorange measurements are considered independently affected by an error that can be modeled as a Gaussian random variable with zero mean and a standard deviation σ_{UERE}. In the total error budget σ_{UERE}, the ionospheric

Parameter	Value
Receiver type	Mass-market/Professional
Ionospheric pseudorange error std	5/0.1 m
Other pseudorange errors std	3 m

Table 2.3: standard deviation σ_{UERE} of Mass Market and Professional receivers

contribution assumes for the two kinds of receivers the values reported in table 2.3.

- **Number of aiding peers:** increasing numbers of aiding peers allow, especially in the outdoor scenario, to provide aiding when needed.

2.2.4   Simulation Results

Simulation results on the P2P algorithms as well as the impact of professional receivers on PVT calculation are carried out. All figures show the obtained position estimates in the X-Y plane centered in the real user position.

Four different scenarios, varying depending on the number and type of aiding peers have been considered:

- Scenario 1: one mass-market aiding peer;

- Scenario 2: one professional aiding peer;

- Scenario 3: three mass-market aiding peers;

- Scenario 4: three professional aiding peers.
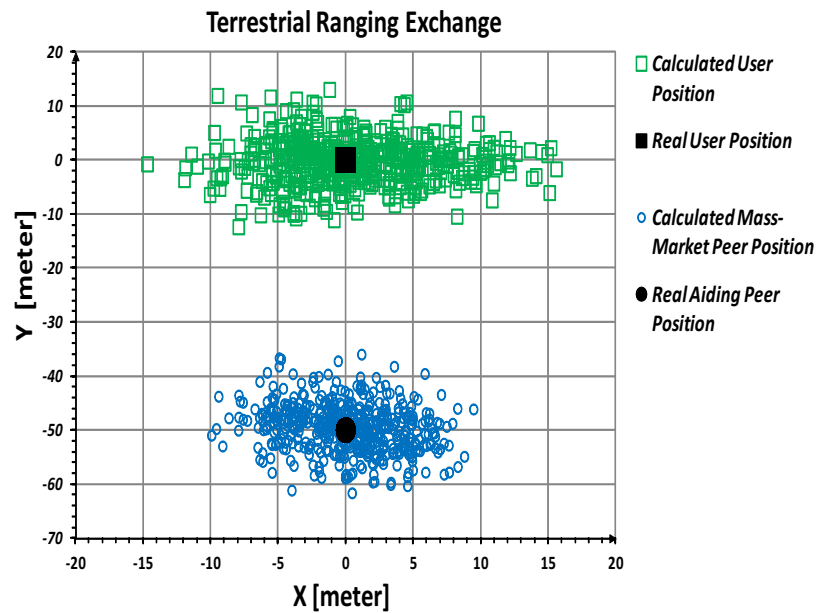
Figure 2.15: Position estimation obtained with the Hybrid technique in Scenario 1
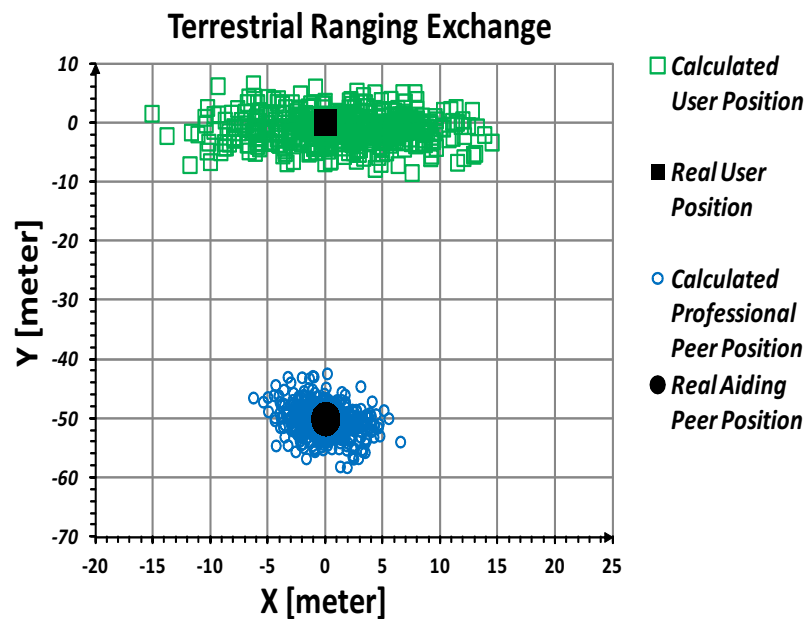
Figure 2.16: Position estimation obtained with the Hybrid technique in Scenario 2
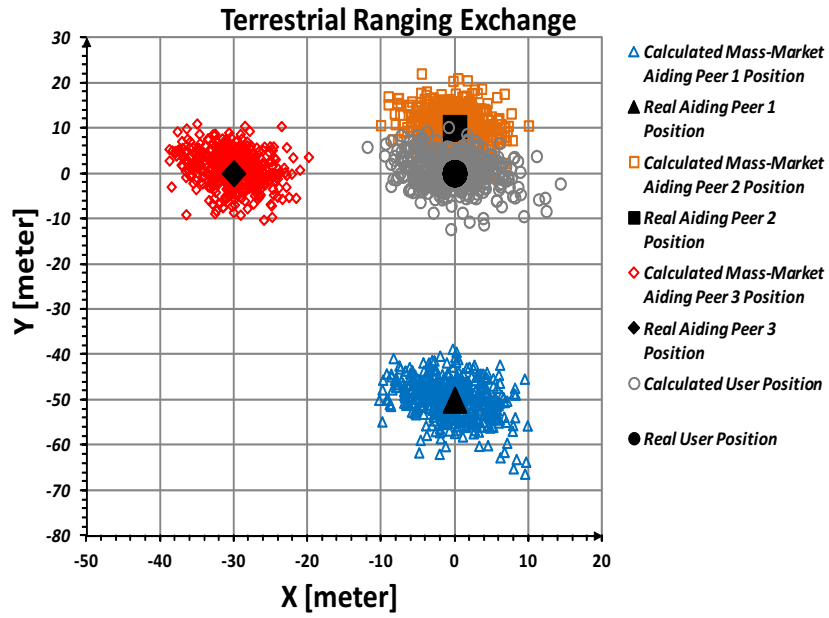
Figure 2.17: Position estimation obtained with the Hybrid technique in Scenario 3
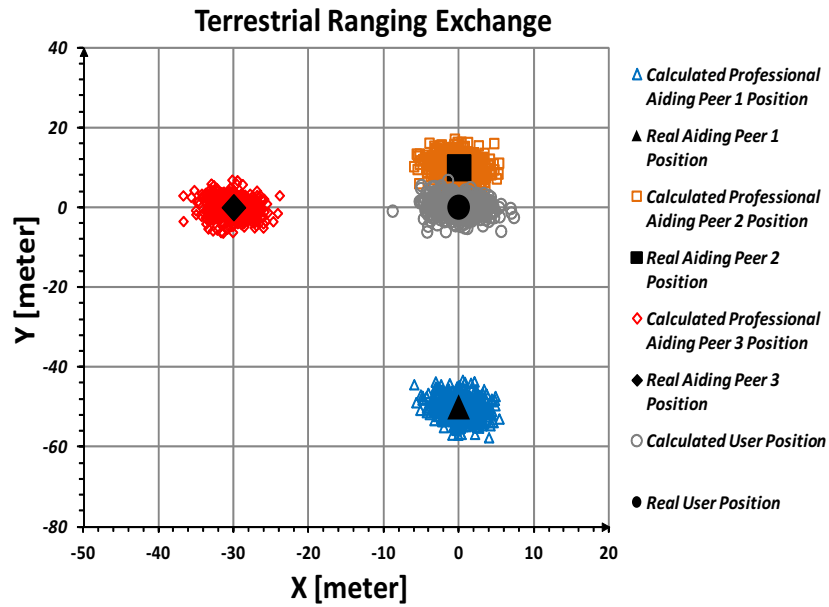
Figure 2.18: Position estimation obtained with the Hybrid technique in Scenario 4

Scenario	$E[e_X]$ [m]	$E[e_Y][m]$	σ_{e_X} [m]	σ_{e_Y} [m]
1	1.3	-0.8	6.3	4.3
2	0.8	-0.8	5.8	2.5
3	-0.2	0.5	4.0	3.5
4	-0.1	0.3	2.3	2.3

Table 2.4: Position estimation performance of positioning based on the Hybrid technique: mean error and standard deviation in the X and Y directions

Figure 2.15, 2.16, 2.17, 2.18 show the results obtained by fusing together direct pseudorange measurements and terrestrial assistance information. It is quite clear that when aiding is provided by professional peer the standard deviation of the position estimations decreases considerably; this is also highlighted by the numerical results reported in table 2.4. The greater impact on user accuracy is given by the presence of professional receivers in the network. Any further development of this study will allow to better define the algorithm and network requirements. In this case, position estimations are closely concentrated around the real user position.

Part II

Physical Level Aiding Techniques

GNSS operations at the physical layer are responsible for estimating the satellite signal parameters and ultimately for computing pseudo-range distances, and demodulating the navigation data. They are the basic operation of a GNSS receiver, and being directly related to the Time To First Fix (TTFF), their behaviour drives the overall performance and impacts on the time needed by the receiver to provide the PVT solution to the user.

Parameter estimation is usually accomplished by synchronizing a locally generated replica with the received signal, in order to determine the transmission delay, carrier frequency and phase. Given the great initial uncertainty on the signal parameters and the very low SNR at the receiver due to the Spread Spectrum (SS) modulation, synchronization cannot be achieved in a single operation. Usually two steps are performed in cascade: acquisition and tracking.

Acquisition is typically the most critical operation to be performed as it is in charge of exploring the entire joint code, timing and frequency domain uncertainty regions in order to identify the code epoch and frequency offsets of a specific satellite signal. To reduce complexity, the uncertainty region is generally discretized in time cells and frequency bins, transforming the epoch estimation problem in a detection problem. Understandably, acquisition requires time consuming operations to identify the correct parameter estimation that may need to be repeated due to the very low SNR values of the received signals. Different search strategies can be envisaged and decision criterion applied depeding on the required complexity and performance.

On the other hand, the tracking phase is responsible of detecting eventual erroneous synchronization events and refining the acquisition estimates to guarantee continuous lock between local replica and received signal. Both carrier and code tracking need to be performed concurrently for correct receiver function: the code tracking process is in fact necessary for pseudorange estimation while the carrier tracking process has to estimate either the frequency or the phase of the carrier wave for correct Doppler offset removal. Tracking is usually performed through closed loop architectures that update constantly the local replica according to feedback information. Generally a Delay Lock Loop (DLL) is employed for code tracking and either a Frequency Lock Loop (FLL) or a Phase Lock Loop (PLL) is used for carrier tracking.

In the following the problem of code acquisition, and code tracking will be tackled and novel aiding techniques operating at the physical layer presented and discussed.

Chapter 3

Code Acquisition Techniques

3.1 The Code Acquisition Problem

The purpose of acquisition is to identify which are the satellites visible to the user and roughly estimate the code epoch and possible frequency offset of each received satellite signal, estimation is thus performed over a three-dimensional uncertainty region. Of course, such a complex problem cannot be handled as a whole, but has to be split in smaller problems. For each possible Pseudo Random Noise (PRN) code identifying a satellite, a twofold discretization process is normally adopted: the time Uncertainty Region (UR) is discretized into time slots, and the frequency domain is discretized into frequency bins [18]. The acquisition search space can thus be seen as a bi-dimensional matrix that must be entirely scanned by the receiver to perform acquisition tests.

A test cell is defined as the combination of a time slot and a frequency bin, each one corresponding to a decision hypothesis, as shown in Figure 3.1. Identifying as hypothesis H_1 the correct test cells (i.e. those cells corresponding to a residual code epoch offset within the pull-in range of the subsequent tracking circuits), and all incorrect cells as hypotheses H_0, the code acquisition engine has the goal to decide, according to a certain decision criterion, in favor of a true H_1 hypothesis (correct detection), while discarding all incorrect H_0 cells (correct rejection), trying to avoid missed detection and false alarm events, which correspond respectively to discarding H_1 cells or selecting H_0 cells as being correct [30]. It is worthwhile repeating that, due to discretization, correct H_1 detection does not resolve completely the problem of code epoch identification. The residual time uncertainty, generally in the order of one chip interval, has to be later refined in the tracking stage.

The typical approach adopted to perform code acquisition in SS systems, is derived from the Maximum Likelihood (ML) criterion and consists in evaluating the correlation of the received signal with a locally generated replica of the desired sequence, in order to identify the correlation peak that corresponds to the H_1 hypothesis. As a result, to explore the entire bi-dimensional UR, a large number of correlations have to be computed, which often becomes a very demanding task for the receiver in terms of computational load and power consumption.
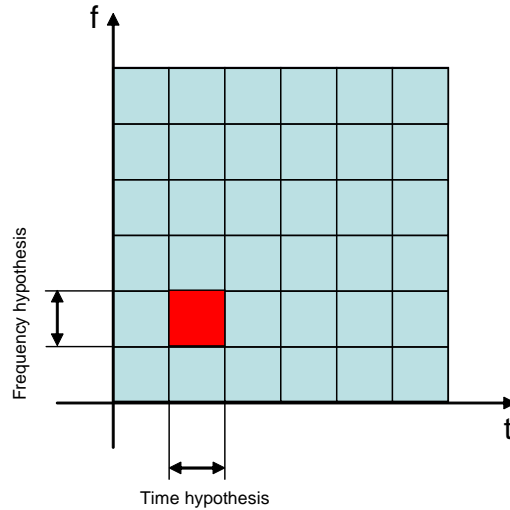
Figure 3.1: Uncertainty region discretization in time and frequency domains

To scan the entire UR, different acquisition strategies can be adopted, more specifically the serial and the parallel search [31]. With the former approach the input signal is multiplied with different PRN code sequences each with a specific code phase, as shown in figure 3.2. However, with this configuration, to improve TTFF parallel branches have to be implemented.
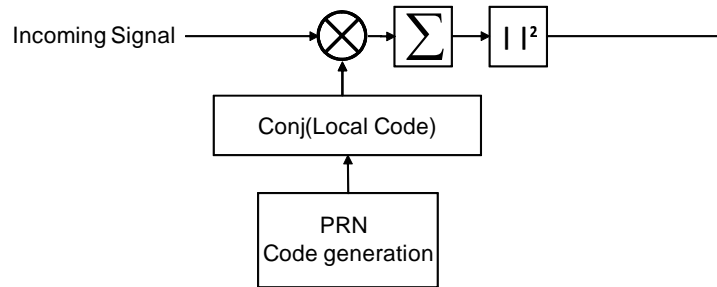
Figure 3.2: Block diagram of the serial code phase search algorithm

Alternatively, in the parallel scheme, the circular cross correlation between the input and the PRN sequence is computed to test all code phases at once [13].

A very efficient way to perform circular correlation is to use the Fast Fourier Transform (FFT) approach. Figure 3.3 reports the blocks comprising a FFT/IFFT search scheme, where the Fourier transform of the input is multiplied with the Fourier transform of the local PRN code. The result of this multiplication is then transformed into the time domain by an Inverse Fast Fourier Transform (IFFT). The correlation between the input and the PRN code is computed as the absolute value of the output obtained through the IFFT.
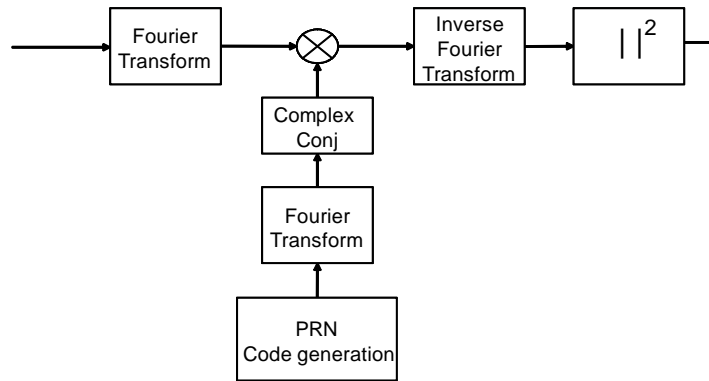
Figure 3.3: Block diagram of the parallel code phase search algorithm

Compared with serial search acquisition methods, the parallel approach allows to reduce the number of parallel branches to be implemented and to compute the Fourier transform of the generated PRN code only once for testing all code phases, but at the price of added complexity.

The choice between the two strategies must thus consider the trade-off between allowed receiver complexity and performance in terms of TTFF. When the UR extension in the time domain is medium to large the FFT/IFFT strategy seems to represent the better choice, whereas different trade-offs can be identified for limited UR time extensions, for which the overhead introduced by the FFT computation can become much larger than the direct computation of correlations.

Independently of the method adopted to evaluate the correlation, the selection of the correct hypothesis can in general be performed by selecting the largest correlation in the UR (MAX criterion) or comparing the correlation outputs with a threshold (Threshold Crossing (TC) criterion) [30], or even the MAX/TC hybrid option [32]. The TC criterion compares the decision variable of each cell with a

threshold and declares acquisition in correspondence of a threshold crossing event. The threshold is set in order to guarantee a Constant False Alarm Rate (CFAR) and must thus adapt to the SNR and to the channel fading statistics. Alternatively, it is possible to obtain TC acquisition strategies independent on channel conditions and multipath affecting the received signal, but using as decision variables the ratio between correlation output local maxima [33]. The MAX criterion acts after having scanned the entire UR, and therefore can be well combined with the FFT/IFFT search strategy. However, the MAX criterion implicitly assumes that the correct hypothesis H_1 is present in the UR and this is not necessarily true in GNSS because, during the very initial stage of operation, the receiver can be unaware of which satellites are in its visibility scope; thus, a verification of the MAX decision becomes necessary. As an alternative to the pure MAX criterion, it is possible to insert the TC criterion by comparing the maximum decision variable with a decision threshold. In general, the best design choice for the decision criterion depends on several factors that need to be considered altogether.

It is worthwhile noting that, while a single FFT/IFFT computation allows for the direct exploration of the entire time dimension of the UR, the uncertainty in the frequency domain must be tackled via a further scan, which can be performed in parallel, but is often too demanding, or via a sequential approach, e.g. reusing the same FFT/IFFT with circular rotations in the frequency domain.

3.2   Aiding Techniques

Limitations of stand-alone GNSS receivers performance are mainly due to the large search space and very low SNR values, that cause acquisition schemes to require a great amount of resource-consuming operations, which may need to be repeated several times to get correct synchronization. To limit complexity and improve receiver performance in terms TTFF, assistance techniques become thus essential. It is worthwhile noting that the TTFF of a navigation receiver is comprised of many contributes, but the most impacting ones are the the time needed to get the navigation data and the time required by acquisition to provide coarse estimations.

To speed-up operations it becomes thus important to reduce the size of the search space during acquisition and to this aim different aiding schemes can be envisaged.

One available technique is the Assisted-GNSS (AGNSS) scheme that allows to speed up inial operations by employing base station broadcasted information to all

the users in their coverage area [34]. This assistance data can then be used to limit the number of tested PRN codes, by sharing almanac information, and reduce the time-frequency search domain, thanks to the pre-computation of the Doppler of each visible satellites.

On the other hand, the diffusion of GNSS users, and the distribution of hybrid navigation-communication (NAV-COM) devices, have laid the foundations for developing innovative cooperation schemes based on the concept of Peer-to-Peer (P2P) cooperation. In [35–38], cooperative techniques operating at physical level with peers sharing primary code time reference, Doppler shift, secondary code and C/N_0 information are presented.

Other configurations, relying on the availability of multi-band receivers, can also provide grounds for research in novel aiding techniques.

My contribution to this topic lies in the design of a fast code acquisition scheme for dual-band GNSS receivers. This novel procedure defined Cross-Band Aiding (CBA) is built on information exchanged between the code acquisition blocks acting in different bands, achieving mutual assistance in code synchronization. In the following the motivation, description and analytical performance evaluation of the proposed aiding schemes are reported.

3.3   Cross-Band Aiding Code Acquisition

The underlying principle of the CBA acquisition technique for dual-band receivers is that the navigation signals in the two bands are transmitted using a common time reference, therefore, it is possible to exploit the reference provided by the synchronization process in a band to reduce the extent of the UR time dimension in the other band, performing the acquisition procedures in the two bands sequentially. Although the signals undergo slightly different propagation conditions and the chip rate and code length are different; information can still be exchanged in order to mutually reduce uncertainty regions, resolve epoch ambiguity, and verify the correctness of decisions taken by the parallel device in the different bands.

The feasibility of this technique stems from the introduction by both the Galileo system and the modernized GPS of multiple band Open Service (OS) signals, more specifically E1 and E5 in Galileo and L1 and L2 starting from in the modernized GPS, that will allow also mass-market and commercial receivers to enjoy the benefits provided by band diversity.

In the following the CBA technique is applied to the fast acquistion of E1 and E5 OS signals, where the pseudo-noise DS-SS (Direct-Sequence Spread-Spectrum) code periods in the two bands can be related according to a specific rule in the time domain. However, it is worthwhile noting that this technique can be generalized to cover the case of N band code acquisition, with $N > 2$.

3.3.1 Galileo Open Service Signals

The main innovation in the signals of the Galileo system is the introduction of the Binary Offset Carrier (BOC) modulation that shifts the signal power from the band center reducing the interference with coexisting systems.

A BOC modulated signal is obtained through the spreading of the input signal with a square wave subcarrier that has a frequency multiple of the chip rate [39]. It is denoted as $\mathrm{BOC}(f_{sc}, f_c)$, where f_{sc} and f_c are the subcarrier frequency and the chip rate, respectively, related by the equation $f_c = \frac{1}{T_c} = \frac{2}{n} f_{sc} = \frac{1}{nT_{sc}}$, where n is the number of subcarrier half periods T_{sc}, in a chip period T_c ($T_c = nT_{sc}$). In the GNSS context, a BOC modulated signal is often indicated as $\mathrm{BOC}(\alpha,\beta)$, where $\alpha = f_{sc}/1.023$ MHz and $\beta = f_c/1.023$ MHz. By setting the f_{sc} and f_c frequencies it is possible to concentrate the signal power in specific parts of the spectrum, in particular the product is a split spectrum that is shifted from the central frequency by an amount equal to the sub-carrier frequency f_{sc} [13].

The waveform can be expressed as

$$p_{\mathrm{BOC}}(t) = \mathrm{rect}_{T_c}(t) \, \mathrm{sign}\left[\sin(2\pi f_{sc} t)\right] \tag{3.1}$$

Analogously, a BOCc (Binary Offset Carrier Cosine) can be described by the following waveform

$$p_{\mathrm{BOCc}}(t) = \mathrm{rect}_{T_c}(t) \, \mathrm{sign}\left[\cos(2\pi f_{sc} t)\right] \tag{3.2}$$

Alternatively the BOC-modulated signals can be described as in [40], where a generalized family denoted double-BOC (DBOC) modulation is introduced to provide an unified framework for analyzing the properties of both GPS and Galileo signals in terms of Power Spectral Density (PSD) and Auto-Correlation Function (ACF).

3.3.1.1 The Galileo E1 Signal

The E1 band contains three channels that are transmitted at the same carrier frequency (1575.42 MHz). The A channel contains encrypted data for Public Regulated

Service (PRS), and will thus not be considered in the following, while the B and C channels contain the OS navigation data and the pilot code, respectively. In particular B and C are described by the Composite BOC (CBOC) modulation [41]. Nevertheless, in the following, the BOC(1,1) modulation has been considered instead of CBOC, since it represent a very good approximation with the advantage of being easily treatable.

E1 OS signals have a 4092 code length with a $f_{c-E1} = 1.023$ [Mcps] chipping rate giving it a duration of 4ms. E1 B and C channels are thus modulated through the BOC(1,1) with subcarrier frequency $f_{sc-E1} = 1.023$ [MHz]. The BOC(1,1) component can be considered as part of the spreading code, but it is also viable to consider it part of the carrier in the acquisition phase and remove it prior to the correlation [13]. The Galileo E1 OS can be defined as:

$$e_{E1_B}(t) = \sum_{i=-\infty}^{+\infty} c_{B,|i|_N} d_{\lfloor i \rfloor_N} \text{rect}_{T_c}(t - iT_c) sc_{E1_B} \tag{3.3}$$

$$e_{E1_C}(t) = \sum_{i=-\infty}^{+\infty} c_{C,|i|_N} \text{rect}_{T_c}(t - iT_c) sc_{E1_C} \tag{3.4}$$

where $sc_{E1_B} = \text{sign}\left[\sin(2\pi f_{sc-E1}t)\right]$, $sc_{E1_C} = \text{sign}\left[\sin(2\pi f_{sc-E1}t)\right]$ and $\lfloor a \rfloor_b$ indicates the integer part of a/b, $|a|_b$ is the a module b operation, $c_{B,i}$ and $c_{C,i}$ are the ith chip of the spreading code of channel B and C, respectively, d_i are the data symbols to transmit the navigation message, N is the spreading factor equal to the code length (4092), T_c is the chip period equal to 977.51 ns, and $\text{rect}_T(t)$ is the rectangular pulse shape function over the time period T [41].

The complete s_{E1} signal id defined as:

$$s_{E1}(t) = \frac{1}{\sqrt{2}}(e_{E1_B}(t) - e_{E1_C}(t)) \tag{3.5}$$

The autocorrelation function of BOC(1,1) modulation is shown in Figure 3.4(a). It can be seen that even limited timing misalignments introduce an attenuation on the useful signal that go up to a null corresponding to $\frac{T_c}{3}$. It is also important to note that the presence of side peaks can create problems during the tracking phases requiring to verify is the lock is achieved on the main peak. The BOC(1,1) PSD is shown in 3.4(b).
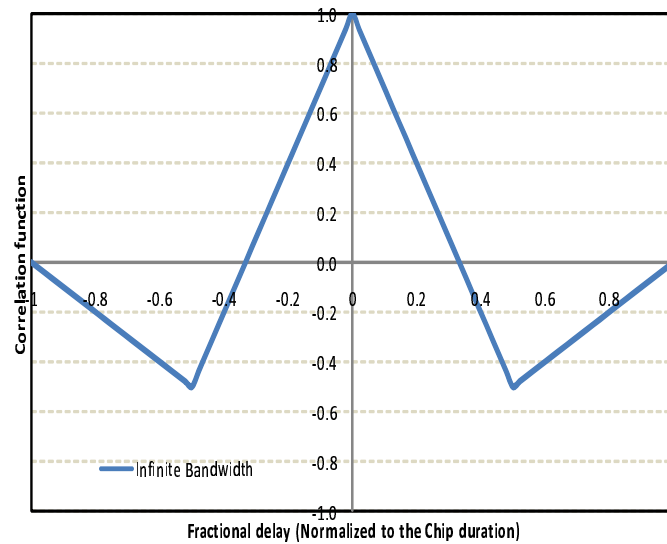
(a) BOC autocorrelation function
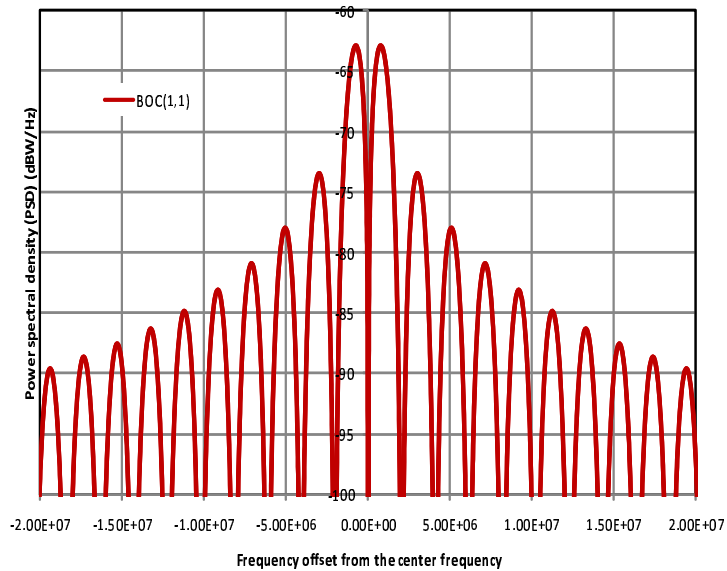
(b) E1 Signal Spectrum

Figure 3.4: E1 OS signal characteristics

3.3.1.2 The Galileo E5 Signal

The wide-band Galileo E5 signal employs a special modulation known as constant envelope Alternate Binary Offset Carrier (AltBOC). In particular, the E5 signal is characterized by the AltBOC(15,10) modulation, with side-band subcarriers of rate $f_{sc-E5} = 15.345$ [MHz] and a spreading code of length 10230 with chipping rate equal to $f_{c-E5} = 10.230$ [Mcps], consequently a duration of 1 ms. The entire E5 signal can be defined according to the expression in equation 3.6, where the spreading code components are e_{E5a-I}, e_{E5a-Q}, e_{E5b-I} and e_{E5b-Q}.

The in-phase components $E5_{aI}$ and $E5_{bI}$ carry the data modulation while the quadrature components $E5_{aQ}$ and $E5_{bQ}$ are pilot signals. The sub-carrier waveforms are chosen so as to obtain a constant envelope at the transmitter.

$$
\begin{aligned}
s_{E5}(t) = & \frac{1}{2\sqrt{2}} (e_{E5a\_I}(t) + j e_{E5a\_Q}(t)) \cdot [SC_{E5-S}(t) - jSC_{E5-S}(t - \frac{T_S}{4})] \\
& + \frac{1}{2\sqrt{2}} (e_{E5b\_I}(t) + j e_{E5b\_Q}(t)) \cdot [SC_{E5-S}(t) + jSC_{E5-S}(t - \frac{T_S}{4})] \\
& + \frac{1}{2\sqrt{2}} (\overline{e}_{E5a\_I}(t) + j\overline{e}_{E5a\_Q}(t)) \cdot [SC_{E5-P}(t) - jSC_{E5-P}(t - \frac{T_S}{4})] \\
& + \frac{1}{2\sqrt{2}} (\overline{e}_{E5b\_I}(t) + j\overline{e}_{E5q\_Q}(t)) \cdot [SC_{E5-P}(t) + jSC_{E5-P}(t - \frac{T_S}{4})]
\end{aligned}
\tag{3.6}
$$

The first two terms of Equation (3.6) represent respectively the $E5a$ and $E5b$ complex signals modulated by the complex sub-carriers. The respective dashed signal components $\overline{e}_{E5a-I}$, $\overline{e}_{E5a-Q}$, $\overline{e}_{E5b-I}$ and $\overline{e}_{E5b-Q}$ represent product signals introduced for constant envelope reasons and they do not carry useful information; however, they correspond to about 16% of the $E5$ total power.

The E5 autocorrelation function is reported in figure 3.5(a) and its spectrum, split around the central frequency (1191.795MHz), is reported in figure 3.5(b) [42].

It is worthwhile noting that processing the complete E5 signal requires a complexity increase at the receiver. More in detail, the bandwidth of $51.15MHz$ imposes a limitation on the minimum sampling frequency that results to be much higher than that required by other GNSS signals (typically 122.76MHz). Moreover, the sharp main peak in the auto correlation function requires a code search step size reduction during acquisition and a consequent increase of the number of cells to test. However, only considering the complete signal, all the signal power can be exploited at the receiver. Furthermore, the presence of side peaks in the auto correlation function poses the problem of false lock analogous to other BOC modulated signals.
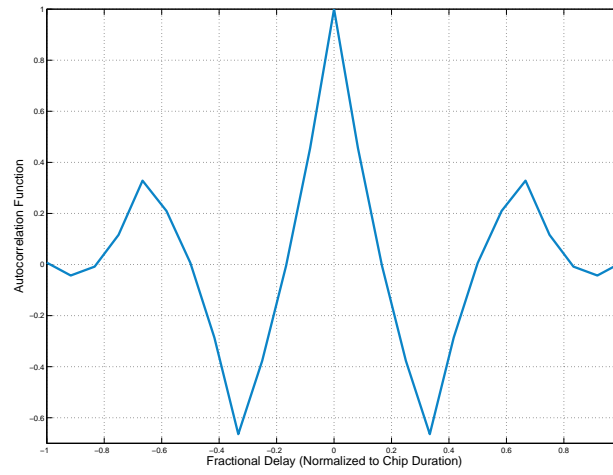
(a) AltBOC autocorrelation function
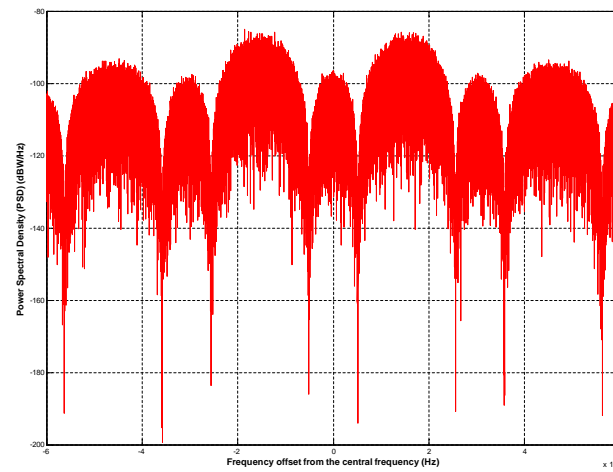
(b) E5 Signal Spectrum

Figure 3.5: E5 signal characteristics

3.3.2 Signal Timing Structures

Having reported the Galileo E1 and E5 signal main characteristics, this section will present the timing structure exploited in the CBA approach. Code acquisition is designed considering pilot channels and roughly estimating for both E1 and E5 the epoch of primary codes only, as partially reported in [1], leaving the alignment of the secondary code to a following non-critical stage.

The signal structure in the E5 band is designed to have a higher chip rate ($Rc_{E5} = 10.23$Mcps) with respect to the E1 signal ($Rc_{E1} = 1.023$Mcps), and a longer primary code length, equal to 10230, against the 4092 length of E1. As a result, there are four E5 repetitions every E1 code, and the E1 chip duration (977.51ns) is exactly ten times longer than the corresponding interval in E5 (97.75ns), as summarized in table 3.1.

Primary Code	E1	E5
Code Length	4092	10230
Chip Rate	1.023Mcps	10.23Mcps
Code Period	4ms	1ms
Chip Duration	977.51ns	97.75ns

Table 3.1: Galileo E1 and E5 main signal characteristics

Since the signals are aligned at the transmitter and the primary code durations are multiple of one another, as depicted in figure 3.6, once the code in the first band has been acquired, a time reference can be provided to the other band in order to reduce the UR extension in the time domain due to the epoch ambiguity. We denote this novel approach as Cross-Band Aided (CBA) acquisition.
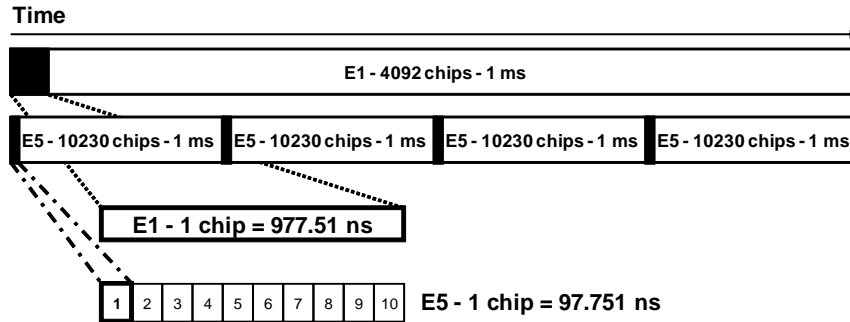
Figure 3.6: E1 and E5 signal timing structure

In order to correctly exploit the time reference between the two Galileo bands, the presence of the ionospheric delay must be accounted for.

Propagation through the ionosphere introduces in fact different delays in the two bands, delaying more signals in the lower frequencies with respect to higher frequencies. In mid-latitude ionospheric propagation condition, the high value of the Total Electron Content (TEC) parameter is in the order of 100TECu (1TECu= 1016el/m2). Considering a low satellite elevation angle (45 degrees), as described in [18], the iono-group delay corresponds to 72.5ns for the E1 band and to 126ns for the E5 band, corresponding to a relative group delay for the composite E1-E5 signal of about 53.5ns, which is smaller than the E5 chip duration. Therefore, in typical conditions the ionospheric delay difference between E1 and E5 is well within the smallest temporal unit used in our dual-band acquisition problem, i.e. the E5 chip duration. The proposed code acquisition technique is thus robust against ionospheric delay misalignments.

The information exchange is implemented here in a *Master-Slave* fashion, where the Master signal is the signal in the frequency band where code acquisition is accomplished first and is characterized by the scan of its Complete Uncertainty Region (CUR), while we identify as the Slave signal the signal in the frequency band where code acquisition is performed over a Reduced Uncertainty Region (RUR), thanks to the time reference provided by the Master signal. For the Galileo E1-E5 dual-band receiver, two alternative options might be adopted to perform CBA:

1. E1-E5 CBA, denoting classical acquisition in E1 over the complete uncertainty region (E1-CUR), followed by acquisition over the E5 with a reduced uncertainty region (E5-RUR); in this case, the signal in E1 is the Master and the signal in E5 the Slave.

2. E5-E1 CBA, denoting classical acquisition in E5 (E5-CUR), followed by acquisition over the E1 (E1-RUR); in this case the signal in E5 is the Master and the signal in E1 the Slave.

In the first case, as reported in figure 3.7, acquisition on E5 starts as soon as acquisition in E1 is achieved. Because of the chip rate diversity in the two bands, after acquisition in E1, the code epoch of the Slave signal E5 must be searched inside a RUR of length:

$$E5_{RUR} = \frac{Rc_{E5}}{Rc_{E1}} = 10 \quad E5 \ chips \tag{3.7}$$
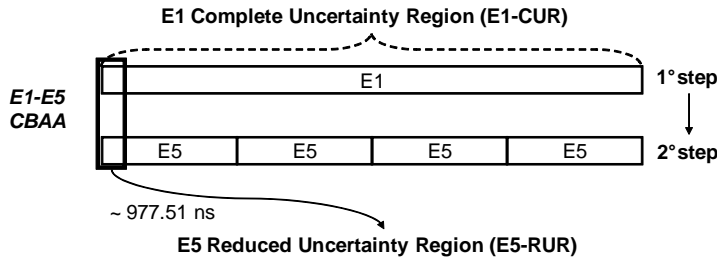
Figure 3.7: Pictorial representation of E1-E5 CBA.

Note that this reduced region corresponds to the duration of one E1 chip, i.e. 977.51ns, that is a just small fraction of the whole E5 CUR, equal to 10230 chips and corresponding to 1ms.

In the case of E5-E1 CBA, shown in figure 3.8, the problem is dual: the E5 signal is the Master signal, and, because its code duration is exactly a quarter of that in E1 (Slave signal), the only operation needed to obtain synchronization in E1 is to distinguish the start of the primary code between four macro-hypotheses due to epoch ambiguity. Note that, because of chip rate diversity a coarser resolution equal to one E1 chip duration is considered for the reduced search in E1 and the entire length of E1 RUR is:

$$E1_{RUR} = \frac{T_{code-E1}}{T_{code-E5}} = 4 \quad E1 \ chips \tag{3.8}$$

Each macro-hypothesis is separated in time by one E5 primary code, corresponding to 1ms.
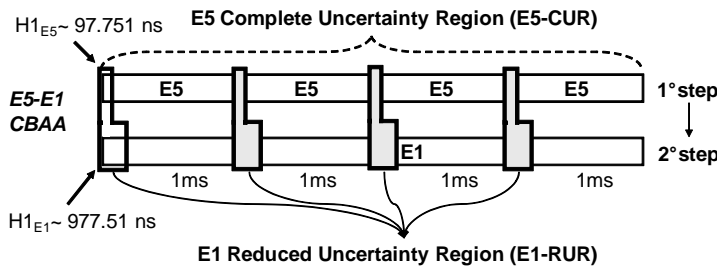
Figure 3.8: Pictorial representation of E5-E1 CBA.

The two approaches are analyzed in the following to determine which one provides the best performance/complexity trade-off.

3.3.3   Analytical mean acquisition time evaluation

As anticipated in 3.1, the selection of the correct hypothesis can be in general made through different decision criteria: namely TC [30], MAX, and MAX/TC [32]. The MAX criterion decides in favor of the cell with the largest detection variable, the decision is thus taken only after having scanned the entire uncertainty region, which can be penalizing when the correct hypothesis is well distinguishable from the misaligned cells. Alternatively, the decision could be anticipated through the use of a TC criterion, by comparing the decision variable of each cell with a threshold and declaring the acquisition in correspondence of a threshold crossing event. In general, the trade-off between MAX and TC is not trivial, and typically depends on the uncertainty region size and the SNR. A common design trend is to prefer MAX with relatively short uncertainty regions, and adopt TC otherwise. In the following, since the uncertainty region is scanned via a FFT/IFFT scheme in its entirety, the MAX criterion will be considered.

The metric introduced to characterize the detection circuit performance is the mean acquisition time (MAT). The acquisition procedure can be completed after a single uncertainty region scan (single-dwell procedure) and evaluated through the flow-graph approach. This approach exploits the fact that the acquisition procedure can be modelled as a discrete Markov chain where the states of the chain become the nodes of the graph, and nodes are interconnected through branches with appropriate gains [43], [44]. The flow graph approach relies on the assumption that different cells provide statistically independent variables. In general, an overall false alarm state is present in the flow graph, which corresponds to the case of false acquisition after the entire single-dwell procedure. This state is classified as absorbing when the procedure does not restart, while it is identified as non-absorbing when the procedure restarts after a penalty time T_P dependent on the employed tracking circuit.

For both alternative approaches proposed in section 3.3.1, performance can be evaluated by computing the mean acquisition time (MAT) in each band, but in addition, an important metric to consider is the Overall Mean Acquisition Time (OMAT), defined as the average time needed to achieve coarse code synchronization in both bands.

Synchronization is achieved by acquiring first the Master signal, and then passing the time reference to the Slave signal. The information exchange can either be unidirectional (from Master to Slave) or bidirectional, when control can be returned to the Master as feedback if the Slave finds errors in the Master information. The

specific information exchange taking place between the two bands is fundamental for building the flow graph of the overall acquisition procedure as presented in the following sections.

3.3.3.1 Unidirectional Information Exchange

In case of unidirectional information exchange from Master to Slave (CBA UD), the entire synchronization procedure in the Master band terminates before passing the reference to the Slave band. Therefore, the $OMAT_{UD}$ of the entire procedure is given by the sum of the time needed by the Master to acquire synchronism over the CUR and the Slave over the RUR.

If both bands employ the MAX decision criterion, the procedure can be summarized as in the following:

- Synchronization commences in the Master band by scanning the CUR (Master Search).

- When a maximum decision variable corresponding to a H_1 hypothesis occurs, with probability of detection P_{DM}, then a transition from the search state (Master Search) to the correct acquisition state (Master ACQ) takes place.

- If the maximum decision is in correspondence of a H_0 cell, with probability of error $P_{EM} = 1 - P_{DM}$, then the transition is to the non-absorbing error state (ERROR), from which the detector exits after a penalty time T_{PM}, which is the processing time spent by the Master band false alarm detection circuit to recognized the erroneous detection.

- After a time T_{CB}, needed to exchange information between the two acquisition engines, the control is passed to the slave band and the scanning stage inside the RUR.

- When a maximum decision variable corresponding to a H_1 hypothesis occurs, with probability of detection P_{DS}, then a transition from the search state (Slave Search) to the correct acquisition state (Slave ACQ) takes place.

- If the maximum decision is in correspondence of a H_0 cell, with probability of error $P_{ES} = 1 - P_{DS}$, then the transition is to the non-absorbing error state (ERROR), from which the detector exits after a penalty time T_{PS}, which is the Slave band penalty time and defines the processing time spent by the Slave band false alarm detection circuit to recognized the erroneous detection.

The dwell time spent by the code acquisition subsystem before performing any transition from the search state is equal to T_{UR}, which indicates the generic uncertainty region duration (T_{URM} and T_{URS} for the Master and Slave band respectively), multiplied by a processing factor P_f, which takes into account the possible further delay introduced by the receiver to perform the computations required for the exploration of the UR also in the frequency domain. The actual value of P_f can vary according to the architecture adopted by the acquisition subsystem, e.g. as a function of the parallelism adopted by the specific hardware implementation.

By reducing the flow-graph, the following transfer function results:

$$P_A(z) = \frac{P_{DM}P_{DS}z^{P_f(T_{URM}+T_{URS})+T_{CB}}}{(1 - P_{EM}z^{P_fT_{URM}+T_{PM}})(1 - P_{ES}z^{P_fT_{URS}+T_{PS}})} \qquad (3.9)$$

which translates into the following Mean Acquisition Time:

$$\begin{aligned}
OMAT_{UD} &= \frac{dP_A(z)}{dz}\Big|_{z=1} \\
&= T_{CB} + \frac{P_{DM}(P_fT_{URS}+T_{PS})}{P_{DM}P_{DS}} \\
&+ \frac{P_{DS}(P_fT_{URM}+T_{PM}-P_{DM}(T_{PM}+T_{PS}))}{P_{DM}P_{DS}}
\end{aligned} \qquad (3.10)$$

Equation (3.10) clearly shows that the $OMAT_{UD}$ performance is given by the sum of the time required for the information exchange T_{CBA} and the MAT required for the acquisition in the Master band over the CUR, the Slave band in the RUR applying the MAX decision criterion. Performance in terms of OMAT with respect to autonomous acquisition in the two bands is thus improved and a complexity reduction is guaranteed.

3.3.3.2   Bi-directional Information Exchange

With the aim of further improving performance in terms of OMAT, bi-directional information exchange (CBA BD) is considered in this section. By allowing the exchange of information between the two bands, control from the Slave band can be returned to the Master in case of erroneous synchronization. More specifically, if acquisition in the Slave band starts as soon as acquisition in the Master band is achieved, before the Master tracking circuit has refined the code epoch estimate accuracy and the false alarm detection circuit has rejected possible erroneous detections, then the Slave feedback can be used as a verification stage for the Master acquisition.

$$P_{EM} \cdot z^{P_f \cdot T_{URM}} = (1 - P_{DM}) z^{P_f \cdot T_{URM}}$$

Master Search

Master Error

$$z^{T_{PM}}$$

$$P_{DM} \cdot z^{P_f \cdot T_{URM}}$$

Master ACQ

$$z^{T_{CB}}$$

$$P_{ES} \cdot z^{P_f \cdot T_{URS}} = (1 - P_{DS}) z^{P_f \cdot T_{URS}}$$

Slave Search

Slave Error

$$z^{T_{PS}}$$

$$P_{DS} \cdot z^{P_f \cdot T_{URS}}$$

Slave ACQ
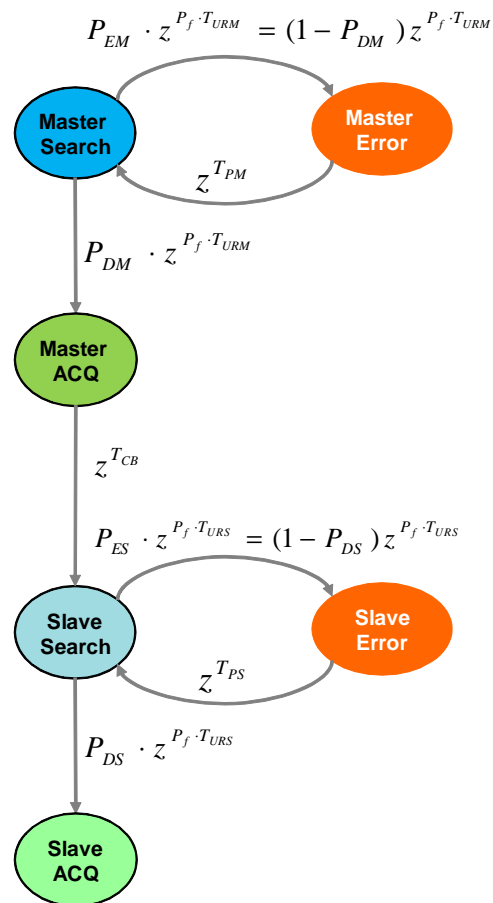
Figure 3.9: Flow graph of the overall acquisition procedure in the case of unidirection information exchange

If the MAX criterion is used in both bands, the corresponding flow graph is reported in figure 3.10 and the overall acquisition procedure can be summarized as:

- Synchronization commences in the Master band by scanning the CUR (Master Search).

- Regardless of having correctly achieved synchronization, the Master band passes the estimated time reference in a time T_{CB} to the Slave band (Slave Search), that is thus in charge of acquiring the signal over its RUR and provide a feedback to the Master band.

  − When the Master decides in favor of a maximum decision variable corresponding to a H_1 hypothesis, with probability of detection P_{DM}, then a transition from the search state (Master Search) to the search state (Slave Search "Full") takes place.

    ∗ From the Slave Search Full state, after scanning the RUR if the maximum decision corresponding to a H_1 hypothesis occurs, with probability of detection P_{DS}, then a transition from the search state (Slave Search) to the correct acquisition state (Master/Slave ACQ) takes place.

    ∗ If the Slave maximum decision is in correspondence of a H_0 cell, with probability of error $P_{ES} = 1 - P_{DS}$, then the transition is to the non-absorbing error state (ERROR), from which the detector exits after a penalty time T_{PS}, after which a feedback is provided to the Master band (Master Search) to restart the search over the CUR.

  − If the Master maximum decision is in correspondence of a H_0 cell, with probability of error $P_{EM} = 1 - P_{DM}$, then the transition is to the search state (Slave Search "Empty").

    ∗ From the Slave Search "Empty" state, after scanning the RUR the transition is to the non-absorbing error state (ERROR) with probability equal to 1, from which the detector exits after a penalty time T_{PS}, after which a feedback is provided to the Master band (Master Search) to restart the search over the CUR.

As in the UD case, the dwell time spent by the code acquisition subsystem before performing any transition from the search state is equal to T_{UR}, which indicates the generic uncertainty region duration (T_{URM} and T_{URS} for the Master and Slave band

respectively), multiplied by a processing factor P_f. The resulting transfer function is thus:

$$P_A(z) = \frac{A(z)}{B(z)} \tag{3.11}$$

where:

$$A(z) = P_{DM} P_{DS} z^{P_f(T_{URM}+T_{URS})+T_{CB}}$$

$$B(z) = 1 - \{(1 - P_{DM})z^{P_f(T_{URM}+T_{URS})+T_{CB}+T_{PS}}$$

$$+ P_{DM} z^{P_f T_{URM}+T_{CB}}(1 - P_{DS})z^{P_f T_{URS}+T_{PS}}\}$$

which translates into the following OMAT:

$$
\begin{aligned}
OMAT_{BD} &= \frac{dP_A(z)}{dz} \Big|_{z=1} \\
&= \frac{T_{CB} + P_f(T_{URM} + T_{URS}) + T_{PS}(1 - P_{DM}P_{DS})}{P_{DM}P_{DS}}
\end{aligned}
\tag{3.12}
$$

Equation 3.12 shows that by delegating the Master acquisition verification to the Slave band, which has to scan only a RUR, the OMAT performance depends on the specific choice of penalty time T_{PS}, leaning in the best scenario where $P_{DS} = 1$ and $P_{DM} = 1$ to only the time needed to perform the scan in the two bands $P_f(T_{URM} + T_{URS})$ plus the time required to exchange information between the bands T_{CB}.

Having determined the analytical formulation of the mean acquisition time, in the following performance evaluation is carried out via a semi-analytical approach, where detection probabilities are obtained from Monte Carlo simulations, and are then combined according to (3.10),(3.12) to evaluate MAT performance. Note that the generic uncertainty region duration TUR is equal to the entire code duration for the CUR step (1ms and 4ms for E5 and E1, respectively), and to a fraction of the Slave signal code duration for the RUR step. In particular, when the RUR approach is performed, T_{UR} amounts to:

$$T_{UR} = 3.000978 \ ms \ \ for \ \ E1 - RUR \tag{3.13}$$

$$T_{UR} = 977.51 \ ms \ \ for \ \ E5 - RUR \tag{3.14}$$

In particular, (3.13) corresponds to 4 hypotheses distributed in a period of 3 E5 code segments plus 1 E5 chip, while (3.14) corresponds to 10 consecutive E5 chips.
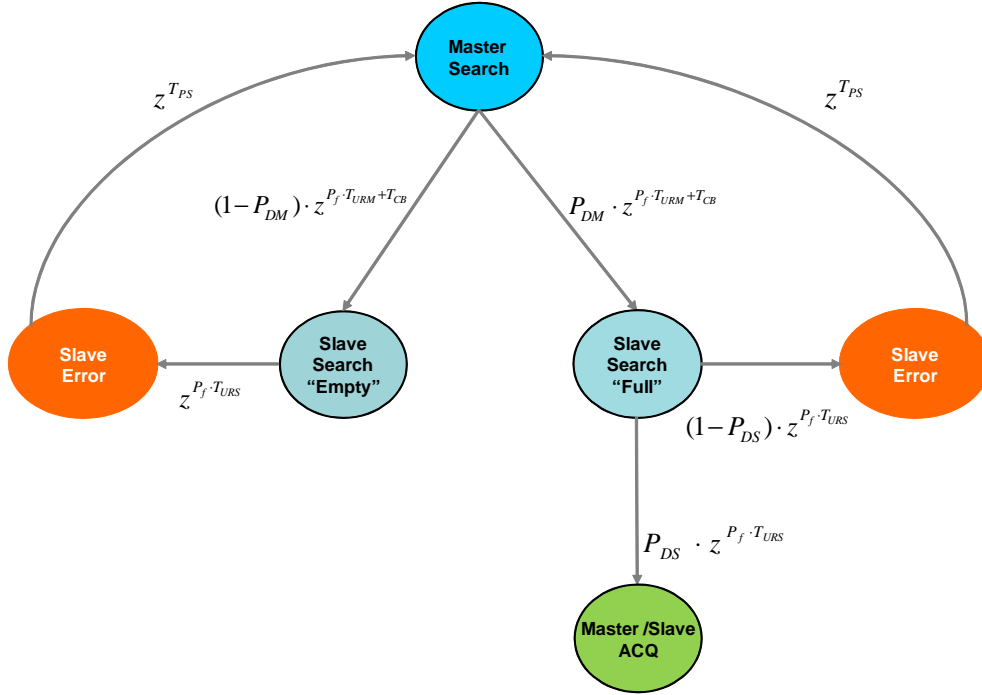
Figure 3.10: Flow graph of the overall acquisition procedure in the case of bi-direction information exchange

The penalty time T_P considered in our semi-analytical evaluation is set equal to 10 times the code duration of the corresponding signals, as shown in (3.15) and (3.16), and it is the same for both CUR and RUR stages:

$$T_{P(E1-acq)} = 10T_{code-E1} \qquad (3.15)$$

$$T_{P(E5-acq)} = 10T_{code-E5} \qquad (3.16)$$

3.3.4   Receiver architecture

As already anticipated, we process pilot codes only to perform code acquisition in the two bands, i.e. the signal component E1c in E1, and the signal component E5aQ in E5 [41].

For the E5 signal acquisition, in order to limit the complexity of the receiver, instead of considering the entire AltBOC architecture a Single Side Band (SSB) processing scheme is considered [45], [46]. With this technique the signals from the two sub-bands are processed independently as simple BPSK signals obtaining an

unambiguous triangular correlation peak.

For both approaches (E1-E5 CBA and E5-E1 CBA), after the dual band front-end, the receiver architecture foresees chip matched filtering (MF), which in E1 is matched to the BOC(1,1) waveform while in E5 is matched to the rectangular BPSK waveform, followed by a decimation block that reduces the number of samples to be processed by the following acquisition blocks to limit the resulting FFT size, so reducing complexity. In particular, we consider a discrete time representation of the signal with 16 samples per E1 chip and 12 samples per E5 chip, corresponding to analogue to digital conversion performed at the sampling frequencies $f_{s-E1} = 16.368$MHz and $f_{s-E5} = 122.76$MHz for the two bands before the digital MF. The output of the MF is then decimated with a sampling frequency f_{k-E1} and f_{k-E5} ($f_s \geqslant f_k$). Figure 3.11 shows the receiver architecture for the E1-E5 CBA approach: the first step consists in the acquisition of the Master signal (E1c code) using a parallel FFT/IFFT search strategy over the entire time UR; then, the CBA acquisition controller manages the obtained rough epoch estimate to perform UR reduction for the E5 band. Because in this second step the search space is limited according to the performed UR reduction, the acquisition of the Slave signal can be obtained through a simple correlator scheme, where the Circular Phase-Shift block selects the timing hypotheses to test among the few that are possible. This approach allows to minimize the hardware complexity with no impact on performance.

Figure 3.12 shows the E5-E1 CBA dual receiver architecture, where the basic concept is the same as in E1-E5 CBA, but here acquisition in E5 is the Master process, while acquisition in E1 is the Slave process. Note that the MAX decision criterion is used both for Master and Slave signals.

It is worthwhile mentioning, that to perform a fair performance comparison, the Total Received Minimum Power (TRMP) for both E5a and E5b is of -155 dBW, corresponding to a TRMP for the entire E5 signal of -152 dBW. On the other hand, the E1 TRMP is equal to -157 dBW [41]. Thus, the entire E5 signal considering both sub-bands a and b together) is on average 5 dB more powerful than the E1 signal, resulting in a difference of 5 dBHz also in terms of signal power over noise power spectral density C/N_0.

First Step - Master Signal E1
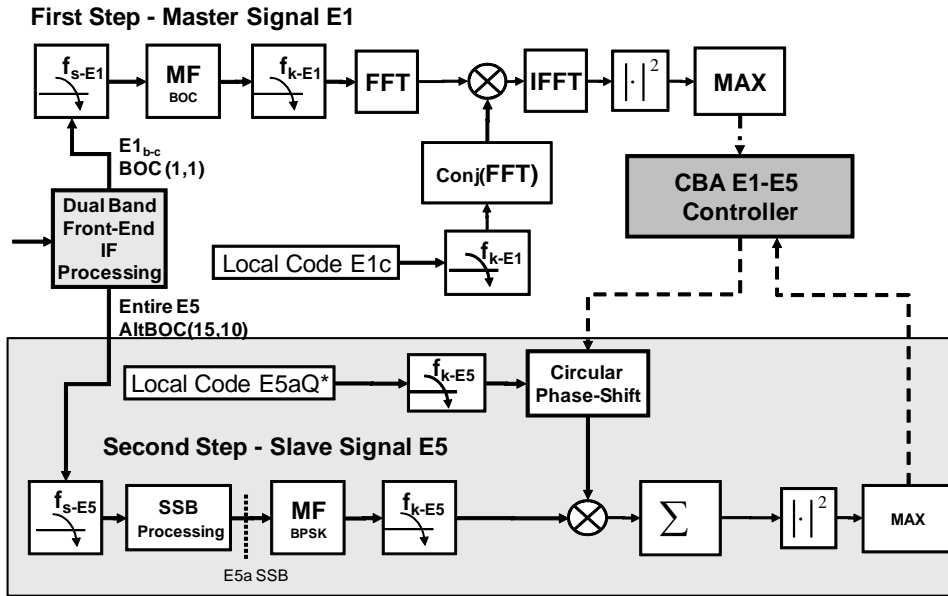
Figure 3.11: E1-E5 CBA receiver architecture

First Step - Master Signal E5
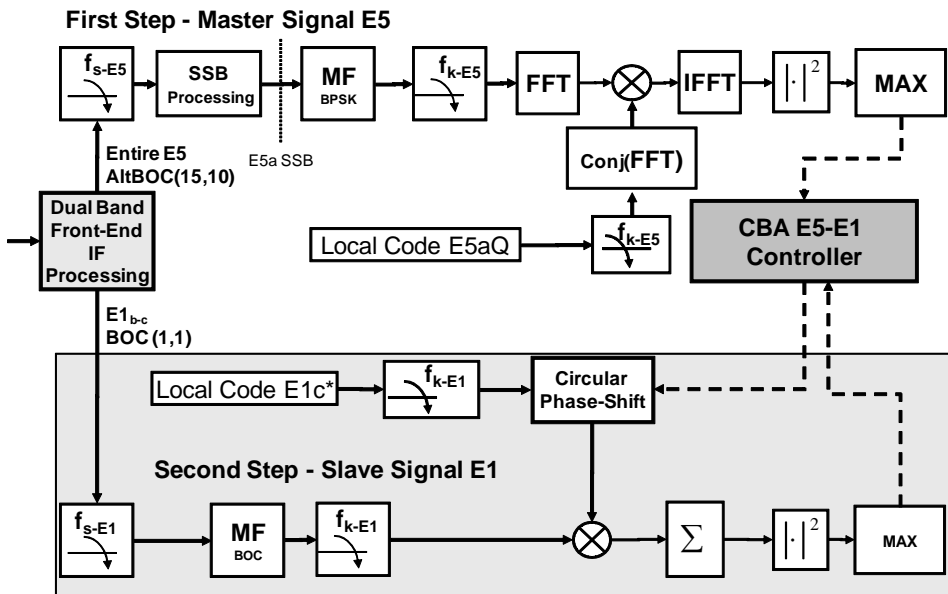
Figure 3.12: E5-E1 CBA receiver architecture

3.3.5   Simulation results with time uncertainty only

To assess the performance of the proposed approach, we consider at first a simplified scenario where the detector has to explore the time domain only. This corresponds for example to a scenario where the multi-frequency receiver exploits a frequency reference obtained from an external network, as it happens for example in Assisted-GNSS systems.

3.3.5.1   Acquisition of the Master Signal

In this section the results of E1 and E5 code acquisition considering the CUR stage are reported with the aim to optimize the choice of the sampling frequency f_k to adopt after the MF, considering actual scenarios affected by timing errors. These results correspond to the acquisition of the Master Signal in the CBA strategy. Figure 3.13 shows the resulting MAT for the E1c pilot code acquisition, at different sampling rates f_k, considering a reasonable fractional timing error in the sampling stage equal to the worst case, a residual frequency error equal to 50 Hz, a processing factor $P_f = 1$, and variable C/N_0 values. As shown in the figure, acquisition performance improves at higher sampling frequencies because the receiver is more robust against timing errors, thanks to the finer discretization in time. On the other hand, higher sampling frequencies require longer FFT, increasing terminal complexity and power consumption. A good complexity-performance trade-off is represented by $f_{k-E1} = 8$ MHz (8 samples per E1 chip, corresponding to an oversampling factor $\eta = 8$).

Figure 3.14 shows MAT performance for the E5aQ pilot code acquisition, taking into account the same impairments considered in E1 simulations. For E5, a good trade-off between complexity and performance is given by the sampling frequency $f_{k-E5} = 61.38$ MHz (6 samples per E5 chip, corresponding to an oversampling factor $\eta = 6$). These two sampling frequencies (f_{k-E1}, f_{k-E5}) have been considered also for the CBA approaches analyzed in the following.
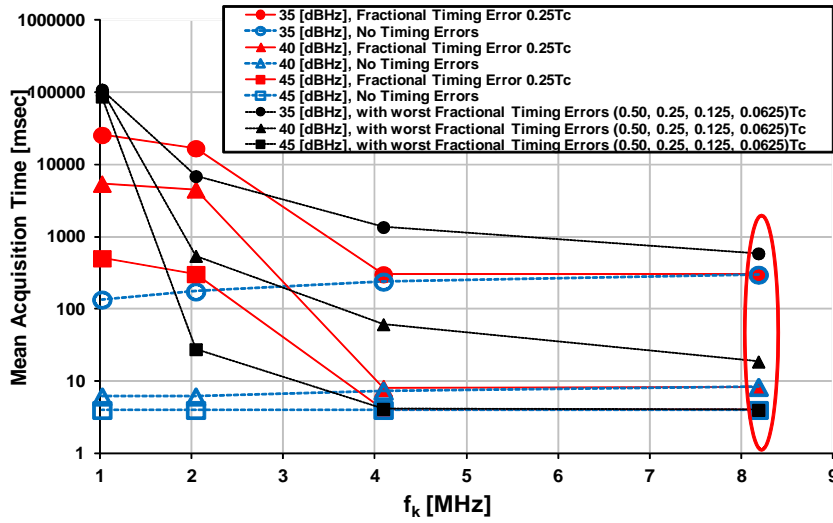
Figure 3.13: E1c CUR code acquisition, MAX criterion, residual frequency error of 50Hz, $f_{s-E1} = 16.368$MHz. The mean acquisition time (MAT) is reported vs. the sampling frequency
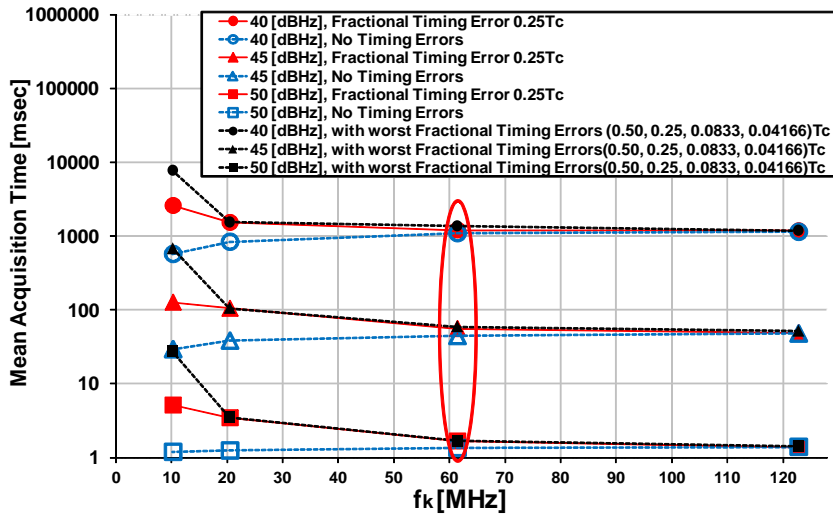
Figure 3.14: E5aQ CUR code acquisition, MAX criterion, residual frequency error 50Hz, $f_{s-E5} = 122.76$MHz. The mean acquisition time (MAT) is reported vs. the sampling frequency

3.3.5.2   Acquisition of the Slave Signal

To understand the advantages of a reduced uncertainty region, figure 3.15 reports MAT performance as a function of the uncertainty region extension for a scenario with high signal power to noise ratio equal to $C/N_0 = 47$dBHz and a frequency error equal to 250Hz. As clearly shown in the figure, the reduction of the uncertainty region in the time domain leads to enormous benefits, with a mean acquisition time which is two orders of magnitude lower when passing from CUR to a RUR of 10 chips.
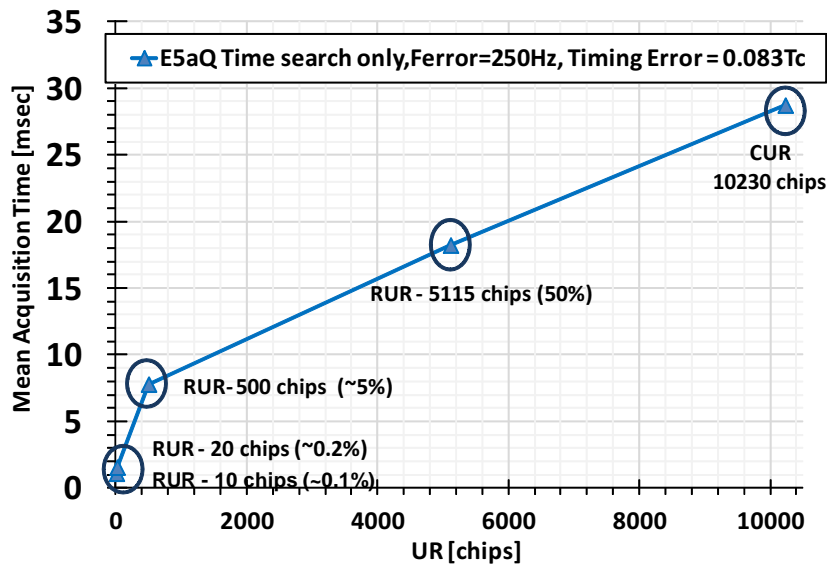
Figure 3.15: Mean Acquisition Time vs. uncertainty region with the MAX criterion and Time Search Only, oversampling $\eta = 6$, frequency error $= 250$ Hz, $C/N_0 = 47$dBHz

The improvements of the cross-band aided approach is shown in figure 3.16 and figure 3.17, where the gain of the RUR approach is clearly evident with respect to the classic CUR strategy, in terms of MAT. The results are obtained with a residual frequency error of 50 Hz, sampling frequencies $f_{k-E1} = 8.184$ MHz and $f_{k-E1} = 16.368$ MHz. Performance is evaluated both in the presence of a sampling error equal to the worst case and with ideal sampling. In both bands, the improvements achievable with the CBA strategies in terms of MAT reduction are compelling. For the E1 signal (figure 3.16), the mean acquisition time is considerably reduced at low C/N_0 values, while, for higher signal to noise ratios, the gain of the RUR approach in terms of MAT is only 1 ms, due to the ambiguity resolution over the 4 macro-

zones. In E5 (figure 3.17), the attainable improvements are even more significant and, at higher C/N_0, MAT tends towards its minimum equal to the E1 chip duration. In particular, the lower bound of the MAT achievable in large SNR conditions is obtained by evaluating the OMAT formula with $P_D = 1$, and corresponds to the duration of the RUR equal to 977.51ns for E5 and 3.000978ms for E1.
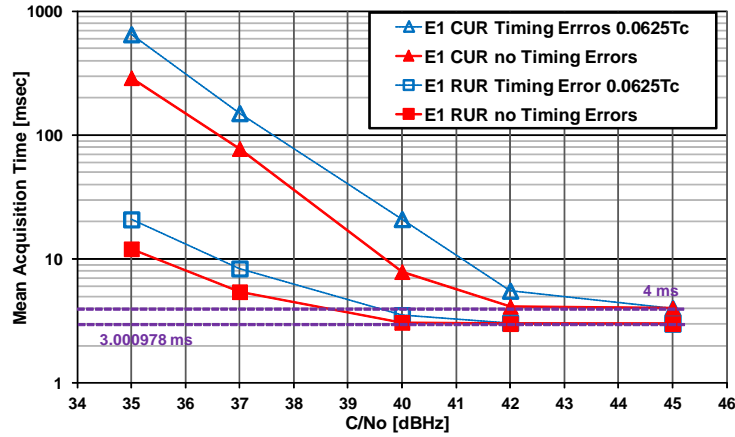
Figure 3.16: E1c CUR vs RUR Code Acquisition, MAX Criterion, residual Frequency Error 50 Hz, $f_{s-E1} = 16.368$ MHz and $f_{k-E1} = 8.184$ MHz.
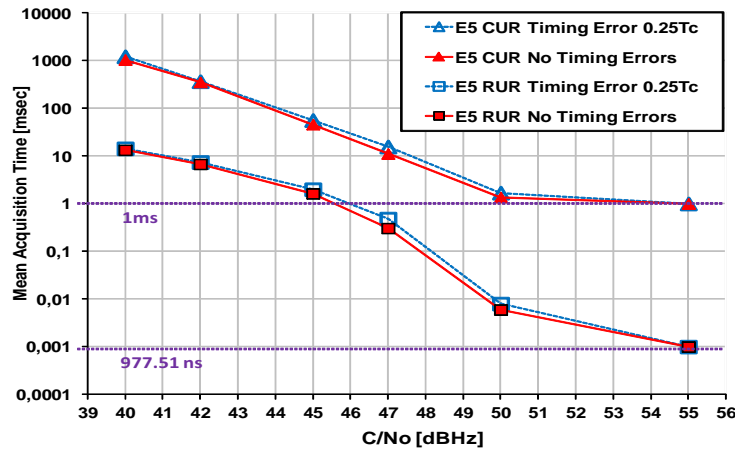
Figure 3.17: E5aQ CUR vs RUR Code Acquisition, MAX Criterion, residual Frequency Error 50 Hz, $f_{s-E5} = 122.76$ MHz and $f_{k-E5} = 61.38$ MHz

3.3.5.3 Cross-band aiding acquisition: unidirectional case

Performance of the CBA process depends on the specific case under consideration, (e.g. unidirectional or bi-directional information flow). The following section reports the performance of each configurations presented in 3.3.3.

Taking into account that the RUR step (acting on the Slave signal) is accomplished after the CUR step (acting on the Master signal in the other band), the total MAT for the overall CBA UD strategy can be evaluated as the sum of MAT in the two sequential steps. Table 3.2 reports the overall MAT results for serial Stand-Alone E1 E5 acquisition, E1-E5 CBA and E5-E1 CBA, respectively. Note that a pair of C/N_0 values is reported for each reference scenario, to take into account the 5dB difference in the received signal power level between E1 and E5, as discussed above and the time T_{CB} is set equal to zero, implying no delay in passing the time reference information.

These results highlight that the E1-E5 CBA UD strategy offers the best performance in terms of overall MAT, particularly at low SNR, as shown also in figure 3.18. For increasing SNR, performance of both CBA strategies improves matching more closely, and finally converging to the same lower bound for the mean acquisition time.

Note that although E1-E5 CBA UD and E5-E1 CBA UD converge towards the same limit for large SNRs, the former is the preferable approach because it considerably improves code acquisition performance in worst-case operating conditions.

Scenario	E1-E5 SNR	No Timing Errors	Timing Errors (worst case)
A	35 dBHz (E1)-40 dBHz	1327.14 ms	1806.2 ms
		1049.7 ms	1233.0 ms
		302.7 ms	662.3 ms
B	37 dBHz (E1)-42 dBHz	428.4 ms	513.9 ms
		356.1 ms	372.5 ms
		84.5 ms	157.1 ms
C	40 dBHz (E1)-45 dBHz	53.7 ms	76.9 ms
		48.9 ms	59.5 ms
		9.5 ms	22.9 ms
D	42 dBHz (E1)-47 dBHz	15.2 ms	21.1 ms
		14.1 ms	18.6 ms
		4.4 ms	6.0 ms
E	42 dBHz (E1)-47 dBHz	5.4 ms	5.7 ms
		4.4 ms	4.7 ms
		4.0 ms	4.0 ms
F	42 dBHz (E1)-47 dBHz	5.0 ms	5.0 ms
		4.0 ms	4.0 ms
		4.0 ms	4.0 ms

Table 3.2: Stand-Alone E1&E5, E5-E1 CBA UD and E1-E5 CBA UD OMAT performance in the time domain only
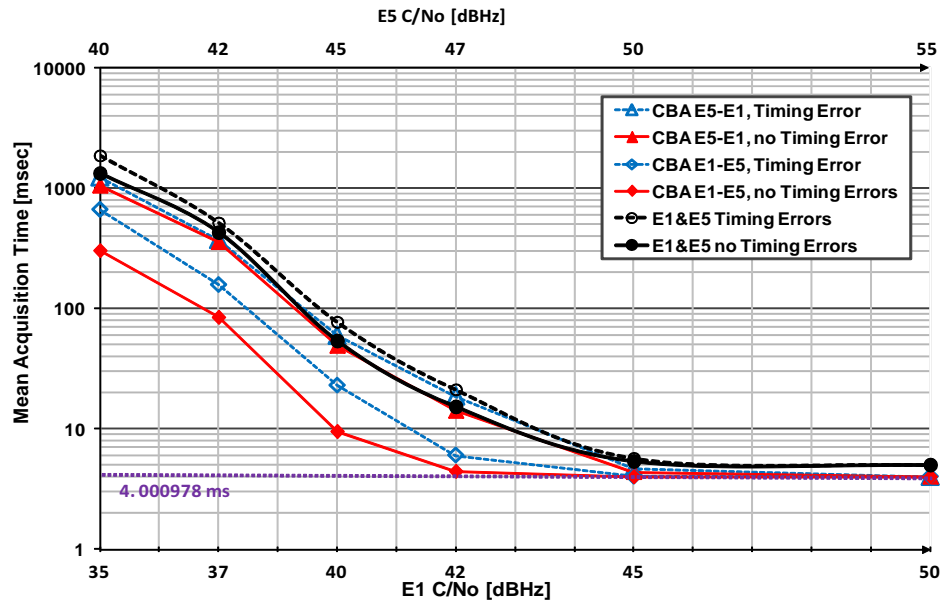
Figure 3.18: Stand-Alone E1&E5, E1-E5 CBA UD and E5-E1 CBA UD performance comparison

3.3.5.4 Cross-band aiding: bi-directional case

When bidirectional information exchanges between the two bands are envisaged, depending on the scenario at hand and the choice of CBA strategy, performance differ considerably as reported in table 3.3.

The results reported in figure 3.19 underline that the E1-E5 CBA BD strategy offers the best performance in terms of OMAT, particularly at low SNR. On the other hand, the E5-E1 CBA BD approach performance at low SNR values does not improve the OMAT, this is due to the fact that verification is delegated to the band with the longest penalty time T_{PS}.

Comparison between unidirectional and bi-directional approaches is reported in figure 3.20. It is worthwhile noting that with our specific choice of penalty times, the bi-directional approach offers the best performance when the Slave band is faster than the Master band. Inversely, delegating the verification to a slower band might degrade considerably performance in terms of OMAT also with respect to the uni-directional information exchange case.

Scenario	E1-E5 SNR	No Timing Errors	Timing Errors (worst case)
A	35 dBHz (E1)-40 dBHz	1327.14ms	1806.2ms
		234.2ms	521.3ms
		4571.4ms	6874.6ms
C	40 dBHz (E1)-45 dBHz	53.7ms	76.9ms
		7.7ms	13.2ms
		183.8ms	226.9ms
E	42 dBHz (E1)-47 dBHz	5.4ms	5.7ms
		4.0ms	4.0ms
		5.5ms	6.7ms
F	42 dBHz (E1)-47 dBHz	5.0ms	5.0ms
		4.0ms	4.0ms
		4.0ms	4.0ms

Table 3.3: Stand-Alone E1&E5, E5-E1 CBA BD and E1-E5 CBA BD OMAT performance in the time domain only
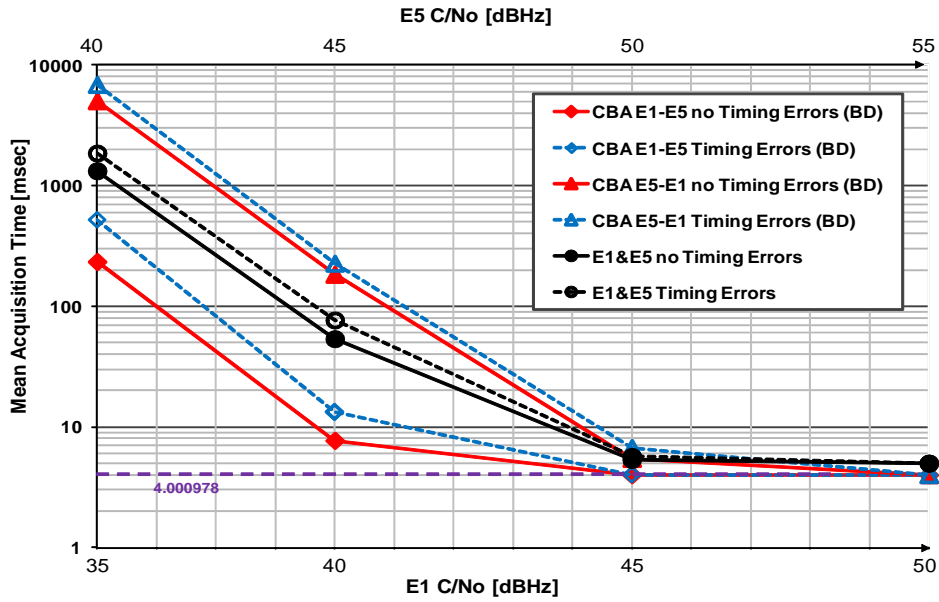
Figure 3.19: Stand-Alone E1&E5, E1-E5 CBA and E5-E1 CBA BD performance comparison
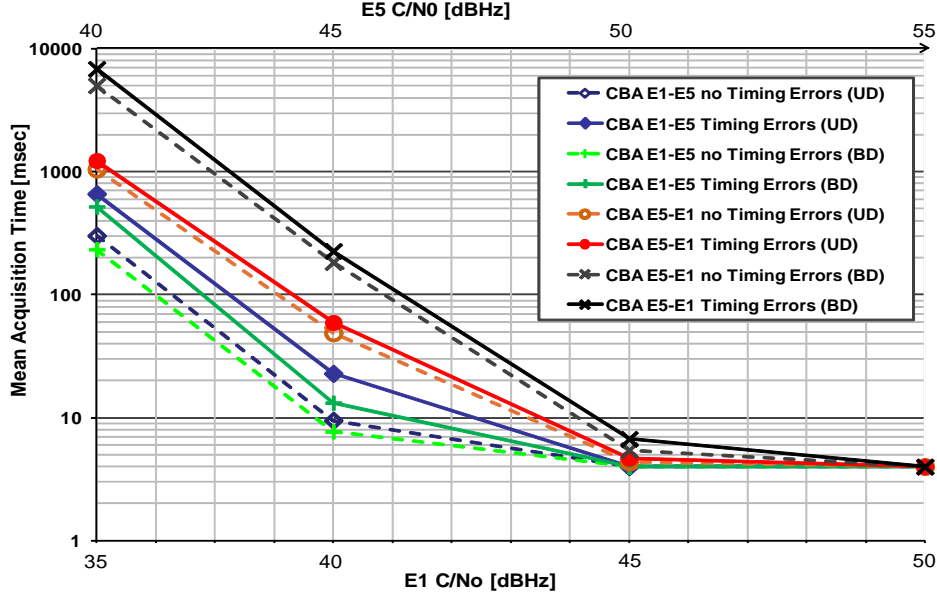
Figure 3.20: Comparison between the UD and BD E1-E5 CBA and E5-E1 CBA performance

3.3.6 Simulation Results with time/frequency domain search

A robust receiver design has to take into account also practical frequency errors affecting the received signal. For this reason, we remove in this section the assumption of ideal frequency recovery, and introduce a typical value for the frequency offset in the order of ± 10 kHz. In this case, the full bi-dimensional UR must be processed in each band of the multi-frequency receiver. Similarly to the approach used for scanning the temporal domain, also the uncertainty in the frequency domain is handled by the code acquisition subsystem via a discretization of the overall uncertainty into bins. The degree of discretization (i.e. the selection of the frequency bin extension) must be selected so that, for the correct frequency bin, the inherent degradation introduced by the maximum residual frequency offset on the decision variable is limited. This degradation is related with the selected accumulation strategy, and in particular with the length of the performed coherent correlation L_{corr}, which for a FFT/IFFT approach is identical to the entire code length. In particular, a practical rule to determine the maximum tolerable frequency error is provided in [47] as:

$$\Delta f \leq \frac{3}{8 L_{corr} T_c} \tag{3.17}$$

Applying this rule, in order to have acceptable performance degradation with

fully coherent correlation, the maximum frequency offset has to be:

- 50 Hz for E1, corresponding to 200 frequency bins of 100 Hz each;

- 250 Hz for E5, corresponding to 40 frequency bins of 500 Hz each.

Note that the number of FFT operations needed to scan the uncertainty region also in the frequency domain increases proportionally with the number of the frequency bins adopted in the discretization, which can become an issue for computationally limited terminals. All parameters for the two Galileo signal are summarized in the following table.

Signal	E1(E1c Pilot Code)	E5(E5aQ Pilot Code)
Frequency Error Range	±10kHz	±10kHz
Sampling Frequency (f_k)	8.184MHz	61.380MHz
Oversampling Factor (η)	8	6
Frequency Domain Resolution (Δf)	100 Hz	500(Hz)
Residual Frequency Error (Ferror)	50(Hz) worst case	250(Hz) worst case
FFT Length in samples (NFFT)	81840	122760
Frequency Bins Number	200	40
Time Hypotheses Number	81840	122760
Time/Frequency Hypotheses	$16.368 * 10^6$	$4.9104 * 10^6$

Table 3.4: E1 and E5 optimized parameters to scan the Time and Frequency domain

To evaluate this aspect, in figure 3.21 the MAT is reported for the E1 signal with time and frequency search vs. C/N_0. Different values of the processing factor P_f are considered because this parameter is determined by the hardware architecture and the available computational capabilities, and thus cannot be fixed a-priori. For example, $P_f = 10$ means that the entire uncertainty region processing (time and frequency) requires 10 times the code duration. According to equation (3.17), 200 frequency bins of 100Hz are considered along with a sampling timing error equal to 0.0625 T_c. The time search only is also reported as a reference while the case $P_f = 1$ represents the performance obtained with no hardware limitations or constraints. Note that considering the computation overhead, the MAT performance slightly degrades with $P_f = 2$, while is severely affected by $P_f = 10$. This provides a clear indication on the hardware requirements that the terminal has to satisfy.

The same behavior can be found for the E5 band, as depicted in figure 3.22 where the MAT for the E5 signal with time and frequency search is reported vs. C/N_0 for different values of the processing factor P_f. According to equation Equation (3.17), 40 frequency bins of 500 Hz are considered along with a sampling timing error equal to 0.0833 T_c. Also in this case, the time search only is reported as a reference.
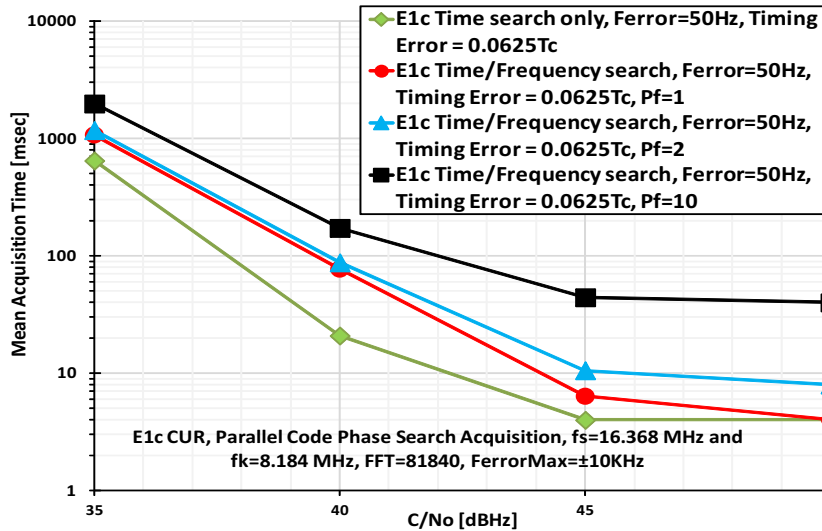
Figure 3.21: Mean Acquisition Time for the E1 signal with time and frequency search vs. C/N_0 for different values of the Processing factor P_f

The comparison of E1 and E5 MAT performance is reported in figure 3.23 with time/frequency search. As discussed above, performance has to be compared considering a 5 dB difference for the C/N_0 in the two bands. Interestingly, different conclusions with respect to the time search only can be drawn. In fact, the performance in the two bands is closer, with a gain of E1 over E5 for low SNRs and an opposite behavior at large SNRs. This is due to the fact that the E5 band signal has a higher chip rate and, for this reason, is inherently more robust against frequency errors. Thus, the search domain in the frequency space, composed by 40 bins, is smaller with respect to the E1 band signal, which requires 200 bins. This penalizes the E1 performance more than the E5 performance, balancing the comparison.
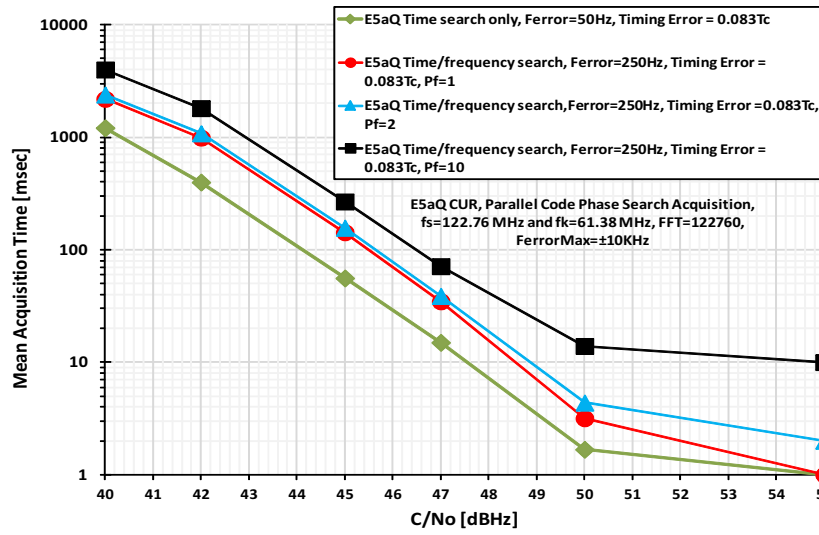
Figure 3.22: Mean Acquisition Time for the E5 signal with time and frequency search vs. C/N_0 for different values of the Processing factor P_f. 40 frequency bins of 500Hz are considered with a sampling timing error equal to $0.083T_c$.
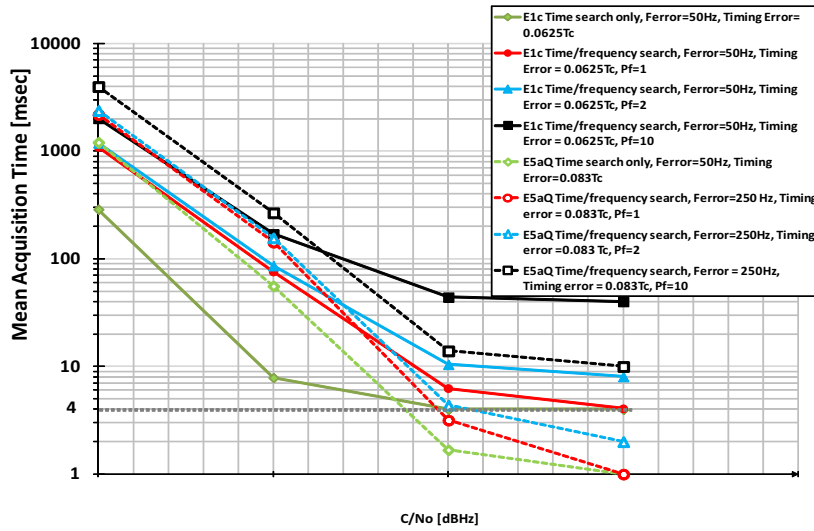
Figure 3.23: Comparison of the Mean Acquisition Time for the E5 and E1 signal with time and frequency search vs. C/N_0 for different values of the Processing factor P_f

3.3.6.1 Cross-band aiding: unidirectional case

In the following the assessment of the CBA UD technique are reported, figure 3.24 depicts the overall E1-E5 CBA UD and E5-E1 CBA UD acquisition time, considering also the acquisition of the Slave signal, for different values of C/N_0 and P_f with 40 frequency bins of 500 Hz and timing error equal to 0.0833 T_c in E5, and 200 frequency bins of 100 Hz and timing error equal to 0.0625 T_c for the E1 signal.
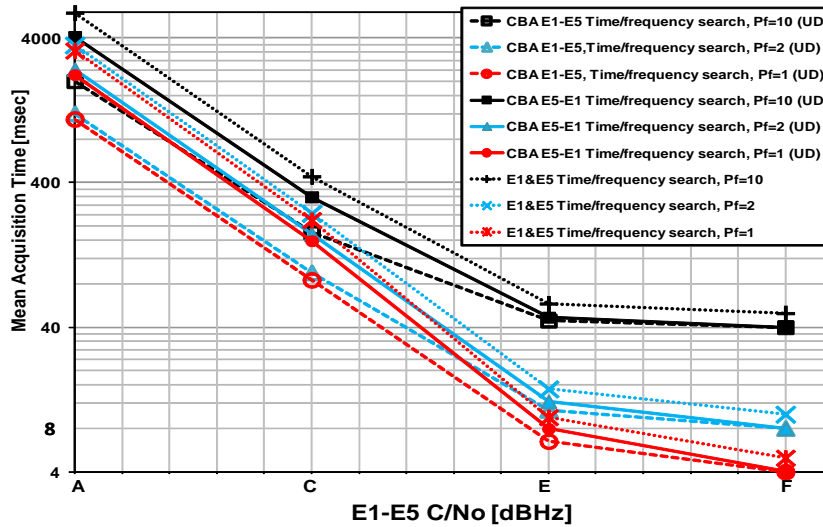
Figure 3.24: Comparison of the Mean Acquisition Time for the entire stand-alone (E1&E5), E1-E5 CBA UD and E5-E1 CBA UD procedures with time and frequency search vs. C/N_0 for different values of the Processing factor P_f.

It is interesting to note that the overall E1-E5 CBA UD acquisition time performance (dashed curves) is always better than E5-E1 CBA UD performance (continuous curves): this is due to the fact that the acquisition of the slave signal in E1 is more time demanding with respect to the acquisition of the E5 slave signal. Thus, also in the actual scenario of Time/Frequency search, E1-E5 CBA UD is the best approach in terms of overall performance. The figure shows also the comparison with the classical approach (dotted curves labeled E1&E5) where the acquisition in the two bands is completed sequentially, but without exploiting the time reference between the two bands. The performance of the proposed E1-E5 CBA UD approach is always better and it is worthwhile noting that this result comes along with the reduction of the complexity of the overall acquisition process. In fact, the acquisition of the slave signal in E5 requires the computation of a very limited number of correlations. To complete the analysis, in table 3.5 the quantitative comparison is

reported to better evaluate the advantages of the proposed approach. For example, in the worst case condition, E1-E5 CBA UD is able to provide a mean acquisition time, 1098 ms, which is one third with respect to the classical approach, equal to 3262.5 ms.

Scenario	E1-E5 SNR	$P_f = 10$	$P_f = 2$	$P_f = 1$
A	35dBHz (E1)-40dBHz	5972.7ms	3563.6ms	3262.5ms
		4071.9ms	2430.1ms	2224.9ms
		2008.2ms	1199.1ms	1098.0ms
C	40dBHz (E1)-45dBHz	440.7ms	244.4ms	220.0ms
		318.1ms	176.0ms	158.3ms
		180.7ms	95.5ms	84.8ms
E	42dBHz (E1)-47dBHz	58.2ms	15.0ms	9.5ms
		46.8ms	12.3ms	7.9ms
		44.4ms	10.7ms	6.5ms
F	42dBHz (E1)-47dBHz	50.0ms	10.0ms	5.0ms
		40.0ms	8.0ms	4.0ms
		40.0ms	8.0ms	4.0ms

Table 3.5: Stand-Alone E1&E5, E5-E1 CBA UD and E1-E5 CBA UD OMAT in the Time/Frequency Domain

3.3.6.2 Cross-band aiding: bi-directional case

The performance of CBA BD are considered in this section, figure 3.25 depicts the overall E1-E5 CBA BD and E5-E1 CBA BD acquisition time, considering also the acquisition of the Slave signal, for different values of C/N_0 and P_f with 40 frequency bins of 500 Hz and timing error equal to 0.0833 T_c in E5, and 200 frequency bins of 100 Hz and timing error equal to 0.0625 T_c for the E1 signal.

It is interesting to note that, also in this case, the overall E1-E5 CBA BD acquisition time performance (dashed curves) is always better than E5-E1 CBA BD performance (continuous curves), due to the fact that the acquisition of the slave signal in E1 is more time demanding with respect to the acquisition of the E5 slave signal. The figure shows also the comparison with the classical approach (dotted curves labeled E1&E5) where the acquisition in the two bands is completed sequentially, but without exploiting the time reference between the two bands. Analogously
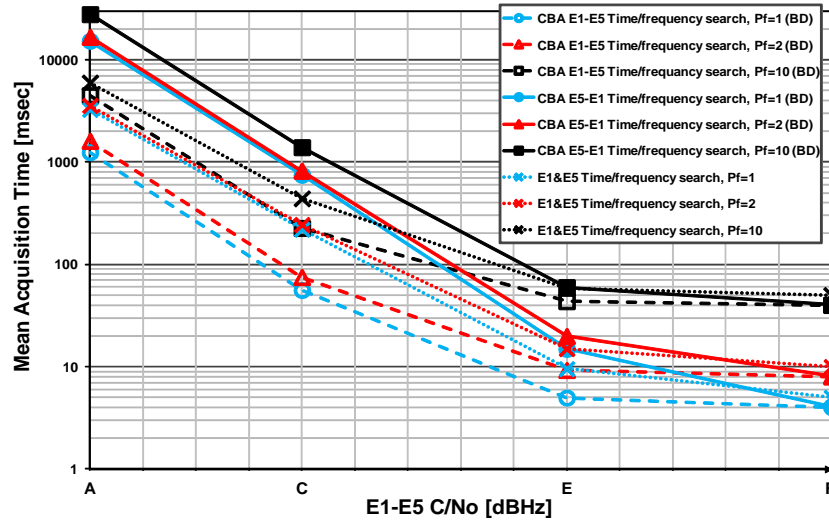
Figure 3.25: Comparison of the Mean Acquisition Time for the entire stand-alone (E1&E5), E1-E5 CBA BD and E5-E1 CBA BD procedures with time and frequency search vs. C/N_0 for different values of the Processing factor P_f.

to the the search in the time domain only the E5-E1 CBA BD strategy performs do not provide improvements due to the longer penalty times of the E1 band and the lower SNR of the Master band E5.

To complete the analysis, the quantitative comparison is reported in table 3.6.

Scenario	E1-E5 SNR	$P_f = 10$	$P_f = 2$	$P_f = 1$
A	35dBHz (E1)-40dBHz	5972.7ms	3563.6ms	3262.5ms
		4478.7ms	1605.8ms	1246.7ms
		27833.1ms	16682.5ms	15288.7ms
C	40dBHz (E1)-45dBHz	440.7ms	244.4ms	220.0ms
		226.0ms	75.0ms	56.0ms
		1394.2ms	820.5ms	748.8ms
E	42dBHz (E1)-47dBHz	58.2ms	15.0ms	9.5ms
		43.4ms	9.2ms	5.0ms
		59.8ms	19.9ms	14.9ms
F	42dBHz (E1)-47dBHz	50.0ms	10.0ms	5.0ms
		40.0ms	8.0ms	4.0ms
		40.1ms	8.1ms	4.1ms

Table 3.6: Stand-Alone E1&E5, E5-E1 CBA BD and E1-E5 CBA BD OMAT in the Time/Frequency Domain

Chapter 4

Code Tracking Techniques

4.1 Code Tracking

Code acquisition can only provide coarse initial estimation of the code delay, therefore the subsequent tracking block aim is to refine these estimations to a higher precision. Thus, code tracking has to follow the code phase of a specific satellite and generate a perfectly time aligned code replica [13]. In traditional GNSS receivers, code tracking is performed through a DLL feedback system as reported in 4.1 where the result of the multiplication of the in-phase and quadra-phase components with different delayed spreading sequences is followed by filtering with the Integrate and Dump (I&D) filters realizing the correlation over a Predetection Integration (PDI) time T_I. Considering that the correlation process takes place over one data bit, the in-phase (I) and quadra-phase (Q) values can be expressed as:

$$I_X = \sqrt{\frac{P}{2}} R(\Delta\tau + \delta_X) D \frac{\sin(\pi\Delta f T_I)}{\pi\Delta_f T_I} \cos(\pi\Delta f T_I + \Delta\phi) + n_I \qquad (4.1)$$

$$Q_X = \sqrt{\frac{P}{2}} R(\Delta\tau + \delta_X) D \frac{\sin(\pi\Delta f T_I)}{\pi\Delta_f T_I} \sin(\pi\Delta f T_I + \Delta\phi) + n_Q \qquad (4.2)$$

where:

- P is the received signal power;

- $R(\Delta\tau + \delta_X)$ is the correlation between the local spreading code and the incoming signal. With X representing the early, prompt and late replicas and δ_X the corresponding delay. In particular $\delta_X = -\frac{T_c}{2}$ for the early, $\delta_X = 0$ for the prompt and $\delta_X = +\frac{T_c}{2}$ for the late replica;

- D is the data bit sign;

- $\Delta\tau$ the misalignment between the local replica $\hat{\tau}$ and the received spreading code delay τ $(\Delta\tau = \tau - \hat{\tau})$;

- $\Delta\phi$ is the carrier phase delay misalignment$(\Delta\phi = \phi - \hat{\phi})$;

- Δf is the frequency error (Doppler) due to the relative motion between satellite and receiver $(\Delta f = f - \hat{f})$;

- n_I and n_Q are Gaussian noises.
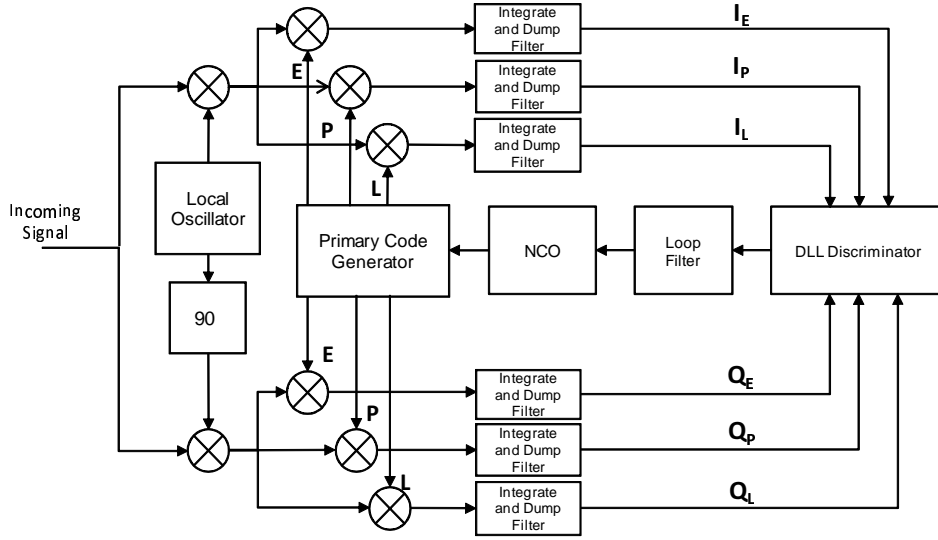
Figure 4.1: DLL architecture

The obtained correlation values are then fed to the code delay discriminator to obtain a measure of the misalignment between the received and the local code phases.

The choice of discriminator is very important, since it provides the estimate of the code tracking error and is responsible for adjusting the local replica code phase. Its gain, represented as the slope at the origin, depends on the type of discriminator, the signal modulation and the presence or absence of bit transitions in the PDI interval as described in [18] and [13]. The discriminator output is then used to steer the Numerically Controlled Oscillators (NCO) to adjust the code phase of the local replica.

At steady state the aim of the tracking block is to generate for each satellite j, a code replica whose phase $\hat{\tau}^j$, is the closest to the received signal code phase τ^j, or

equivalently $\Delta\tau = (\tau^j - \hat{\tau}^j) \to 0$. Considering a non-coherent discriminator, like the Early-minus-Late Power (EMLP), perfect knowledge of the carrier phase and data symbol is not required. The discriminator output is defined as:

$$D_{EMLP} = \frac{P}{2}\left[R^2\left(\Delta\tau + \frac{T_c}{2}\right) - R^2\left(\Delta\tau - \frac{T_c}{2}\right)\right] \cong K_d\Delta\tau \qquad (4.3)$$

where K_d is the gain of the discriminator, representing the slope of the discriminator at the origin and assumes a value dependent on the particular discriminator type and signal modulation.

The received signal is considered correctly tracked as long as $|\Delta\tau| \leq \frac{T_c}{2}$.

In a classical DLL configuration, no feedback from the navigation processor is foreseen and each block works independently from the others. Scalar receivers, in fact, process each channel independently, resulting in a relatively easy implementation that is robust against errors propagating from one channel to the other [48]. However, in highly dynamic scenarios or when the signals are severely attenuated, traditional tracking architectures are not able to keep track of the signals [49] [50].

Aiding at the tracking stage is employed to improve robustness against errors affecting the received signal that may cause the receiver to lose lock and require re-acquisition. In this context, different techniques that fuse information within the tracking loops have been the subject of widespread research efforts. Aiding can be supplied either by additional external sensors as in Ultra-Tight integration or by allowing assistance between the different channels and exploiting the connection between the signal delays and user position as in Vector Tracking Loops (VTL).

4.2 Ultra-Tight Integration

There are many possible ways to integrate a GNSS receiver with inertial platforms [21]. The level of integration depends on the available measurements, the requirements, the objective applications, and the receiver architecture according to which the data fusion takes place [18]. In 1.4 position level techniques have been briefly introduced but a deepest level of integration can be pursued by going inside the processing core of the GNSS receiver and entering into its tracking loop circuits. Hybridization of two completely different positioning systems, such as GNSS and an Inertial Navigation System (INS), is gaining increasing attention, especially in scenarios where reliable navigation is needed but radio signal detection is hindered by obstacles. The strength of integration schemes is in fact built upon the complementarities between these two navigation systems.

More in detail, INS are able to calculate the change of user position, velocity and attitude by measuring and processing user acceleration and angular rate [51], thereby, given a known initial condition, they can provide user position and velocity with continuity. Moreover, being entirely self-contained, they can be considered absolutely non-jammable. GNSS receivers, on the contrary, being based on satellite signal detection, depend on the correct reception of signals and are potentially subject to service outages. Furthermore, these two systems can balance out their errors. INS accuracy is limited by the quality of the inertial sensors used and by the knowledge of the Earth gravity field and rate. This is why INS performance tends to degrade in accuracy with time due to the integration drift: very small acceleration and angular rate biases that grow progressively into potentially unbounded errors in position after integration. GNSS, on the other hand, have bounded errors and offers good performance over long periods. Thus, fusion of the two systems can be very effective: high-fidelity GNSS position can be used to calibrate the INS and INS estimates can either substitute or be helpful to the GNSS measurements during signal drop-outs or in the case of radio frequency interference.

4.2.1   Inertial Navigation Systems

Inertial Navigation is a self-contained navigation technique in which measurements provided by two types of devices, accelerometers and gyroscopes, are used to track the position and orientation (attitude) of an object relative to a known initial state (position, velocity and orientation). An INS usually is composed by two functional parts: the first one is the Inertial Measurement Units (IMU), that typically contains three rate gyroscopes and three accelerometers mounted with mutually orthogonal sensitive axes which are able to measure the angular velocity ω and linear acceleration a respectively; the second part is the processing block, where the velocity and position are derived by mathematical integrations.

INS can either be gimballed or strap-down. The strap-down technology is so called because its sensors (both accelerometers and gyroscopes) are strapped to the object and they provide measurements with respect to the object reference frame called body frame (a^b, ω^b). Strap down technology is characterized by lower costs, the absence of gimbal locks, fewer calibrations phases and easier fabrication processes with respect to gimballed technology [51]. The navigation is performed with respect to the Cartesian ECEF (Earth-Centered, Earth-Fixed) frame that represents velocity v^e as (v_x^e, v_y^e, v_z^e) coordinates and positions r^e as (x^e, y^e, z^e) coordinates, where

the point (0, 0, 0) denotes the mass center of the Earth. A simplified block diagram representation of the INS mechanization is reported in figure 4.2.
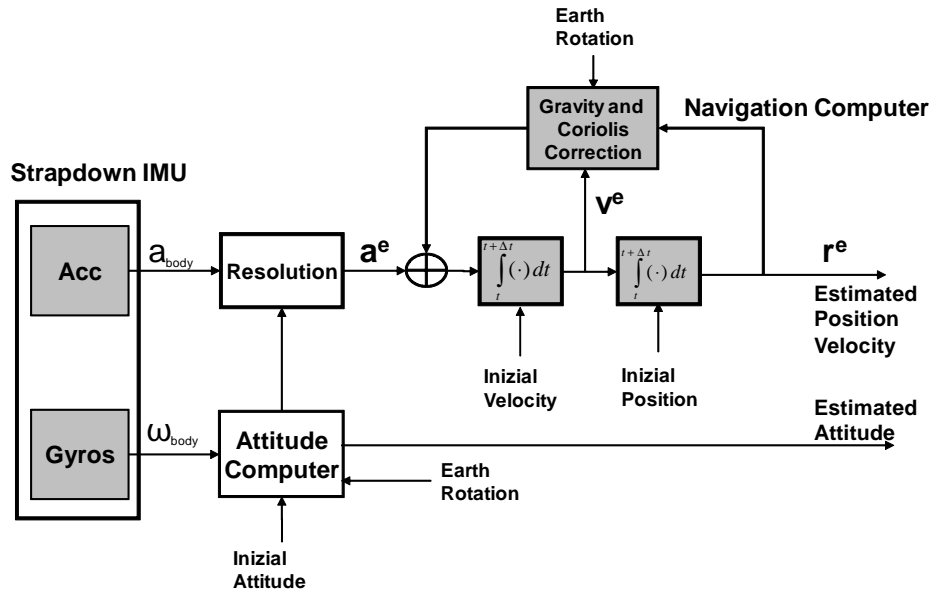
Figure 4.2: Inertial Navigation Systems mechanization

As pointed out earlier, INS measurements are affected by errors that cause INS-only navigation to degrade rapidly. The simplest INS error model takes into account only two error sources for accelerometers and gyroscopes. The first one is a constant bias that is the average output of the measuring devices when they are not undergoing any forces. The bias is expressed in $[m/s^2]$ for acceleration and in $[deg/h]$ for angular velocity. The effects of a constant bias error on acceleration, when double integrated, is an error in position which grows quadratically with time. The second error source considered,depends on thermo-mechanical noise which fluctuates at a rate much greater than the sampling rate of the sensors. As a result, the samples obtained from the sensors are perturbed by a disturbance which can be modeled as a white Gaussian noise sequence, with zero-mean and a finite variance σ_w^2.

Figure 4.3 reports the performance of a high quality INS where only accelerometers measurement errors are considered: the error budget for all three sensing axis consists in a constant bias equal to 50 μg and white noise characterized by a standard deviation (σ_w), equal to 5 μg/ Hz (g = 9.8 m/s^2). Due to the bias an initial position error at 20 s on the x-axis of about 10 cm grows to 10 m after 200 s.
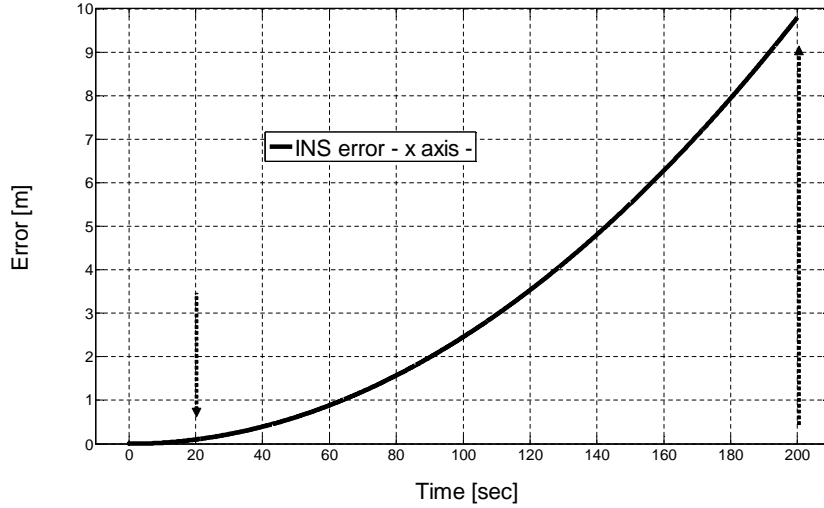
Figure 4.3: INS x axis error considering only accelerometer errors

4.2.2   Ultra-tight Integration Implementation

The conventional approach to perform the Ultra-tight integration consists in the use of the INS information to update the local replica into the tracking feedback [52]. However, despite providing a very strict combination of the two systems, this approach does not solve the problems of outages or jamming vulnerabilities.

Additionally an integration filter can be used to fuse the data provided by the inertial navigation system to calculate on the one hand the integrated navigation solution (i.e. the variations in user position and velocity) and on the other hand control the update of the oscillator and the tracking loop. The integration filter is thus responsible of fusing together the observations provided by the tracking block (either directly the outputs I and Q generated by the correlation process or the discriminator outputs) with a dynamic error model of the Inertial Measurement Unit (IMU) error states in a linear or non-linear Kalman filter formulation.

My contribution to Ultra-tight techniques is in the design of a novel scheme where an artificial peak is generated starting from the information coming from the INS, and then is non-coherently summed to the correlator outputs. By using this approach, the tracking loops are no longer vulnerable to signal outages or jamming, since they can rely solely on the synthetic INS information. The proposed ultra-tight approach, identified as Gaussian AUtocorrelation Scaled Sum (GAUSS), is based on the concept that a completely artificial autocorrelation peak can be generated starting from the information coming from the INS, as shown in figure 4.4. This

artificial peak is synthesized through a Gaussian function, centered at the delay estimated by the INS, μ_{INS}, and with a variance selected according to the early-late spacing ($\sigma^2_{INS} = \Delta$), as detailed in the following formula:

$$G(t) = \frac{1}{\sqrt{2\pi\sigma^2_{INS}}} \exp \frac{-(t - \mu_{INS})^2}{2\sigma^2_{INS}} \tag{4.4}$$

This synthetic correlation is calculated at two points, corresponding to the Early and Late branches, called G_E and G_L:

$$G_E = G(\tau_{GNSS} - \Delta) \tag{4.5}$$

$$G_L = G(\tau_{GNSS} + \Delta) \tag{4.6}$$

Therefore, two completely different sets of correlations are considered: the ones coming from the GNSS received signal, and the artificial ones created by the INS information. The correlations are then summed non-coherently, each one scaled by its estimated Mean Square Error (MSE). By combining together the two autocorrelation functions code tracking robustness and correlation sensitivity are greatly improved. The tracking discriminator D_{GAUSS} can be defined as:

$$D_{GAUSS} = \frac{MSE_{INS}D_{GNSS} + MSE_{GNSS}D_{INS}}{MSE_{INS} + MSE_{GNSS}} \tag{4.7}$$

where D_{INS} is the discriminator output obtained with the synthetic autocorrelation function and D_{GNSS} is the GNSS-only discriminator output:

$$D_{INS} = \frac{G_E^2 - G_L^2}{G_E^2 + G_L^2}$$

$$D_{GNSS} = \frac{(I_E^2 + Q_E^2) - (I_L^2 + Q_L^2)}{(I_E^2 + Q_E^2) + (I_L^2 + Q_L^2)} \tag{4.8}$$

Figure 4.4, is reported as an example of the GAUSS approach in ideal conditions (i.e. no errors affecting the received signal and INS perfectly calibrated and aligned with the GNSS receiver). As time progresses the INS synthetic correlation function will drift due to the errors affecting the measurements and will be accordingly weighted less in the combination. However, it is worthwhile noting that the impact of a calibrated INS is to sharpen, in the combined autocorrelation, the main correlation peak and filter out eventual distortions due to errors affecting the received signals.
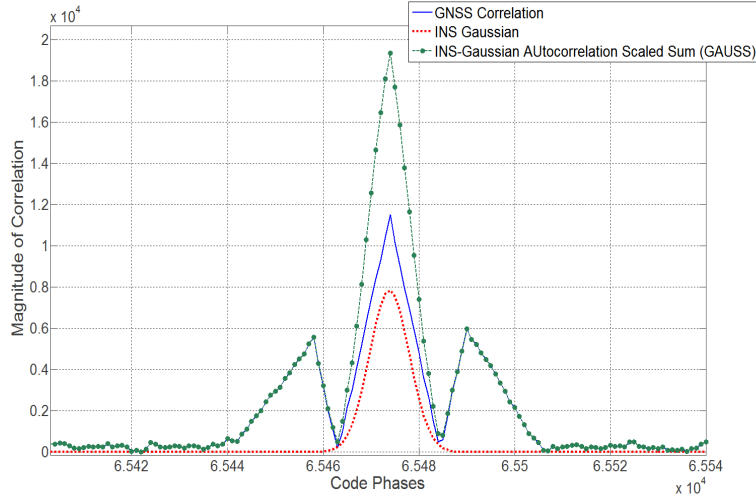
Figure 4.4: GAUSS approach correlation functions

This system can be straightforwardly inserted in the receiver processing chain before the classical Kalman filter or Least Square estimation for the GNSS PVT calculation, since it operates the hybridization completely inside the tracking loops, and does not require any outside optimization as reported in figure 4.5. Furthermore, this scheme is able to work without four satellites in visibility since the artificial Gaussian peak retains its significance even in the case of satellite blockage, thereby at least four pseudorange measurements can be provided at any time to the navigation processor.
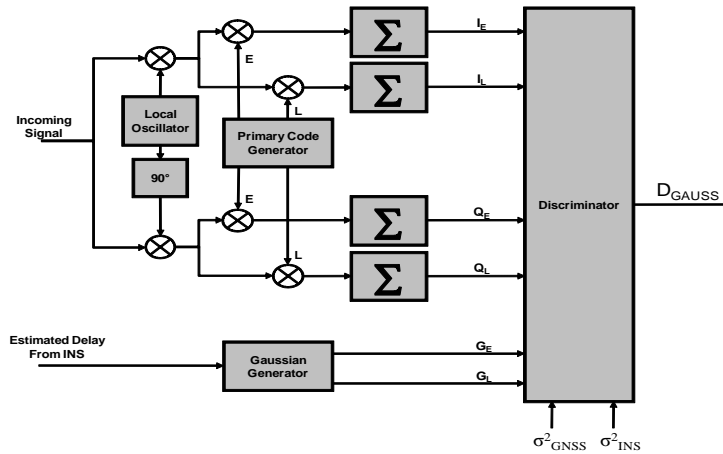
Figure 4.5: GAUSS schematic block diagram

4.2.3   Performance Evaluation

In order to evaluate the performance of the proposed technique both in terms of fractional timing estimate and position accuracy, simulations considering the tracking of the pilot channel $E1_C$ only will be reported in this section.

As for all integrations, the key aspect to be considered in this fusion scheme is the weight given to the information coming from the INS and the GNSS receiver. In order to improve performance the most reliable information must be weighted more in the integrated discriminator.

For the GNSS a second order loop with the following characteristics has been considered:

- Early Late Spacing $\Delta = 0.5$ chips

- Damping ratio $= 0.7$

- DLL Bandwidth: 5Hz

For the INS, errors affecting the measurements are not recalibrated during the simulations and no additional external aiding (e.g. mechanical altimeter or speedometer) is provided. In particular two different conditions, depending on the degradation stage (20s, 200s, after the initial calibration) are considered.

The simulations were carried out considering:

- Four satellites in visibility

- Signal to noise ratio C/N_0 dependent on the elevation angle (i.e. four satellites at 41, 52, 29, 48 dBHz)respectively

- Sampling frequency $f_s = 16$MHz

Figure 4.6 shows the tracking timing estimation behavior with and without INS aiding. It can be seen that the integrated output is heavily dependent upon the reliability of the INS. In case of a highly accurate INS solution, the integrated autocorrelation function follows closely the INS Gaussian, otherwise, it relies more closely on the GNSS correlation function.

In order to evaluate the impact of multipath on the tracking circuit and test the added robustness of the GAUSS approach a two-path case has been simulated. The reflected signal component has the following characteristics:

- Delay = 3e-7 sec
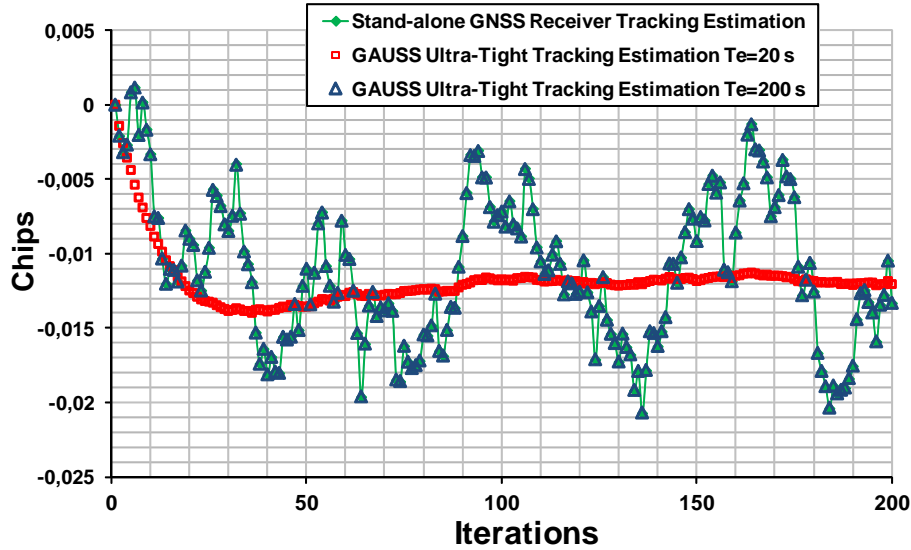
Figure 4.6: Tracking circuit fractional time estimation trend: GNSS stand alone Vs. GAUSS method

- Phase = 0 rad

- Signal to Multipath Ratio = 3dB

Figure 4.7 and figure 4.8, show the positioning performance at two different INS degradation conditions. It can be seen that by exploiting INS information, tracking performance can be greatly improved also in the presence of a strong reflected signal and that integration helps to enhance position accuracy even with less reliable INS information.

These results show that great improvements in terms of position accuracy can be achieved using the GAUSS approach when the INS information is very reliable. In the other cases, the GAUSS approach follows more closely the GNSS output. The optimization of the weights of GNSS and INS information in the integration is the key for achieving good performance in all application scenarios. Fine tuning of the discriminator value becomes thus a priority for future researches in this area.

With the advent of new satellite constellations for positioning, it is reasonable to hypothesize that at any given moment the receiver will have visibility of more than 4 satellites, therefore the problem of satellite blockage will be easily overcome without the need of exploiting INS information. However, the GAUSS approach can still offer compelling improvements since it can enhance receiver robustness by filtering out distortions to the autocorrelation function caused by errors.
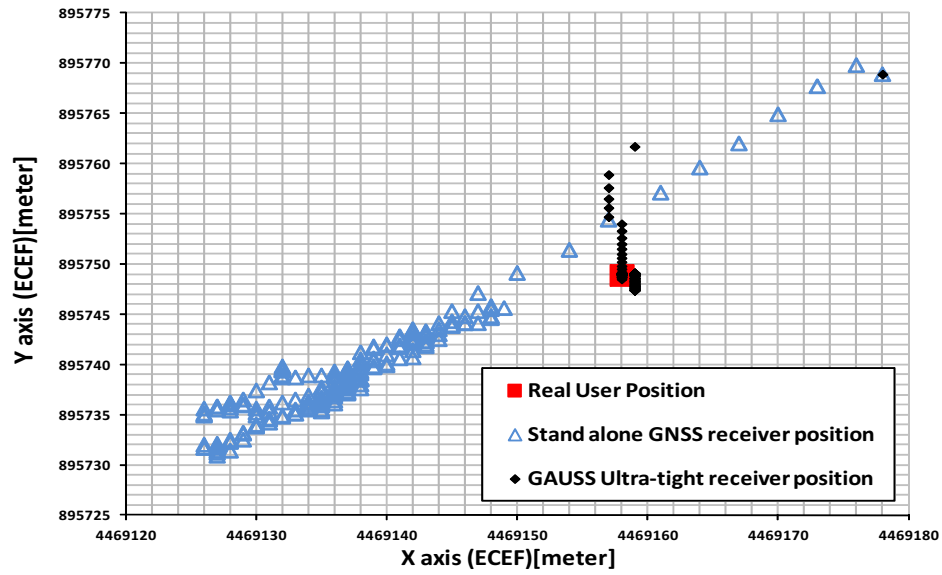
Figure 4.7: Multipath effects on the position accuracy. GNSS stand alone Vs. GAUSS method. Time elapsed after initial calibration T_e=20s
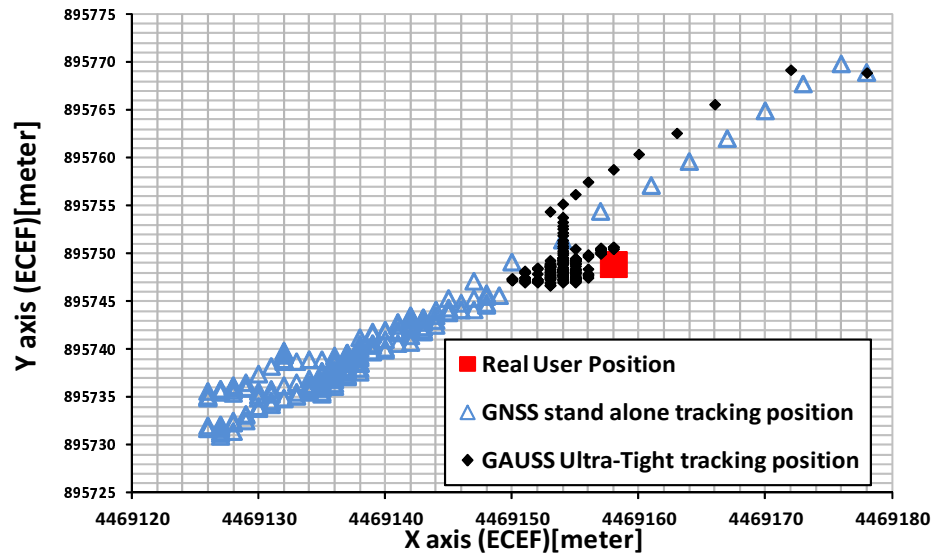
Figure 4.8: Multipath effects on the position accuracy. GNSS stand alone Vs. GAUSS method. Time elapsed after initial calibration T_e=200s

4.3   Vector Tracking Loops

Another alternative technique for code tracking aiding is the vector configuration. Differently from traditional receivers where all signals are processed by parallel independent blocks, vector tracking loops are based on processing all received signals collectively and using the navigation filter outputs as feedback to drive the loop code and carrier generators. By linking together all received signals through the receiver position it is in fact possible to exploit the stronger signals to aid the weaker ones thus helping them to remain locked even when affected by errors or strongly attenuated. The navigation processor becomes thus the block in charge of closing the tracking loops and providing the tracking control information to drive the NCO.

4.3.1   Vector Delay Lock Loops

The Vector Delay Lock Loops (VDLL) scheme is proposed in [53] as a way to combine the tracking of multiple channels and the navigation filter into a single algorithm. The idea at the base of VDLL is to use the user and satellite positions to predict the phases of the received PRN codes. With this architecture, instead of having two sets of shorter loops (one for the tracking DLL and the other for the navigation processor), one single block is responsible for tracking the received signals and for computing the navigation solution. The reason vector tracking is possible is built on the fact that all received signals are effectively linked together by the receiver position that can thus be used to steer the tracking loops of all the channels [54]. This way, information from the stronger satellite signals can be used to estimate the user position and in turn the weak signals can be predicted on the basis of user estimations [55].

Figure 4.9 reports the schematic of the VDLL block diagram where the input to the navigation block are the discriminator outputs and the feedback to the code generator is provided by the navigation solution. Since only code phase differences are provided to the navigation processor, the output solution is represented by position and clock bias drifts. Actual estimations of the user position and clock bias have to be updated and maintained outside of the navigation block.

4.3.1.1   VDLL Model

The use of vector configuration for tracking is especially advantageous in harsh scenarios, as in the presence of high dynamics and propagation errors affecting the
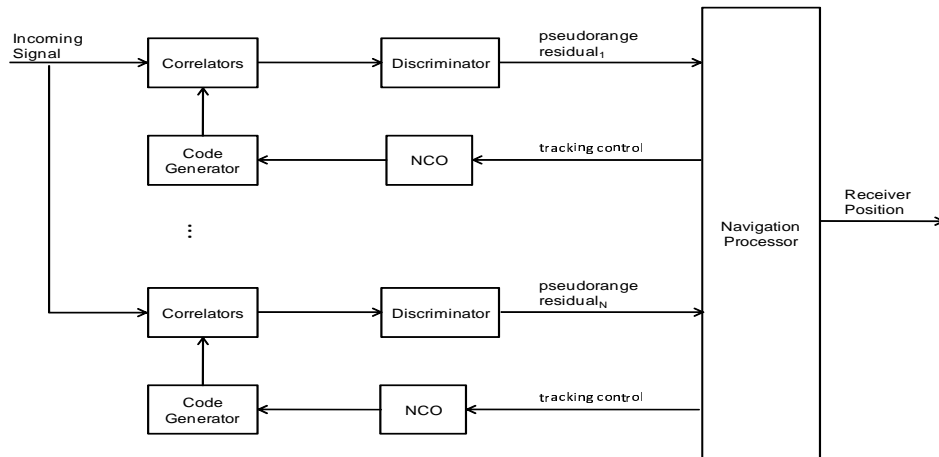
Figure 4.9: VDLL architecture

received signals, since local replicas are no longer updated independently for each channel but through the receiver position information and the aid of all received signals.

In VDLLs the feedback is generated from the user position that is computed either through a LS estimator or a Kalman filter. In order to initialize the estimators and commence vector tracking an initial position and at least four tracked satellites are essential. Thus, conventional tracking algorithms are needed to initialize vector tracking that can start only after lock is achieved ($|\Delta\tau| \leq T_c/2$).

While in scalar loops the local replica is determined using only information coming from the correlators and each singular contribution to the propagation delay is not considered separately but only as a sum; in vector loops the local replica is generated starting from the computed user position and clock bias and all error contributions should be accounted for and added in the feedback loop. In [53], the relationship between the DLL discriminator output and the user position is described in detail. However, literature lacks a clear definition of the local replica update operation, therefore, the analytical study of the feedback loop has been considered and reported in this section.

By considering a LS implementation it is possible to highlight the VDLL mechanization and the relationship between discriminator output and position drift.

At each iteration of the LS estimator, parameters are identified by the corresponding time instant. For each channel j, the discriminator output, computed by correlating the received signal with the local replica at time instant t_{i+1}, is $\Delta\tau_{i+1}^j$ and it provides information on the difference between the received signal propaga-

Figure 4.10: VDLL architecture with Least Squares

tion delay τ_{i+1}^j and the local replica delay $\hat{\tau}_i^j$. As shown in figure 4.10, the output provided by the discriminator is used to obtain an estimate of the state vector:

$$\Delta \hat{X}_i = S \Delta \tau_i \tag{4.9}$$

where:

$$S = (H^T H)^{-1} H^T \tag{4.10}$$

and H is the matrix linking the discriminator output to the position and clock bias variation as described in [53].

The F block represents a bank of loop filters, designed to track the user dynamics. They must be chosen as a trade-off between the ability of following high dynamics and the capacity of filtering noise $\Delta \tilde{X}_i = F \Delta \hat{X}_i$. The final block is responsible for computing the updated $\Delta \tau$ as:

$$\Delta \tau_i = H \Delta \tilde{X}_i \tag{4.11}$$

that will be used for the correlation at the next time step.

The local replica code phase $\hat{\tau}_i^j$, is obtained through the feedback of the previous time step computation.

At the receiver, the propagation delay from satellite j at time instant t_{i+1} can be defined as:

$$\tau_{i+1}^j = \frac{1}{c} \left(\sqrt{(x_{i+1} - x^j)^2 + (y_{i+1} - y^j)^2 + (z_{i+1} - z^j)^2} + (b_{i+1} - b^j) + I_{i+1}^j + T_{i+1}^j + n \right)$$

where:

- $(x_{i+1}, y_{i+1}, z_{i+1})$ is the receiver position at time instant t_{i+1};

- (x^j, y^j, z^j) is the satellite position at transmission time t_t;

- b_{i+1}^j is the satellite clock bias in meters;

- b_{i+1} is the receiver clock bias in meters at time instant t_{i+1};

- I_{i+1}^j and T_{i+1}^j are the ionospheric and tropospheric delay respectively;

- n is the receiver noise.

The propagation delay is thus a function of the satellite and receiver position, satellite and receiver clock bias and atmospheric delays.

Defining: $h(X_{i+1}) = \frac{1}{c}(\sqrt{(x^j - x_{i+1})^2 + (y^j - y_{i+1})^2 + (z^j - z_{i+1})^2} + (b_{i+1}))$ and the state vector $X_i = [x_i, y_i, z_i, b_i]^T$ it is possible to linearize the previous equation at the last available estimate X_i as:

$$
\begin{aligned}
\tau_{i+1}^j &= \frac{1}{c}\left(\sqrt{(x_{i+1}-x^j)^2+(y_{i+1}-y^j)^2+(z_{i+1}-z^j)^2}+(b_{i+1}-b_{i+1}^j)+I_{i+1}^j+T_{i+1}^j+n\right) \\
&= h(X_{i+1}) + \frac{1}{c}(-b_{i+1}^j + I_{i+1}^j + T_{i+1}^j + n) \\
&\cong h(\hat{X}_i) + \frac{\partial h(\hat{X}_i)}{\partial X_i}\Delta X_{i+1} + \frac{1}{c}(-b_{i+1}^j + I_{i+1}^j + T_{i+1}^j + n) \\
&= h(\hat{X}_i) + H\Delta X_{i+1} + \frac{1}{c}(-b_{i+1}^j + I_{i+1}^j + T_{i+1}^j + n) \qquad (4.12)
\end{aligned}
$$

where $H = \frac{\partial h(\hat{X}_i)}{\partial X_i}$ and $X_{i+1} = \hat{X}_i + \Delta X_{i+1}$.

ΔX_{i+1} is the difference between the real receiver position and clock bias and their last estimated values. Analogously, the local replica can be defined as:

$$
\hat{\tau}_i^j = h(\hat{X}_i) + \frac{1}{c}(-\hat{b}_i^j + \hat{I}_i^j + \hat{T}_i^j) \qquad (4.13)
$$

Therefore the discriminator output is computed as:

$$
\begin{aligned}
\Delta\tau_{i+1}^j &= \tau_{i+1}^j - \hat{\tau}_i^j \\
&= h(\hat{X}_i) + H\Delta X_{i+1} + \frac{1}{c}(-b_{i+1}^j + I_{i+1}^j + T_{i+1}^j + n) \\
&\quad - h(\hat{X}_i) - \frac{1}{c}(-\hat{b}_i^j + \hat{I}_i^j + \hat{T}_i^j) \\
&= H\Delta X_{i+1} + \Delta E \qquad (4.14)
\end{aligned}
$$

where:

- $\Delta X_{i+1} = X_{i+1} - \hat{X}_i$ the receiver position and clock bias correction from the last estimated state vector $\hat{X}_i$;

- ΔE are the error variations affecting the discriminator output (atmospheric errors, satellite clock bias, noise).

The local replica, is obtained using the last available delay estimation and the feedback from the navigation processor.

$$\hat{\tau}_i^j = \hat{\tau}_{i-1}^j + \Delta\hat{\tau}_i^j \tag{4.15}$$

In order to clarify the local replica update process, the partial computed values at the previous step t_i which is used to obtain the new timing estimate, will be defined in the following.

As already noted the discriminator output is given by:

$$\Delta\tau_i^j = \tau_i^j - \hat{\tau}_{i-1}^j = H\Delta X_i + \Delta E \tag{4.16}$$

Given the discriminator outputs from at least four channels $\Delta\tau_i = [\Delta\tau_i^j]_{j=1}^N$ and $N \geq 4$, the position and clock bias variations in ΔX_i are estimated in $\Delta\hat{X}_i$ and can be obtained as:

$$
\begin{aligned}
\Delta\hat{X}_i &= (H^T H)^{-1} H^T \Delta\tau_i \\
&= (H^T H)^{-1} H^T (H\Delta X_i + \Delta E) \\
&= \Delta X_i + (H^T H)^{-1} H^T \Delta E
\end{aligned}
\tag{4.17}
$$

The state vector at time step t_i is calculated by adding the innovation value $\Delta\hat{X}_i$ to the previous state:

$$
\begin{aligned}
\hat{X}_i &= \hat{X}_{i-1} + \Delta\hat{X}_i \tag{4.18} \\
\Delta\hat{X}_i &= \hat{X}_i - \hat{X}_{i-1} \tag{4.19}
\end{aligned}
$$

The impact of the discriminator output error on the state vector can be expressed using 4.18 as:

$$\Delta X_i - \Delta\hat{X}_i = \Delta X_i - \Delta X_i - (H^T H)^{-1} H^T \Delta E = -H(H^T H)^{-1} H^T \Delta E \tag{4.20}$$

The feedback to the code NCO is then provided by the position drift and clock bias variation obtained in 4.18:

$$\Delta\hat{\tau}_i = H\Delta\hat{X}_i = H(\Delta X_i + (H^T H)^{-1} H^T \Delta E) = H\Delta X_i + H(H^T H)^{-1} H^T \Delta E \tag{4.21}$$

By defining $\Delta\hat{\tau}_i$ the estimated value of $\Delta\tau_i$, the local replica code phase shift is updated for each channel j considering the j-th element of $\Delta\hat{\tau}_i$ as in the following. Using 4.12, 4.18, 4.20 and 4.21, through mathematical manipulation it can be

obtained:

$$
\begin{aligned}
\hat{\tau}_i^j &= \hat{\tau}_{i-1}^j + \Delta\hat{\tau}_i^j = \hat{\tau}_{i-1}^j + H\Delta\hat{X}_i \\
&= \hat{\tau}_{i-1}^j + H(\hat{X}_i - \hat{X}_{i-1}) \\
&= \hat{\tau}_{i-1}^j + H\Delta X_i + H(H^T H)^{-1} H^T \Delta E \\
&= \hat{\tau}_{i-1}^j + H(X_i - \hat{X}_{i-1}) + H(H^T H)^{-1} H^T \Delta E \\
&= h(\hat{X}_{i-1}) + \frac{1}{c}(-\hat{b}_{i-1}^j + \hat{I}_{i-1}^j + \hat{T}_{i-1}^j) + H(X_i - \hat{X}_{i-1}) + H(H^T H)^{-1} H^T \Delta E \\
&= h(X_i) + \frac{1}{c}(-\hat{b}_{i-1}^j + \hat{I}_{i-1}^j + \hat{T}_{i-1}^j) + H(H^T H)^{-1} H^T \Delta E \\
&= h(\hat{X}_i) + H(X_i - \hat{X}_i) + \frac{1}{c}(-\hat{b}_{i-1}^j + \hat{I}_{i-1}^j + \hat{T}_{i-1}^j) + H(H^T H)^{-1} H^T \Delta E \\
&= h(\hat{X}_i) + H(\hat{X}_{i-1} + \Delta X_i - \hat{X}_{i-1} - \Delta\hat{X}_i) + \frac{1}{c}(-\hat{b}_{i-1}^j + \hat{I}_{i-1}^j + \hat{T}_{i-1}^j) + H(H^T H)^{-1} H^T \Delta E \\
&= h(\hat{X}_i) + H(\Delta X_i - \Delta\hat{X}_i) + \frac{1}{c}(-\hat{b}_{i-1}^j + \hat{I}_{i-1}^j + \hat{T}_{i-1}^j) + H(H^T H)^{-1} H^T \Delta E \\
&= h(\hat{X}_i) - H(H^T H)^{-1} H^T \Delta E + H(H^T H)^{-1} H^T \Delta E + \frac{1}{c}(-\hat{b}_{i-1}^j + \hat{I}_{i-1}^j + \hat{T}_{i-1}^j) \\
&= h(\hat{X}_i) + \frac{1}{c}(-\hat{b}_{i-1}^j + \hat{I}_{i-1}^j + \hat{T}_{i-1}^j) \qquad (4.22)
\end{aligned}
$$

If no correction at the feedback are foreseen, the local replica might deviate from the received signal because atmospheric and satellite clock errors are not updated. To limit the impact of the additive propagation delays and error contributions, additional states can be introduced in the state filter vector [54], or navigation data information can be used to correct the delay estimation before the NCO [53], [56].

4.3.1.2   VDLL Implementations

The schemes proposed in the literature to realize a VDLL differ depending on the choice of navigation algorithm employed. Possible implementation may consider the LS or the Kalman Filter (KF). While the LS scheme has been amply described in 4.3.1.1, the Kalman filter implementation is reported in 5.2.

As demonstrated previously, since correlation is performed with the received uncorrected signal, the estimation of the atmospheric and satellite clock bias errors are instrumental in updating correctly the local replica. For a LS implementation in a single band receiver, it is not possible to augment the state vector by adding the error components as the estimator requires at least as many equations as unknowns. Therefore, in this case, error correction information should be inserted by using external assistance information, as shown in figure 4.10. On the other hand, in the KF scheme, two different solutions could be implemented: either satellite clock

information and ionospheric models can be used in the feedback generation [56], as in figure 4.11; or additional states can be considered (the KF can be used also in the presence of more unknowns that measurements).
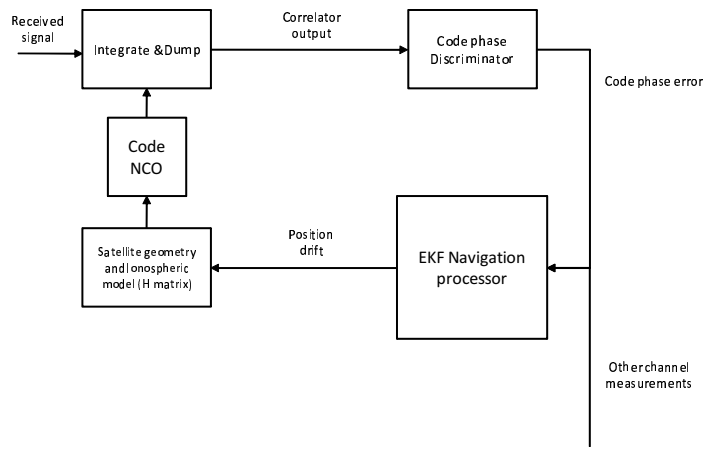
Figure 4.11: VDLL architecture with Least Squares

Chapter 5

Carrier Tracking

Correct signal demodulation is obtained by employing carrier tracking loops to replicate exactly the received signal carrier. Carrier tracking can be performed either through a FLL or a PLL. Their difference lies in the fact that while PLLs aim at replicating the exact phase and frequency of the received signal, FLLs replicate an approximate frequency allowing the phase to rotate.

5.1 Frequency Lock Loops

The FLL discriminator computes the frequency error collecting integrated and dumped I and Q samples at two consecutive times t_1 and t_2. The phase change in the considered interval is in fact proportional to the frequency error. To guarantee correct tracking the interval under consideration $(t_2 - t_1)$ should not straddle the data bit transition. However, since in the first synchronization phases, the receiver does not know the data bit boundaries, by considering a FLL it is easier to maintain lock. In a FLL the phasor given by the sum of I and Q rotates at a rate proportional to the frequency error. When frequency lock is achieved the phasor stops rotating but it may stop at any angle and thus cannot be used in combination with a coherent DLL [18].

In the following we consider a Dot-Cross discriminator that guarantees robustness against bit transitions:

$$cross = I_{PS1} \times Q_{PS2} - I_{PS2} \times Q_{PS1} \tag{5.1}$$

$$dot = I_{PS1} \times I_{PS2} + Q_{PS1} \times Q_{PS2} \tag{5.2}$$

$$D_{dotcross} = \frac{cross \times dot}{t_2 - t_1} \tag{5.3}$$

Analogously to code tracking, also for the frequency it is possible to consider a vector architecture where the receiver velocity is used to link together all received signals. In fact it is possible to define the link between Doppler frequency and velocity through :

$$f_j = \frac{f_T}{1+\dot{b}} \left[1 - \frac{1}{c}\left[(v_j - v)a_j\right]\right] \tag{5.4}$$

where f_T is the signal transmission frequency. The received signal frequency differs from the transmit frequency because of the relative motion of the user and the satellite and the user clock drift. v_j and a_j are the satellite velocity vector and the line-of-sight unit vector from the user to the satellite, respectively. The satellite velocity is calculated from the ephemeris in the data message. The user velocity vector is denoted as v and the user clock drift is $\dot{b}$ in units of seconds per second and is the rate at which the user diverges from GNSS system time.

5.2 Vector Frequency Lock Loop

A widely employed vector configuration considers both DLL and FLL in a common processing block. In this Vector Delay Frequency Lock Loop (VDFLL) architecture the vector tracking loops operate by receiving as input code phase error and Doppler frequency error and by using a KF to estimate user position, velocity, clock bias and clock drift and steer the code and carrier generators.

The filter system model used to describe the receiver motion can be expressed as:

$$X_i = \mathbf{F}_i X_{i-1} + \mathbf{B}_i w_i \tag{5.5}$$

where X_i is the filter state vector, $\mathbf{F}_i$ is the transition matrix and w_i are the uncertainties affecting the model.

The states of the central Kalman filter in the position-state formulation differ depending on the architecture and the application scenario. Typically, a P model is used in static scenarios while a PV model is used in dynamic scenarios. For the VDLL, only the position and clock bias states are required while the VDFLL requires additional velocity and clock drift states. In the following the PV model is considered:

$$
X_i = \begin{bmatrix} \Delta x_i \\ \Delta y_i \\ \Delta z_i \\ \Delta b_i \\ \Delta v x_i \\ \Delta v y_i \\ \Delta v z_i \\ \Delta \dot{b}_i \end{bmatrix}
$$

$$
\mathbf{F}_i = \begin{bmatrix}
1 & 0 & 0 & 0 & T & 0 & 0 & 0 \\
0 & 1 & 0 & 0 & 0 & T & 0 & 0 \\
0 & 0 & 1 & 0 & 0 & 0 & T & 0 \\
0 & 0 & 0 & 1 & 0 & 0 & 0 & T \\
0 & 0 & 0 & 0 & 1 & 0 & 0 & 0 \\
0 & 0 & 0 & 0 & 0 & 1 & 0 & 0 \\
0 & 0 & 0 & 0 & 0 & 0 & 1 & 0 \\
0 & 0 & 0 & 0 & 0 & 0 & 0 & 1
\end{bmatrix}
$$

where b is the bias expressed in meters due to the clock misalignment between receiver and satellites, $\dot{b}$ is the clock drift and $T = t_i - t_{i-1}$ is the time interval between two consecutive estimations.

The process noise in the system comes from two sources: receiver dynamics and clock noise. The dynamic noise sources (w_x, w_y, w_z) drive their respective velocity states while the user local clock phase and frequency error (w_b, w_d) impact on the clock bias and clock drift.

$$
w_i = \begin{bmatrix} w_x \\ w_y \\ w_z \\ w_b \\ w_d \end{bmatrix}
$$

$$\mathbf{B}_i = \begin{bmatrix} T & 0 & 0 & 0 & 0 \\ 0 & T & 0 & 0 & 0 \\ 0 & 0 & T & 0 & 0 \\ 0 & 0 & 0 & 1 & T \\ 1 & 0 & 0 & 0 & 0 \\ 0 & 1 & 0 & 0 & 0 \\ 0 & 0 & 1 & 0 & 0 \\ 0 & 0 & 0 & 0 & 1 \end{bmatrix}$$

where w_i is a Gaussian noise process with zero mean and variance $\mathbf{Q}_i$.

$$\mathbf{Q}_i = \begin{bmatrix} \sigma_x^2 & 0 & 0 & 0 & 0 \\ 0 & \sigma_y^2 & 0 & 0 & 0 \\ 0 & 0 & \sigma_z^2 & 0 & 0 \\ 0 & 0 & 0 & \sigma_b^2 & 0 \\ 0 & 0 & 0 & 0 & \sigma_d^2 \end{bmatrix}$$

The values for $\sigma_x^2, \sigma_y^2, \sigma_z^2$ are chosen based on the expected level of receiver dynamics, while σ_b^2, σ_d^2 account for the clock oscillator errors.

The state filter estimate is corrected by the available measurements. In the following pseudorange and pseudorange-rate residuals are used in the measurement model equation. At the end of every integrate and dump operation, the correlator outputs are used by the code phase and frequency discriminator to produce a code phase and Doppler frequency residual. The code phase error is scaled to convert it to units of meters and similarly, the Doppler frequency residual is scaled to convert it to units of meters per second. The scaled code phase error represents the error in the predicted line-of-sight range from the satellite to the receiver plus the receiver clock bias (pseudorange residual) and the scaled Doppler frequency is the error in the predicted line-of-sight velocity from the satellite to the receiver plus the receiver clock drift (pseudorange-rate residual) [54].

$$z_i = \mathbf{H}_i X_i + n_i \tag{5.6}$$

where z_i is the vector of available measurements, $\mathbf{H}_i$ is the measurement model

matrix and n_i is the observation noise process.

$$z_i = \begin{bmatrix} \Delta\rho_1 \\ \vdots \\ \Delta\rho_N \\ \Delta\dot{\rho}_1 \\ \vdots \\ \Delta\dot{\rho}_N \end{bmatrix}$$

$$\mathbf{H}_i = \begin{bmatrix} a_x^1 & a_y^1 & a_z^1 & 0 & 0 & 0 & 1 & 0 \\ \vdots & \vdots & \vdots & \vdots & \vdots & \vdots & \vdots & \vdots \\ a_x^N & a_y^N & a_z^N & 0 & 0 & 0 & 1 & 0 \\ 0 & 0 & 0 & a_x^1 & a_y^1 & a_z^1 & 0 & 1 \\ \vdots & \vdots & \vdots & \vdots & \vdots & \vdots & \vdots & \vdots \\ 0 & 0 & 0 & a_x^N & a_y^N & a_z^N & 0 & 1 \end{bmatrix}$$

where a_x^j, a_y^j, a_z^j are the components of the line-of-sight unit vector from the user to the j-th satellite. The measurement noise is modeled as Gaussian noise with zero mean and covariance R_i.

The measurements provided by the different channels are linked together through the navigation solution as shown in the $\mathbf{H}_i$ matrix. Pseudoranges are linked together through the user position and pseudorange-rates through the velocity.

Position and velocity estimates are then used to predict the control information for the code and carrier NCO.

5.3 Phase Lock Loops

The carrier wipe-off could also be performed considering PLLs and thus following the phase variations caused by variations in the satellite and receiver positions. The basic block diagram is given in figure 5.1, where the PRN code is eliminated by considering the DLL prompt replica signal.

The discriminator block is used to find the phase error on the local replica. The output of the discriminator is then filtered to remove the noise and used to generate the feedback for the NCO. The choice of discriminators depends on signal parameters and the presence or absence of data bits. The classical arctangent (Atan) discriminator provides robustness against data bit transitions:
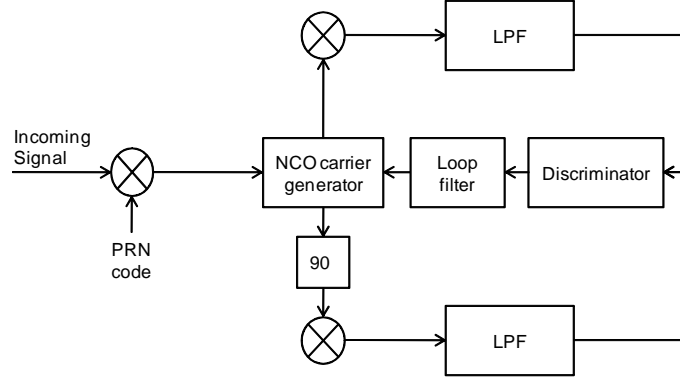
Figure 5.1: Phase Lock Loop block diagram

$$D_{Atan} = \arctan \frac{Q_P}{I_P} = mod(\phi_i^j - \hat{\phi}_i^j, 2\pi) = mod(\Delta\phi_i^j, 2\pi) \qquad (5.7)$$

where:

- Q_P is the signal quadra-phase prompt correlation component;

- I_P is the signal in-phase prompt correlation component;

- ϕ_i^j is the phase of the received carrier from the j satellite at time instant t_i;

- $\hat{\phi}_i^j$ is the phase of the local replica carrier j at time instant t_i.

By defining:

$$\delta\phi_i^j = mod(\phi_i^j, 2\pi) \qquad (5.8)$$

$$\delta\hat{\phi}_i^j = mod(\hat{\phi}_i^j, 2\pi) \qquad (5.9)$$

$$\delta\phi_i^j = (\delta\phi_i^j - \delta\hat{\phi}_i^j) = mod(\Delta\phi_i^j, 2\pi) \qquad (5.10)$$

then the discriminator output can be defined as $D_{Atan} \propto \delta\phi_i^j$.

Therefore the discriminator output gives information about the fractional phase misalignment between the received and local signal. At steady state, in order to guarantee perfect lock, the discriminator output D_{Atan} must be as small as possible. The phase tracking phase can thus be used to compute to a high precision the relative changes in user position. In order to be able to compute the user absolute position, however, also the phase integer ambiguity must be resolved.

5.4 Vector Carrier Lock Loops

The feedback provided by the navigation filter position solution could, in principle, be used both for predicting code and carrier phases. Nevertheless, it is worth noting that carrier phase tracking poses additional challenges. The receiver estimated position, in fact, is not sufficiently accurate to unambiguously predict the phase of the carrier signals, because of the impact of propagation errors and satellite clock bias. The demand for position accuracy become thus quite stringent and hard to provide in order to guarantee that the errors affecting the position estimate are in the cm-level order [57].

Because of the difficulties in implementing a pure VPLL, the literature lacks a common baseline and different schemes have been proposed.

In [58], [59], an approximate VPLL is implemented through a cascaded scheme, where the carrier NCOs are controlled by a local Kalman filter and the navigation filter. In this configuration, each channel has an associated local filter that estimates the channel tracking errors, as presented in figure 5.2. The advantage of this technique is two-fold: first, depending on the implementation of the local filter, the order of the navigation filter state vector can be reduced; second, the output from the local filter can be sent to the navigation filter at a lower rate, thus improving efficiency. In particular the local Kalman filter could only be used for carrier phase feedback, since the navigation solution accuracy is insufficient without corrections for carrier phase tracking. Aiding to the phase tracking can nonetheless be provided in the form of VFLL assistance.

Different system and measurement models for the local filter and their impact in terms of carrier phase tracking are investigated in [48].

In [60] a VPLL architecture is presented. In the Co-op architecture the common navigation filter (G) receives phase information in input and computes the user position and clock bias. The user state estimates are then filtered to remove noise and transformed to get the frequency correction for the NCO. In order to consider also the atmospheric delays impacting on the received signals, each individual channel has one additional filter for computing these residual effects. The two control information are thus summed together to steer the carrier NCO as shown in figure 5.3.

In the proposed scheme there are N scalar DLL loops dedicated to the received signals while the phase tracking is performed by considering two different types of PLLs: one dedicated to tracking the user dynamics (common filter) and the other
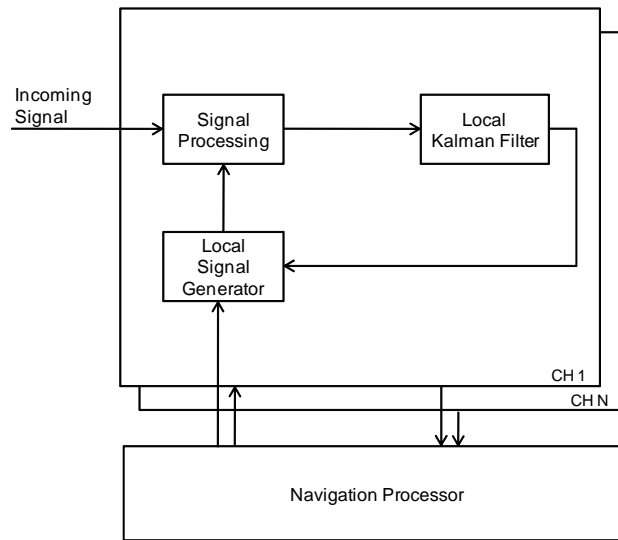
Figure 5.2: Vector-based cascaded architecture
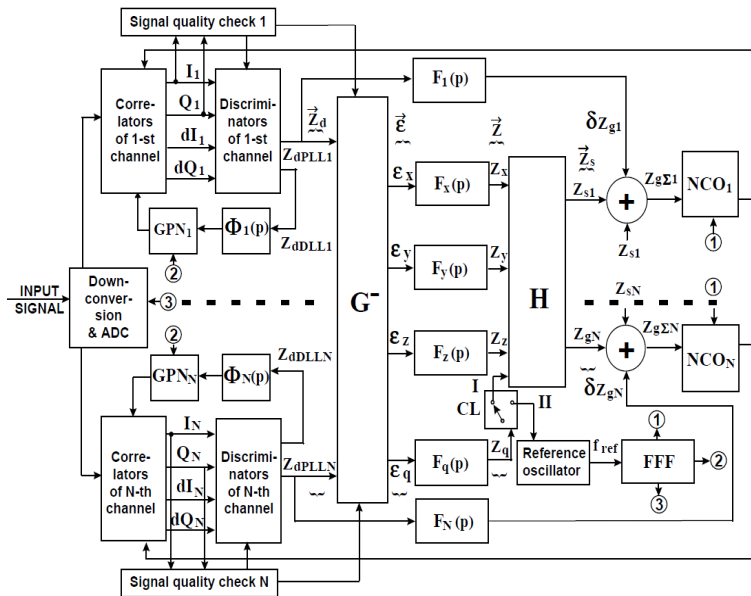
Figure 5.3: Co-op tracking architecture

dedicated to tracking satellite dynamics and atmospheric errors and perturbations (individual tracking loops). The two different contributions are separated by considering their different dynamics and choosing different filter bandwidths. The relative receiver motion and the receiver oscillator, require to follow higher dynamics than the other effects (e.g. atmospheric effects, satellite oscillator), therefore the bandwidth of the common carrier tracking is selected much wider and of higher order than the individual tracking loops filters. Performance of this tracking configuration are presented in [60] considering a vector and a standard stationary receivers with the same noise levels and oscillators. The Co-op scheme operates similarly to a VFLL aided PLL, since the feedback to the carrier generator is provided by both the common filter but also the independent PLL loops.

In [61], [62], the authors propose a Multi-carrier Multi-Satellite VPLL (MC-MS-VPLL) to deal with ionosphere scintillation and improve tracking performance. Redundancies are exploited decomposing each satellite signal into its physical components:

$$X = [\Delta x, \Delta y, \Delta z, \Delta b, \Delta I^1, \dots, \Delta I^N, \Delta T_z] \tag{5.11}$$

where:

- $(\Delta x, \Delta y, \Delta z, \Delta b)$ are the drifts in the user position and clock;

- $(\Delta I^1, \dots, \Delta I^N)$ are the ionospheric drift (tracked separately for each channel);

- ΔT_z is the tropospheric drift (tracked as zenith delay then transformed into delays by mapping functions).

The authors propose a LS scheme similar to the the ones presented by [56] and [53]. In this case it is possible to accommodate all additional states in the vector since more than one measurement are available per satellite. The filtered position error, clock drift, and atmospheric errors are transformed back into phase errors which are then accumulated in the NCO. This VPLL scheme, however, does not consider the impact of the satellite clock bias on the discriminator output. Performance are reported using simulated data only.

5.4.1 Conclusion

In order to refine carrier phase tracking, the best solution seems to be to use aiding from the Vector Frequency Lock Loop (VFLL) in a VFLL-assisted PLL architecture thus combining the robustness of vector frequency tracking that exploits cross-channel aiding with the accuracy of PLL carrier phase tracking. This combination

feeds the carrier NCO with outputs from both the VFLL and PLL discriminators and filters. This way the VFLL is in charge of tracking the line-of-sight (LOS) dynamics and the PLL has just to track the residual carrier mismatch

5.5   Vector architecture: advantages and drawbacks

The main advantages offered by the vector architectures relate to the possibility of aiding between the different channels:

- Noise reduction: the threshold energy that guarantees tracking of the signal without loss of lock can thus be lowered and satisfactory performance can be obtained even in the presence of degraded signals;

- Robustness to temporary blockages: if a sufficient number of satellites remains in view, tracking can operate with momentary blockages of one or more satellites, since the stronger signals can output sufficiently good estimates [53]. After restoring connection with the blocked satellite, it is necessary to perform re-acquisition of the signal but over a reduced uncertainty region and guarantee robust lock before reconnecting it to the common filter;

- Better optimization: since a single loop substitutes the tracking and navigation phases, a global optimum solution is computed while traditional scalar tracking-loops track each satellite signal independently followed by a separate navigation solution processing;

- Performance improvement with respect to scalar loops: obtained from the efficient use of the redundant number of available satellites and their geometry. The improved performance of vector tracking algorithms over scalar tracking loops in terms of variance in the pseudorange and pseudorange-rate estimates are proposed in [54] and in [63] for fading signals, through a weighted least squares example. The improvement in the vectorized architecture is due to the coupling of the measurements and due to several different variables, like the number of satellite signals available and the geometry of the visible satellite constellation. In the case of four visible satellites, the two approaches yield the same results.

The primary drawback is that all satellites are intimately related, and any error in one channel can potentially adversely affect other channels. It is therefore of

great importance the monitoring of the received signal quality at the output of the correlator in order to disconnect the corrupted signals from the common loop. The quality check can be performed by considering the in phase and quadrature signals at the output of the correlator. For every monitoring technique, however, a delay before the exclusion of a channel must be considered. The filter matrices are then recalculated for the remaining channels [60].

Conclusions and Future Developments

This thesis has addressed the problem of aiding techniques for GNSS receivers operating both at the position and at the physical level. In particular the feasibility and advantages offered by the proposed aiding schemes have been analyzed and discussed.

The first part of the dissertation has tackled the problem of improving receiver availability in challenging scenarios where satellite visibility is limited. In Chapter 1 traditional positioning techniques have been presented and aiding schemes introduced by describing their framework and some of the implementations proposed in literature. In Chapter 2, novel positioning techniques relying on peer-to-peer interaction and exchange of information have been introduced. More specifically two different schemes have been proposed: the PSA technique, based on the exchange of GNSS data, that allows to obtain coarse positioning even in the cases where the user has scarce satellite visibility, and the Hybrid approach, which permits to improve the accuracy of the positioning solution. Performance have been assessed also considering the impact on performance of the presence of professional receivers in the network.

The second part of this thesis investigates the issue of aiding techniques at the physical level to improve receiver synchronization with satellite signals. In Chapter 3, code acquisition strategies have been presented and a novel code acquisition strategy for dual-band receivers has been introduced. The presented CBA approach is based on the principle that the navigation signals in the two bands are transmitted using a common time reference, therefore, it is possible to exploit the reference provided by the synchronization process in a band to reduce the extent of the UR time dimension in the other band, performing the acquisition procedures in the two bands sequentially. The acquisition strategy has thus been described in detail considering

the advantages of different information exchange policies between the two bands. In Chapter 4, the problem of code tracking has been introduced and an innovative ultra-tight integration scheme based on the synthesis of an artificial correlation peak has been proposed and discussed. VDLL architectures have also been analyzed as a viable solution to improve tracking robustness and particular attention has been devoted to the description and analysis of the feedback generation. In Chapter 5, the feasibility of VPLL schemes has been introduced and different implemented solution presented and discussed.

This thesis has dealt with the design and analysis of aiding techniques that have become and will continue to be a definite trend for research in the GNSS context. By identifying gaps in GNSS performance many viable solutions that rely on fusing together different systems can be proposed. In the future, the diffusion of multi-system capable devices and the introduction of new positioning systems and technologies will provide easy access to a well of assistance information that can be effectively merged in a single device to enjoy the benefits of each available system. In particular the idea of peer-to-peer positioning offers the means for developing many new applications. Even though in this thesis cooperation has been considered only at position level, interesting results can be achieved also considering exchange of assistance information at the physical level and more specifically the acquisition phase. Indeed, the sharing of timing and frequency information between peers in a network can limit considerably the time needed for the initial synchronization. However, several critical issues will have to be taken in due consideration to ensure that the full potential of P2P techniques is exploited. Particular attention will have to be addressed to the design of suitable energy-aware communication protocols for information exchange, coordination and monitoring of the network of devices and user incentives to foster cooperation and disincentives to avoid malicious behavior. Also vector configurations will continue to be the focus of many research efforts. A particularly challenging application environment that would profit from the exchange of information between strong and weak channels is the presence of ionospheric scintillations that causes deep power fades and rapid changes in the signal phases thus impacting severely on phase lock loop (PLL) circuits. The robustness of the carrier tracking phase could definitely improve by using VDFLL feedback information that relies on the combined processing of all received signals. Moreover, integration schemes based on the fusion of information coming from different systems will continue to be the topic of investigation. A trend, that has not been considered in

this thesis but will nevertheless offer very interesting applications, will be the exploitation of Signal of Opportunity (SoO) for localization purposes; that is, the use for positioning purposes of already deployed radio-communication wireless systems. SoO will garner a lot of attention in the future since it allows to take advantage of the pervasive presence of SoO emitters, especially in densely populated areas, and their high radiated power, to improve coverage and availability, complementing nicely GNSS systems in urban and indoor scenarios [64] [65].

Personal Publications

[1] F. Bastia, L. Deambrogio, C. Palestini, R. Pedone, M. Villanti, and G. E. Corazza, "Hierarchical Code Acquisition for Dual Band GNSS Receivers," *Proceedings of IEEE/ION Position Location and Navigation Symposium (PLANS2010)*, May 2010.

[2] L. Deambrogio, F. Bastia, C. Palestini, R. Pedone, M. Villanti, and G. E. Corazza, "Cross-band aided code acquisition in dual band gnss receivers," *Submitted to IEEE Trans. on Aerospace and Electronic Systems*, November 2011.

[3] C. Palestini, L. Deambrogio, F. Bastia, and G. E. Corazza, "An Insider View on Tracking Loops: a Novel Ultra-Tight GNSS/INS Hybridization Approach," *Proceedings of IEEE/ION Position Location and Navigation Symposium (PLANS2010)*, May 2010.

[4] L. Deambrogio, O. Julien, C. Macabiau, and G. E. Corazza, "Improvement of carrier tracking robustness in the presence of degraded gnss signals using vector tracking loops," *Abstract accepted for the IEEE/ION Position Location and Navigation Symposium (PLANS2012)*, April 2012.

[5] I. Thibault, G. E. Corazza, and L. Deambrogio, "Random, Deterministic, and Hybrid Algorithms for Distributed Beamforming," *Proceedings of IEEE Advanced Satellite Multimedia Systems Conference (ASMS/SPSC 2010)*, September 2010.

[6] L. Deambrogio, C. Palestini, , F. Bastia, G. Gabelli, G. E. Corazza, and J. Samson, "Impact of High-End Receivers in a Peer-To-Peer Cooperative Localization System," *Proceedings of IEEE Ubiquitous Positioning, Indoor Navigation and Location-Based Service (UPINLBS 2010)*, October 2010.

[7] I. Thibault, G. E. Corazza, and L. Deambrogio, "Phase Synchronization Algorithms for Distributed Beamforming with Time Varying Channels in Wireless

Sensor Networks," *Proceedings of IEEE International Wireless Communications and Mobile Computing Conference (IWCMC 2011)*, July 2010.

[8] G. Gabelli, L. Deambrogio, C. Palestini, , F. Bastia, G. E. Corazza, and J. Samson, "Cooperative Code Acquisition based on the P2P Paradigm," *Proceedings of ION International Technical Meeting (ION ITM 2012)*, January 2012.

Bibliography

[9] EC FP7 GALILEO Research and Development Activities (Second Call Area 1B), *FP7 GAMMA-A (Galileo Receiver for Mass Market Applications in the Automotive Area)*.

[10] ESA contract no. 22868/09/NL/AT, *P2P Positioning*.

[11] ASI Project, *SWAN (Sistemi softWare per Applicazioni di Navigazione)* .

[12] R. E. Kalman, "A new approach to linear filtering and prediction problems," *Transactions of the ASME-Journal of Basic Engineering*, vol. 82, no. Series D, pp. 35–45, 1960.

[13] K. Borre, D.M. Akos, N. Bertelsen, P. Rinder, and S.H. Jensen, *A Software-Defined GPS and Galileo Receiver: A Single-Frequency Approach*, Springer, 2007.

[14] G.F. Welch and G. Bishop, "An introduction to the kalman filter," Tech. Rep., University of North Carolina, Chapel Hill, NC, USA, 1995.

[15] P. Closas Gomez, "Bayesian Signal Processing Techniques for GNSS Receivers:from multipath mitigation to positioning," *PhD Thesis, Department of Signal Theory and Communications, Universitat Politecnica de Catalunya*, 2009.

[16] K. Kovach, "New User Equivalent Range Error (UERE) Budget for the Modernized Navstar Global Positioning System (GPS)," *Proceedings of Institute Of Navigation National Technical Meeting (ION NTM 2000)*, pp. 550–573, Jan 2000.

[17] GPS Joint Program Office, "NAVSTAR GPS USER EQUIPMENT (Public Release Version)," Feb 1991.

[18] E.D. Kaplan, *Understanding GPS, Principles and Applications*, Artech House, Boston, 1996.

[19] A. Klobuchar, "Ionospheric Effects on GPS," *GPS world*, 1991.

[20] H. Isshiki and J. Wang, "Estimation of ionospheric delays in dual frequency gnss positioning," *Artificial Satellites*, vol. 43, no. 1, 2008.

[21] A. Wieser, D. Gebre-Egziabher, G. Lachapelle, and M. Petovello, "Weighting GNSS Observations and Variations of GNSS/INS Integration," *Inside GNSS*, pp. 26–33, 2007.

[22] K. Kuusniemi, G. Lachapelle, and J. Takala, "Position and velocity reliability testing in degraded gps signal environments," *GPS Solutions*, pp. 226–237, October 2004.

[23] GSSF Team, "Galileo system simulation facility - appendix - gssf reference scenarios," *GSSFP2.OM.001*, 2005.

[24] Y. Benigue, B. Forte, S. Radicella, H.J. Strangeways, V. Gherm, and N. Zernov, "Scintillations effects on satellite to earth links for telecommunication and navigation purposes," *Annals of Geophysics, Supplement to Vol. 47*, pp. 1179–1199, 2004.

[25] F. Berefelt, B. Boberg, J. Nygards, P. Stromback, and S.L. Wirkander, "Collaborative GPS/INS Navigation in Urban Environment," *Proceedings of the 2004 National Technical Meeting of the Institute of Navigation (ION GNSS 2004)*, January 2004.

[26] P. Groves, *Principles of GNSS, Inertial, and Multisensor Integrated Navigation Systems*, Artech House, 2008.

[27] M.S. Grewal, L.R. Weill, and A.P. Andrews, *Global Positioning Systems, Inertial Navigation, and Integration. Second Edition*, Wiley, 2007.

[28] I. Kraemer and B. Eissfeller, "A-GNSS. A Different Approach.," *Inside GNSS*, pp. 52–61, 2009.

[29] D. Skournetou and E.S. Lohan, "Ionosphere-corrected range estimation in dual frequency global navigation satellite systems receivers," *IET Radar, Sonar and Navigation*, vol. 5, no. 3, pp. 215–224, 2011.

[30] H. L. Van Trees, *Detection, Estimation, and Modulation Theory. Part I: Detection, Estimation, and Linear Modulation Theory*, John Wiley and Sons, Inc., New York, 1968.

[31] B.J. Kang and I.K. Lee, "A performance comparison of code acquisition techniques in DS-CDMA system," *Wireless Personal Communications*, vol. 25, pp. 163 – 176, 2003.

[32] G.E. Corazza, "On the MAX/TC Criterion for Code Acquisition and Its Application to DS-SSMA Systems," *Communications, IEEE Transactions on*, vol. 44, no. 9, pp. 1173–1182, Sep 1996.

[33] E. Pajala, E.S. Lohan, and M. Renfors, "CFAR detectors for hybrid-search acquisition of Galileo signals," *Proceedings of European Navigation Conference (ENC-GNSS 2005)*, July 2005.

[34] F. van Diggelen, *A-GPS: Assisted GPS, GNSS, and SBAS*, Artech House, Boston, 2009.

[35] G. Gabelli, L. Deambrogio, C. Palestini, , F. Bastia, G.E. Corazza, and J. Samson, ," *Proceedings of Institute of Navigation International Technical Meeting (ION ITM 2012)*, January 2012.

[36] L. Lo Presti, D. Margaria, and J. Samson, "A novel peer to peer aided acquisition strategy tailored to galileo e1 receivers," *Proceedings of 52nd International Symposium ELMAR-2010*, September 2010.

[37] D. Margaria, L. Lo Presti, N. Kassabian, and J. Samson, "A new peer-to-peer aided acquisition approach exploiting c/no aiding," *Proceedings of 5th ESA Workshop on Satellite Navigation Technologies - NAVITEC 2010*, December 2010.

[38] P. Luo and M.G. Petovello, "Collaborative acquisition of weak gps signals," *Proceedings of IEEE/ION Position Location and Navigation Symposium (PLANS 2010)*, May 2010.

[39] J.W. Betz, "Binary Offset Carrier Modulations for Radionavigation," *Journal of The Institute of Navigation*, vol. 48, no. 4, pp. 227–246, Winter 2001-2002.

[40] E.S. Lohan, A. Lakhzouri, and M. Renfors, "Binary-offset-carrier modulation techniques with applications in satellite navigation system," *Wiley Journal of*

Wireless Communications and Mobile Computing, vol. 7, pp. 767 – 779, July 2006.

[41] "Signal in Space Interface Control Document," Tech. Rep. OS SIS ICD, Draft 1, GNSS Supervisory Authority, Feb. 2008.

[42] N.C. Shivaramaiah and A.G. Dempster, "The Galileo E5 AltBOC: Understanding the Signal Structure," *International Global Navigation Satellite Systems Society Symposium (IGNSS 2009)*, December 2009.

[43] A. Polydoros and C.L. Weber, "A Unified Approach to Serial Serach Spread-Spectrum Code Acquisition-Part I: General Theory," *Communication, IEEE Transactions on*, vol. COM-32, n.5, pp. 542–549, May 1984.

[44] A. Polydoros and C.L. Weber, "A Unified Approach to Serial Search Spread Spectrum Code Acquisition -Part II: A matched-filter receiver," *Communication, IEEE Transactions on*, vol. COM-32, n.5, pp. 550–560, May 1984.

[45] N.C. Shivaramaiah and A.G. Dempster, "An Analysis of Galileo E5 Signal Acquisition Strategies," *Proceedings of the European Navigation Conference (ENC-GNSS 2008)*, December 2008.

[46] D. Margaria, F. Dovis, and P. Mulassano, "An innovative Data Demodulation Technique for Galileo AltBOC Receivers," *Journal of Global Positioning Systems*, vol. 6, 2007.

[47] M. Villanti, P. Salmi, and G.E. Corazza, "Differential Post Detection Integration Techniques for Robust Code Acquisition," *Communications, IEEE Transactions on*, vol. 55, no. 11, pp. 2172 – 2184, Nov. 2007.

[48] M.G. Petovello and G. Lachapelle, "Comparison of vector-based software receiver implementations with application to ultra-tight gps /ins integration," *Proceedings of Institute of Navigation GNSS (ION GNSS 2006)*, pp. 1790–1799, 2006.

[49] E.S. Lohan, A. Lakhzouri, and M. Renfors, "Feedforward delay estimators in adverse multipath propagation for Galileo and modernized GPS signals," *EURASIP Journal of Applied Signal Processing*, vol. 2006, pp. 1 – 19.

[50] M.H. Bhuiyan and E.S. Lohan, "Advanced multipath mitigation techniques for satellite-based positioning applications," *Hindawi International Journal on Navigation and Observation*, vol. 2010, pp. 1 – 15.

[51] D.H. Titterton and J.L. Weston, *Strapdown inertial navigation technology*, Stevenage, U.K.: Peregrinus, 1997.

[52] S. Gunawardena, A. Soloviev, and F. van Graas, "Real Time Implementation of Deeply Integrated Software GPS Receiver and Low Cost IMU for Processing Low-CNR GPS Signals," *Proceedings of the 60th Annual Meeting of the Institute of Navigation*, 2004.

[53] B.W. Parkinson and J.J. Spilker Jr, *Global Positioning Systems: Theory and Applications: Volume I*, vol. 163, Progress in Astronautics and Aeronautics, 1996.

[54] M. Lashley, "Modeling and Performance Analysis of GPS Vector Tracking Algorithms," *PhD Thesis, Graduate Faculty of Auburn University*, 2009.

[55] D. Benson, "Intereference Benefits of a Vector Delay Lock Loop (VDLL) GPS Receiver," *Proceedings of the 63rd Annual Meeting Institute of Navigation*, 2007.

[56] J.J. Spilker Jr, *Vector Delay Lock Loop Processing of Radiolocation Transmitter Signals*, US Patent 5,398,034 March14, 1995.

[57] D. Sun, "Ultra-Tight GPS/Reduced IMU for Land Vehicle Navigation," *PhD Thesis, University of Calgary, Department of Geomatics Engineering*, 2010.

[58] T. Li, "Use of Wheel Speed Sensors to Enhance a Reduced IMU Ultra-Tight GNSS Receiver," *Graduate Thesis, University of Calgary, Department of Geomatics Engineering*, 2009.

[59] M.G. Petovello, C. O ' Driscoll, and G. Lachapelle, "Carrier Phase Tracking of Weak Signals Using Different Receiver Architectures," *Proceedings of Institute of Navigation National Technical Meeting (ION NTM 2008)*, 2008.

[60] M. Zhodzishsky, S. Yudanovand, V. Veitsel, and J. Ashjaee, "Co-Op Tracking for Carrier Phase," *Proceedings of Institute of Navigation - GPS 98 also U.S. patent (6,313,789 B1) June*, pp. 653–664, 1998.

[61] P. Henkel, G. X. Gao, T. Walter, and C. Gunther, "Robust Multi-Carrier, Multi-Satellite Vector Phase Locked Loop with Wideband Ionospheric Correction and Integrated Weighted RAIM," *Proceedings of European Navigation Conference (ENC- GNSS 2009)*, 2009.

[62] P. Henkel, K. Giger, and C. Gunther, "Multifrequency, Multisatellite Vector Phase-Locked Loop for Robust Carrier Tracking," *IEEE Journal of Selected Topics in Signal Processing*, pp. 674–681, 2009.

[63] J. Won and B. Eissfeller, "Effectiveness Analysis of Vector-Tracking-Loop in Signal Fading Environment," *Proceedings of Navitec 2010*, 2010.

[64] J.F. Raquet, M.M. Miller, and T. Q. Nguyen, "Issues and Approaches for Navigation Using Signals of Opportunity," *Proceedings of the Institute of Navigation National Technical Meeting (ION NTM 2007)*, Jan. 2007.

[65] P. Thevenon, D. Serant, O. Julien, C. Macabiau, M. Bousquet, L. Ries, and S. Corazza, "Positioning Using Mobile TV Based on the DVB-SH Standard," *Journal of the Institute of Navigation*, vol. 58, no. 2, Summer 2011.

[66] M.K. Simon, *Probability Distributions Involving Gaussian Random Variables: A Handbook for Engineers and scientists*, Kluwer Academic Publishers - Springer, May 2002.

[67] M. Abramowitz and I.A. Stegun, *Handbook of Mathematical Functions with Formulas, Graphs, and Mathematical Tables*, Dover Publicatipns, Inc., New York.

[68] K.S. Miller, *Multidimensional Gaussian Distributions*, The SIAM Series in Applied Mathematics, R.F. Drenick and H. Hochstadt, Editors. John Wiley and Sons, Inc., New York, 1964.

[69] M.K. Simon, J.K. Omura, R.A. Scholtz, and B.K. Levitt, *Spread Spectrum Communications Handbook*, Mc Graw Hill, Inc., 1994.

[70] U. Mengali and A.N. D'Andrea, *Synchronization Techniques for Digital Receivers*, Plenium Publishing Corporation, New York, 1997.

[71] J.G. Proakis, *Digital Communications. Third Edition.*, McGraw Hill International Editions, 1989.

[72] K. Brammer and G. Siffling, *Kalman-Bucy Filters*, Artech House, 1989.

[73] H. Meyr, M. Moeneclaey, and S.A. Fechtel, *Digital Communication Receivers*, Wiley, 1998.

[74] M.S. Grewal and A.P. Andrews, *Kalman Filtering: Theory and Practice Using MATLAB, 3rd Edition.*, Wiley, 2008.

[75] F. van Grass, A. Soloviev, M. Uijt de Haag, S. Gunawardena, and M. Braasch, "Comparison of two approaches for GNSS receiver algorithms: batch processing and sequential processing considerations," *Institute of Navigation GNSS 18th International Technical Meeting of the Satellite Division*, Sep. 2005.

[76] D. Kubran, "Hybridization of a GPS Receiver with Low-Cost Sensors for Personal Positioning in Urban Environment," *Doctoral Thesis Ecole Nationale Supèrieure des Tèlècomunications, Telecom Paris*, 2004.

[77] Ch. Kreye, B. Eissfeller, and G. Ameres, "Architecture of GNSS/INS Integrations Theoretical Approach and Practical Tests," .

[78] M. Lashley and D.M. Bevly, "GNSS Solutions: What are vector tracking loops and what are their benefits and drawbacks?," *Inside GNSS*, vol. 4, no. 3, pp. 17–21, 2009.

[79] G.E. Corazza, *Digital satellite communications*, Springer-Verlag, Inc., New York, 2007.

[80] M. Casadei, G.E. Corazza, M. Iubatti, A. Vanelli-Coralli, and M. Villanti, "Robust Code Acquisition with Parallel Frequency Testing for Indoor GNSS," *3rd ESA Workshop on Satellite Navigation User Equipment Technologies Navitec*, Dec. 2006.

[81] H. W. Sorenson, "Least-squares estimation: from gauss to kalman," *IEEE Spectrum*, vol. 7, pp. 63–68, July 1970.

[82] P. Kintner, T. Humphreys, and J. Hinks, "GNSS and Ionospheric Scintillation: How to Survive the Next Solar Maximum," *InsideGNSS*, Jul. 2009.

[83] P. Ward, "Performance Comparisons Between FLL, PLL and Novel FLL-Assisted PLL Carrier Tracking Loop Under RF Interference Conditions," *Proceedings of the 11th International Technical Meeting of The Satellite Divisions of The Institute of Navigation*, 1998.

[84] T. Chiou, J. Seo, T. Walter, and P. Enge, "Performance of a Doppler-Aided GPS Navigation System for Aviation Applications under Ionospheric Scintillation," *Proceedings of 21st Institute of Navigation International Technical Meeting.*

[85] R. Pagny, J.C. Dardelet, and Chenebault J., "From EGNOS to Galileo: A European Vision of Satellite-Based Radio Navigation," *Annals of telecommunications*, vol. 60, no. 3-4, Intelligent transportation systems, March-April 2004.

[86] P. Fertl, A. Hottinen, and G. Matz, "Perturbation-based Distributed Beamforming for Wireless Relay Networks," *Proceedings of the IEEE Global Telecommunications Conference*, 2008.

[87] R. Mudumbai, B. Wild, U. Madhow, and K. Ramchandran, "Distributed beamforming using 1 bit feedback: from concept to realization," *Proceedings of the 44th Allerton Conference on Communication, Control, Computation*, 2006.

[88] R. Mudumbai, J. Hespanha, U. Madhow, and G. Barriac, "Scalable feedback control for distributed beamforming in sensor networks," *Proceedings of the IEEE International Symposium on Information Theory*, 2005.

[89] D.R. Brown III and H.V. Poor, "Time-slotted round trip carrier synchronization for distributed beamforming," *Signal Processing, IEEE Transaction on*, pp. 5630–43, 2008.

[90] I. Ozil and D.R. Brown III, "Time-slotted round trip carrier synchronization," *Proceedings of the 41st Asilomar Conference on Signals*, 2007.

[91] D.R. Brown III, G. Prince, and J. McNeill, "A method for carrier frequency and phase synchronization of two autonomous cooperative transmitters," *Proceedings of the 5th IEEE Signal Processing Advances Wireless Communication*, pp. 278–282, 2005.

[92] G. Barriac, R. Mudumbai, and U. Madhow, "Distributed beamforming for information transfer in sensor networks," *Proceedings of the 3rd International Symposium on Information Processing in Sensor Networks (IPSN 2004), Berkeley*, pp. 81–88, 2004.

Acknowledgements

This thesis is the synthesis of the last three years I have spent working and researching in the Digicomm group of the University of Bologna and I would like to take the chance here to thank some very special and important people.

First and foremost my deepest gratitude goes to my supervisor Professor Giovanni E. Corazza for welcoming me in his research group and guiding me through all these years. I would like to thank him for his profound knowledge but most of all for teaching me that through hard work and dedication I can reach all my goals. Thank you for your support and for believing in me.

Many thanks are also due to all my colleagues at the Digicomm group, for their technical support but more so for their friendship. In particular I would like to thank the navigation group: Raffaella Pedone and Marco Villanti, for their continuous guidance and never-ending encouragement, Claudio Palestini, for his out-of-this-world motivational speeches and for always pushing me to think bigger and do better, Francesco Bastia, for being with me through the good and the bad times from the beginning almost to the very end and Giulio "fondamentalmente" Gabelli, for his infectious enthusiasm, wit and kindness. It has truly been a pleasure working with all of you.

My gratitude goes also to the communication guys and in particular to Professor Alessandro Vanelli-Coralli for finding the time in his busy schedule to make suggestions and exchange kind words, Enzo Alberto Candreva, for his eccentricities and for being a great listener and a good advisor, Marco Papaleo, for his brilliance and for always being there even when time zones away, Stefano Rosati, for his enviable motivation and appreciated support, Valentina Pullano, for being a whirlwind of emotions but above all for being a very good friend, Alessandro Guidotti, for the laughter and the advice, Valeria Petrini, Ilaria Thibault, Francesco Lombardo, Riccardo Baroni, Daniele Tarchi, Rosalba Suffritti, Massimo Neri, my past colleagues and friends Cecilia Bersani, Rosario Firrincieli and Stefano Cioni, and the new en-

tries Stefano Andrenacci and Roberta Casile, for making work and even the DEIS lab a fun place to be.

I am sincerely grateful to Dr. Christophe Macabiau and Dr. Olivier Julien for giving me the opportunity of working within the LTST laboratory of ENAC for six months. I would like to thank them both for welcoming me in their group and for their supervision and patience. Special thanks go to Antoine Blais for his help, Daniel Salos and Leslie Montloin and all the guys at ENAC for the friendly environment.

I would also like to acknowledge my international reviewers, Prof. Gonzalo Seco-Granados, and Prof. Elena Simona Lohan, for their precious and greatly appreciated comments and suggestions.

Finally, my greatest thanks go to my family for their constant support and cheer. Ortensio, for his good humor and kindness. My father and mother for being an inspiration, for celebrating the good times and consoling me through the bad. My sister for being my best friend, for her unwavering support and for always believing in me. You have been my strength and I wouldn't have done it without you.